Center for X-Ray Optics and Advanced Light Source

X-RAY DATA BOOKLET

Albert Thompson Ingolf Lindau
David Attwood Yanwei Liu
Eric Gullikson Piero Pianetta
Malcolm Howells Arthur Robinson
Kwang-Je Kim James Scofield
Janos Kirz James Underwood
Jeffrey Kortright Gwyn Williams

Herman Winick

October 2009

Lawrence Berkeley National Laboratory University of California Berkeley, CA 94720

This work was supported in part by the U.S. Department of Energy under Contract No. DE-AC02-05CH11231

CENTER FOR X-RAY OPTICS ADVANCED LIGHT SOURCE

X-RAY DATA BOOKLET

Albert C. Thompson, Janos Kirz, David T. Attwood, Eric M. Gullikson, Malcolm R. Howells, Jeffrey B. Kortright, Yanwei Liu, and Arthur L. Robinson

-Lawrence Berkeley National Laboratory

James H. Underwood

— EUV Technology, Inc.

Kwang-Je Kim

- Argonne National Laboratory

Ingolf Lindau, Piero Pianetta, and Herman Winick
— Stanford Synchrotron Radiation Laboratory

Gwyn P. Williams
— *Iefferson Laboratory*

Iames H. Scofield

-Lawrence Livermore National Laboratory

Compiled and edited by

Albert C. Thompson

-Lawrence Berkeley National Laboratory

Lawrence Berkeley National Laboratory University of California Berkeley, California 94720

Third edition, September 2009

This work was supported in part by the U.S. Department of Energy under Contract No. DE-AC02-05CH11231

UPDATES AND FURTHER INFORMATION The content of the X-Ray Data Booklet, together with additional information and further references, can be found on the web at http://xdb.lbl.gov. This site will also be updated with corrections to any errors found in this edition of the Booklet.

CONTENTS

X-Ray Properties of the Elements

1.1 Electron Binding Energies
 Gwyn P. Williams 1 1.2 X-Ray Emission Energies

Preface

	Jeffrey B. Kortright and
	Albert C. Thompson 1-8
	1.3 Fluorescence Yields For K And L Shells
	Jeffrey B. Kortright 1-28
	1.4 Principal Auger Electron Energies 1-30
	1.5 Subshell Photoionization Cross Sections
	Ingolf Lindau 1-32
	1.6 Mass Absorption Coefficients
	Eric M. Gullikson 1-38
	1.7 Atomic Scattering Factors
	Eric M. Gullikson 1-44
	1.8 Energy Levels of Few-Electron Ionic Species
	James H. Scofield 1-53
2.	Synchrotron Radiation 2-1
	2.1A Characteristics of Synchrotron Radiation
	Kwang-Je Kim 2-1
	2.1B Free Electron Lasers (FELs) at Extreme Ultraviolet
	and X-Ray Wavelengths
	Yanwei Liu 2-17
	2.2 History of Synchrotron Radiation
	Arthur L. Robinson 2-21

1-1

	Herman Winick and David Attwood 2-29	
3.	Scattering Processes	3-1
	3.1 Scattering of X-Rays from Electrons and Atoms Janos Kirz 3-1	
	3.2 Low-Energy Electron Ranges In Matter Piero Pianetta 3-5	
4.	Optics and Detectors	4-1
	4.1 Multilayers and Crystals James H. Underwood 4-1	
	4.2 Specular Reflectivities for Grazing-Incidence Mirro Eric M. Gullikson 4-13	ors
	4.3 Gratings and Monochromators Malcolm R. Howells 4-16	
	4.4 Zone Plates Janos Kirz and David Attwood 4-27	
	4.5 X-Ray Detectors Albert C. Thompson 4-32	
5.	Miscellaneous	5-1
	5.1 Physical Constants 5-1	

5.2 Physical Properties of the Elements
5.4
5.3 Electromagnetic Relations
5-10
5.4 Radioactivity and Radiation Protection
5-13

5-16

5.5 Useful Equations

2.3 Synchrotron Radiation Facilities

PREFACE

This edition of the X-Ray Data Booklet has minor revisions to some sections since the second edition in 2001. The booklet has been very popular. All 12,000 copies of the second edition were distributed several years ago. This edition is being published to provide a new supply of booklets. The booklet was first published in 1985. The Booklet is also posted on the web at http://xdb.lbl.gov, together with additional detail and further references for many of the sections.

As before, the compilers are grateful to a host of contributors who furnished new material or reviewed and revised their original sections. Also, as in the original edition, many sections draw heavily on work published elsewhere, as indicated in the text and figure captions. I would like to thank Doug Vaughan for his excellent work as co-editor of the second edition. I also want to express my continuing thanks to Janos Kirz, who conceived the *Booklet* as a service to the community and who remains an active contributor to this edition.

I take full responsibility for any errors in this new edition, and I invite readers to bring them to my attention at the Center for X-Ray Optics, 2-400, Lawrence Berkeley National Laboratory, Berkeley, California 94720, or by e-mail at xdb@grace.lbl.gov. Corrections will be posted on the web and incorporated in subsequent printings.

Albert C. Thompson

1 September 2009

SECTION 1

X-RAY PROPERTIES OF THE ELEMENTS

1.1 ELECTRON BINDING ENERGIES

Gwyn P. Williams

Table 1-1 gives the electron binding energies for the elements in their natural forms. The energies are given in electron volts relative to the vacuum level for the rare gases and for H_2 , N_2 , O_2 , F_2 , and Cl_2 ; relative to the Fermi level for the metals; and relative to the top of the valence bands for semiconductors. Values have been taken from Ref. 1 except as follows:

*Values taken from Ref. 2, with additional corrections †Values taken from Ref. 3.

^aOne-particle approximation not valid owing to short core-hole lifetime.

bValue derived from Ref. 1.

Thanks also to R. Johnson, G. Ice, M. Olmstead, P. Dowben, M. Seah, E. Gullikson, F. Boscherini, W. O'Brien, R. Alkire, and others.

REFERENCES

- J. A. Bearden and A. F. Burr, "Reevaluation of X-Ray Atomic Energy Levels," Rev. Mod. Phys. 39, 125 (1967).
- M. Cardona and L. Ley, Eds., Photoemission in Solids 1: General Principles (Springer-Verlag, Berlin, 1978).
- J. C. Fuggle and N. Mårtensson, "Core-Level Binding Energies in Metals," J. Electron Spectrosc. Relat. Phenom. 21, 275 (1980).

7-1

Table 1-1. Electron binding energies, in electron volts, for the elements in their natural forms.

Element	K 1s	L ₁ 2s	L ₂ 2p _{1/2}	L ₃ 2p _{3/2}	M ₁ 3s	M ₂ 3p _{1/2}	M ₃ 3p _{3/2}	M ₄ 3d _{3/2}	M ₅ 3d _{5/2}	N ₁ 4s	N ₂ 4p _{1/2}	N ₃ 4p _{3/2}
1 H	13.6											
2 He	24.6*											
3 Li	54.7*											
4 Be	111.5*											
5 B	188*											
6 C	284.2*											
7 N	409.9*	37.3*										
8 O	543.1*	41.6*										
9 F	696.7*											
10 Ne	870.2*	48.5*	21.7*	21.6*								
11 Na	1070.8†	63.5†	30.65	30.81								
12 Mg	1303.0†	88.7	49.78	49.50								
13 Al	1559.6	117.8	72.95	72.55								
14 Si	1839	149.7*b	99.82	99.42								
15 P	2145.5	189*	136*	135*								
16 S	2472	230.9	163.6*	162.5*								
17 Cl	2822.4	270*	202*	200*								
18 Ar	3205.9*	326.3*	250.6†	248.4*	29.3*	15.9*	15.7*					
19 K	3608.4*	378.6*	297.3*	294.6*	34.8*	18.3*	18.3*					
20 Ca	4038.5*	438.4†	349.7†	346.2†	44.3 †	25.4†	25.4†					
21 Sc	4492	498.0*	403.6*	398.7*	51.1*	28.3*	28.3*					
22 Ti	4966	560.9†	460.2†	453.8†	58.7†	32.6†	32.6†					

23 V	5465	626.7†	519.8†	512.1†	66.3†	37.2†	37.2†					
24 Cr	5989	696.0†	583.8†	574.1†	74.1†	42.2†	42.2†					
25 Mn	6539	769.1†	649.9†	638.7†	82.3†	47.2†	47.2†					
26 Fe	7112	844.6†	719.9†	706.8†	91.3†	52.7†	52.7†					
27 Co	7709	925.1†	793.2†	778.1†	101.0†	58.9†	59.9†					
28 Ni	8333	1008.6†	870.0†	852.7†	110.8†	68.0†	66.2†					
29 Cu	8979	1096.7†	952.3†	932.7	122.5†	77.3†	75.1†					
30 Zn	9659	1196.2*	1044.9*	1021.8*	139.8*	91.4*	88.6*	10.2*	10.1*			
31 Ga	10367	1299.0*b	1143.2†	1116.4†	159.5†	103.5†	100.0†	18.7†	18.7†			
32 Ge	11103	1414.6*b	1248.1*b	1217.0*b	180.1*	124.9*	120.8*	29.8	29.2			
33 As	11867	1527.0*b	1359.1*b	1323.6*b	204.7*	146.2*	141.2*	41.7*	41.7*			
34 Se	12658	1652.0*b	1474.3*b	1433.9*b	229.6*	166.5*	160.7*	55.5*	54.6*			
35 Br	13474	1782*	1596*	1550*	257*	189*	182*	70*	69*			
36 Kr	14326	1921	1730.9*	1678.4*	292.8*	222.2*	214.4	95.0*	93.8*	27.5*	14.1*	14.1*
37 Rb	15200	2065	1864	1804	326.7*	248.7*	239.1*	113.0*	112*	30.5*	16.3*	15.3 *
38 Sr	16105	2216	2007	1940	358.7†	280.3†	270.0†	136.0†	134.2†	38.9†	21.3	20.1†
39 Y	17038	2373	2156	2080	392.0*b	310.6*	298.8*	157.7†	155.8†	43.8*	24.4*	23.1*
40 Zr	17998	2532	2307	2223	430.3†	343.5†	329.8†	181.1†	178.8†	50.6†	28.5†	27.1†
41 Nb	18986	2698	2465	2371	466.6†	376.1†	360.6†	205.0†	202.3†	56.4†	32.6†	30.8†
42 Mo	20000	2866	2625	2520	506.3†	411.6†	394.0†	231.1†	227.9†	63.2†	37.6†	35.5†
43 Tc	21044	3043	2793	2677	544*	447.6	417.7	257.6	253.9*	69.5*	42.3*	39.9*
44 Ru	22117	3224	2967	2838	586.1*	483.5†	461.4†	284.2†	280.0†	75.0†	46.3†	43.2†
45 Rh	23220	3412	3146	3004	628.1†	521.3†	496.5†	311.9†	307.2†	81.4*b	50.5†	47.3†
46 Pd	24350	3604	3330	3173	671.6†	559.9†	532.3†	340.5†	335.2†	87.1*b	55.7†a	50.9†
47 Ag	25514	3806	3524	3351	719.0†	603.8†	573.0†	374.0†	368.3	97.0†	63.7†	58.3†

Table 1-1. Electron binding energies (continued).

Element	K 1s	L ₁ 2s	L ₂ 2p _{1/2}	L ₃ 2p _{3/2}	M ₁ 3s	M ₂ 3p _{1/2}	M ₃ 3p _{3/2}	M ₄ 3d _{3/2}	M ₅ 3d _{5/2}	N ₁ 4s	N ₂ 4p _{1/2}	N ₃ 4p _{3/2}
48 Cd	26711	4018	3727	3538	772.0†	652.6†	618.4†	411.9†	405.2†	109.8†	63.9†a	63.9†a
49 In	27940	4238	3938	3730	827.2†	703.2†	665.3†	451.4†	443.9†	122.9†	73.5†a	73.5†a
50 Sn	29200	4465	4156	3929	884.7†	756.5†	714.6†	493.2†	484.9†	137.1†	83.6†a	83.6†a
51 Sb	30491	4698	4380	4132	946†	812.7†	766.4†	537.5†	528.2†	153.2†	95.6†a	95.6†a
52 Te	31814	4939	4612	4341	1006†	870.8†	820.0‡	583.4†	573.0†	169.4†	103.3†a	103.3†a
53 I	33169	5188	4852	4557	1072*	931*	875*	630.8	619.3	186*	123*	123*
54 Xe	34561	5453	5107	4786	1148.7*	1002.1*	940.6*	689.0*	676.4*	213.2*	146.7	145.5*
55 Cs	35985	5714	5359	5012	1211*b	1071*	1003*	740.5*	726.6*	232.3*	172.4*	161.3*
56 Ba	37441	5989	5624	5247	1293*b	1137*b	1063*b	795.7†	780.5*	253.5†	192	178.6†
57 La	38925	6266	5891	5483	1362*b	1209*b	1128*b	853*	836*	274.7*	205.8	196.0*
58 Ce	40443	6549	6164	5723	1436*b	1274*b	1187*b	902.4*	883.8*	291.0*	223.2	206.5*
59 Pr	41991	6835	6440	5964	1511	1337	1242	948.3*	928.8*	304.5	236.3	217.6
60 Nd	43569	7126	6722	6208	1575	1403	1297	1003.3*	980.4*	319.2*	243.3	224.6
61 Pm	45184	7428	7013	6459	-	1471	1357	1052	1027	_	242	242
62 Sm	46834	7737	7312	6716	1723	1541	1420	1110.9*	1083.4*	347.2*	265.6	247.4
63 Eu	48519	8052	7617	6977	1800	1614	1481	1158.6*	1127.5*	360	284	257
64 Gd	50239	8376	7930	7243	1881	1688	1544	1221.9*	1189.6*	378.6*	286	271
65 Tb	51996	8708	8252	7514	1968	1768	1611	1276.9*	1241.1*	396.0*	322.4*	284.1*
66 Dy	53789	9046	8581	7790	2047	1842	1676	1333	1292.6*	414.2*	333.5*	293.2*
67 Ho	55618	9394	8918	8071	2128	1923	1741	1392	1351	432.4*	343.5	308.2*
68 Er	57486	9751	9264	8358	2207	2006	1812	1453	1409	449.8*	366.2	320.2*
69 Tm	59390	10116	9617	8648	2307	2090	1885	1515	1468	470.9*	385.9*	332.6*
70 Yb	61332	10486	9978	8944	2398	2173	1950	1576	1528	480.5*	388.7*	339.7*

Table 1-1. Electron binding energies (continued).

Element	N ₄ 4d _{3/2}	N ₅ 4d _{5/2}	N ₆ 4f _{5/2}	N ₇ 4f _{7/2}	O ₁ 5s	O ₂ 5p _{1/2}	O ₃ 5p _{3/2}	$O_4 5d_{3/2}$	$O_5 5d_{5/2}$	P ₁ 6s	$P_2 6p_{1/2}$	P ₃ 6p _{3/2}
48 Cd	11.7†	10.7†										
49 In	17.7†	16.9†										
50 Sn	24.9†	23.9†										
51 Sb	33.3†	32.1†										
52 Te	41.9†	40.4†										
53 I	50.6	48.9										
54 Xe	69.5*	67.5*	_	-	23.3*	13.4*	12.1*					
55 Cs	79.8*	77.5*	_	-	22.7	14.2*	12.1*					
56 Ba	92.6†	89.9†	_	-	30.3†	17.0†	14.8†					
57 La	105.3*	102.5*	_	-	34.3*	19.3*	16.8*					
58 Ce	109*	-	0.1	0.1	37.8	19.8*	17.0*					
59 Pr	115.1*	115.1*	2.0	2.0	37.4	22.3	22.3					
60 Nd	120.5*	120.5*	1.5	1.5	37.5	21.1	21.1					
61 Pm	120	120	_	_	-	_	_					
62 Sm	129	129	5.2	5.2	37.4	21.3	21.3					
63 Eu	133	127.7*	0	0	32	22	22					
64 Gd	-	142.6*	8.6*	8.6*	36	28	21					
65 Tb	150.5*	150.5*	7.7*	2.4*	45.6*	28.7*	22.6*					
66 Dy	153.6*	153.6*	*0.8	4.3*	49.9*	26.3	26.3					
67 Ho	160*	160*	8.6*	5.2*	49.3*	30.8*	24.1*					
68 Er	167.6*	167.6*	-	4.7*	50.6*	31.4*	24.7*					
69 Tm	175.5*	175.5*	-	4.6	54.7*	31.8*	25.0*					
70 Yb	191.2*	182.4*	2.5*	1.3*	52.0*	30.3*	24.1*					

Table 1-1. Electron binding energies (continued).

Element	K 1s	L ₁ 2s	L ₂ 2p _{1/2}	L ₃ 2p _{3/2}	M ₁ 3s	M ₂ 3p _{1/2}	M ₃ 3p _{3/2}	M ₄ 3d _{3/2}	M ₅ 3d _{5/2}	N ₁ 4s	N ₂ 4p _{1/2}	N ₃ 4p _{3/2}
71 Lu	63314	10870	10349	9244	2491	2264	2024	1639	1589	506.8*	412.4*	359.2*
72 Hf	65351	11271	10739	9561	2601	2365	2108	1716	1662	538*	438.2†	380.7†
73 Ta	67416	11682	11136	9881	2708	2469	2194	1793	1735	563.4†	463.4†	400.9†
74 W	69525	12100	11544	10207	2820	2575	2281	1872	1809	594.1†	490.4†	423.6†
75 Re	71676	12527	11959	10535	2932	2682	2367	1949	1883	625.4†	518.7†	446.8†
76 Os	73871	12968	12385	10871	3049	2792	2457	2031	1960	658.2†	549.1†	470.7†
77 Ir	76111	13419	12824	11215	3174	2909	2551	2116	2040	691.1†	577.8†	495.8†
78 Pt	78395	13880	13273	11564	3296	3027	2645	2202	2122	725.4†	609.1†	519.4†
79 Au	80725	14353	13734	11919	3425	3148	2743	2291	2206	762.1†	642.7†	546.3†
80 Hg	83102	14839	14209	12284	3562	3279	2847	2385	2295	802.2†	680.2†	576.6†
81 TI	85530	15347	14698	12658	3704	3416	2957	2485	2389	846.2†	720.5†	609.5†
82 Pb	88005	15861	15200	13035	3851	3554	3066	2586	2484	891.8†	761.9†	643.5†
83 Bi	90524	16388	15711	13419	3999	3696	3177	2688	2580	939†	805.2†	678.8†
84 Po	93105	16939	16244	13814	4149	3854	3302	2798	2683	995*	851*	705*
85 At	95730	17493	16785	14214	4317	4008	3426	2909	2787	1042*	886*	740*
86 Rn	98404	18049	17337	14619	4482	4159	3538	3022	2892	1097*	929*	768*
87 Fr	101137	18639	17907	15031	4652	4327	3663	3136	3000	1153*	980*	810*
88 Ra	103922	19237	18484	15444	4822	4490	3792	3248	3105	1208*	1058	879*
89 Ac	106755	19840	19083	15871	5002	4656	3909	3370	3219	1269*	1080*	890*
90 Th	109651	20472	19693	16300	5182	4830	4046	3491	3332	1330*	1168*	966.4†
91 Pa	112601	21105	20314	16733	5367	5001	4174	3611	3442	1387*	1224*	1007*
92 U	115606	21757	20948	17166	5548	5182	4303	3728	3552	1439*b	1271*b	1043†

Table 1-1. Electron binding energies (continued).

Element	N ₄ 4d _{3/2}	N ₅ 4d _{5/2}	$N_6 4f_{5/2}$	N ₇ 4f _{7/2}	O ₁ 5s	$O_2 5p_{1/2}$	${\rm O}_35p_{3/2}$	O ₄ 5d _{3/2}	$\mathrm{O}_55d_{5/2}$	P ₁ 6s	P ₂ 6p _{1/2}	P ₃ 6p _{3/2}
71 Lu	206.1*	196.3*	8.9*	7.5*	57.3*	33.6*	26.7*					
72 Hf	220.0†	211.5†	15.9†	14.2†	64.2†	38*	29.9†					
73 Ta	237.9†	226.4†	23.5†	21.6†	69.7†	42.2*	32.7†					
74 W	255.9†	243.5†	33.6*	31.4†	75.6†	45.3*b	36.8†					
75 Re	273.9†	260.5†	42.9*	40.5*	83†	45.6*	34.6*b					
76 Os	293.1†	278.5†	53.4†	50.7†	84*	58*	44.5†					
77 Ir	311.9†	296.3†	63.8†	60.8†	95.2*b	63.0*b	48.0†					
78 Pt	331.6†	314.6†	74.5†	71.2†	101.7*b	65.3*b	51.7†					
79 Au	353.2†	335.1†	87.6†	84.0	107.2*b	74.2†	57.2†					
80 Hg	378.2†	358.8†	104.0†	99.9†	127†	83.1†	64.5†	9.6†	7.8†			
81 Tl	405.7†	385.0†	122.2†	117.8†	136.0*b	94.6†	73.5†	14.7†	12.5†			
82 Pb	434.3†	412.2†	141.7†	136.9†	147*b	106.4†	83.3†	20.7‡	18.1†			
83 Bi	464.0†	440.1†	162.3†	157.0†	159.3*b	119.0†	92.6†	26.9†	23.8†			
84 Po	500*	473*	184*	184*	177*	132*	104*	31*	31*			
85 At	533*	507	210*	210*	195*	148*	115*	40*	40*			
86 Rn	567*	541*	238*	238*	214*	164*	127*	48*	48*	26		
87 Fr	603*	577*	268*	268*	234*	182*	140*	58*	58*	34	15	15
88 Ra	636*	603*	299*	299*	254*	200*	153*	68*	68*	44	19	19
89 Ac	675*	639*	319*	319*	272*	215*	167*	80*	80*		-	_
90 Th	712.1†	675.2†	342.4†	333.1†	290*a	229*a	182*a	92.5†	85.4†	41.4†	24.5†	16.6†
91 Pa	743*	708*	371*	360*	310*	232*	232*	94*	94*	_	_	_
92 U	778.3†	736.2†	388.2*	377.4†	321*ab	257*ab	192*ab	102.8†	94.2†	43.9†	26.8†	16.8†

1.2 X-RAY EMISSION ENERGIES

Jeffrey B. Kortright and Albert C. Thompson

In Table 1-2, characteristic K, L, and M x-ray line energies are given for elements with $3 \le Z \le 95$. Only the strongest lines are included: $K\alpha_1, K\alpha_2, K\beta_1, L\alpha_1, L\alpha_2, L\beta_1, L\beta_2, L\gamma_1$, and $M\alpha_1$. Wavelengths, in angstroms, can be obtained from the relation $\lambda = 12,398/E$, where E is in eV. The data in the table were based on Ref. 1, which should be consulted for a more complete listing. Widths of the $K\alpha$ lines can be found in Ref. 2.

Table 1-3 provides a listing of these, and additional, lines (arranged by increasing energy), together with relative intensities. An intensity of 100 is assigned to the strongest line in each shell for each element. Figure 1-1 illustrates the transitions that give rise to the lines in Table 1-3.

REFERENCES

- J. A. Bearden, "X-Ray Wavelengths," Rev. Mod. Phys. 39, 78 (1967).
- M. O. Krause and J. H. Oliver, "Natural Widths of Atomic K and L Levels, Kα X-Ray Lines and Several KLL Auger Lines," J. Phys. Chem. Ref. Data 8, 329 (1979).

Table 1-2. Photon energies, in electron volts, of principal K-, L-, and M-shell emission lines.

Μα ₁																			
ΓÄ																			
Γβ																			
$\Gamma \beta_1$																		344.9	399.6
LØ2																		341.3	395.4
LØ1																		341.3	395.4
Kβı									1,071.1	1,302.2	1,557.45	1,835.94	2,139.1	2,464.04	2,815.6	3,190.5	3,589.6	4,012.7	4,460.5
Κα								848.6	1,040.98	1,253.60	1,486.27	1,739.38	2,012.7	2,306.64	2,620.78	2,955.63	3,311.1	3,688.09	4,086.1
Κα ₁	54.3	108.5	183.3	277	392.4	524.9	8.929	848.6	1,040.98	1,253.60	1,486.70	1,739.98	2,013.7	2,307.84	2,622.39	2,957.70	3,313.8	3,691.68	4,090.6
Element	3 Li	4 Be	5 B	9 C	7 Z	8 0	9 F	10 Ne	11 Na	12 Mg	13 Al	14 Si	15 P	16 S	17 CI	18 Ar	19 K	20 Ca	21 Sc

Table 1-2. Energies of x-ray emission lines (continued).

$K\alpha_1$		$K\beta_1$	$\mathbf{L}\alpha_{\mathbf{l}}$	ΓŒ	$\Gamma \beta_1$	rβ	Г'n	Μα _l
		4,931.81	452.2	452.2	458.4			
0		5,427.29	511.3	511.3	519.2			
		5,946.71	572.8	572.8	582.8			
		6,490.45	637.4	637.4	648.8			
		7,057.98	705.0	705.0	718.5			
		7,649.43	776.2	776.2	791.4			
		8,264.66	851.5	851.5	8.898			
	8 8,027.83	8,905.29	929.7	929.7	949.8			
		9,572.0	1,011.7	1,011.7	1,034.7			
		10,264.2	1,097.92	1,097.92	1,124.8			
		10,982.1	1,188.00	1,188.00	1,218.5			
		11,726.2	1,282.0	1,282.0	1,317.0			
		12,495.9	1,379.10	1,379.10	1,419.23			
		13,291.4	1,480.43	1,480.43	1,525.90			
		14,112	1,586.0	1,586.0	1,636.6			
		14,961.3	1,694.13	1,692.56	1,752.17			
		15,835.7	1,806.56	1,804.74	1,871.72			
		16,737.8	1,922.56	1,920.47	1,995.84			
	15,775.1 15,690.9	17,667.8	2,042.36	2,039.9	2,124.4	2,219.4	2,302.7	

180'1	8/11/2	985,6	1.202,8	0.600,8	1.858,2	£14'St	39,522.4	1.811,04	mS 29
_	768'9	666,9	196'⊊	8.704,8	2.254,2	43,826	3.171,85	7.427,85	m4 19
846	1.209,8	4.680,8	9.127,8	7.702,8	4.052,2	£.172,24	4.748,85	0.136,76	PN 09
676	1.225,3	058'5	6.884,8	5.610,8	7.650,2	7.847,04	3.028,28	5.920,95	¹ 4 65
883	750'9	4.613,2	2,262.2	4,823.0	4,840.2	£.722,6£	34,278.9	7.617,45	28 Cc
833	2.887,8	2,585,2	1.240,8	4,634.23	76.028,4	0.108,75	1.450,55	8.144,EE	57 La
	1.152,2	5,851,8	4,827.53	06.024,4	92.994,4	2.875,85	1.718,15	9.591,25	26 Ba
	4.082,2	6.256,4	8.619,4	4,272.2	2.882,4	6.986,45	30,625.1	8.276,05	22 C8
		_	_	_	6.601,4	33,624	884,62	644,62	54 Xe
	6.008,4	5.702,4	4,220.72	3,926.04	59.7£9,£	7.462,25	2.718,82	0.216,82	I ES
	6.072,4	7.108,4	4,029.58	8.887,8	££.697,£	7.866,08	7.102,72	£.274,72	52 Te
	62.748,4	87.001,4	72.E48,E	3,595.32	3,604.72	9.827,62	8.011,62	1.925,32	9S 1 <i>S</i>
	4,131.12	3,904.86	3,662.80	3,435.42	86.544,5	0.884,85	0.440,82	25,271.3	us os
	18.026,£	18.517,5	12.784,5	3,279.29	₹6.982,€	6.272,72	24,002.0	7.602,42	u _I 6†
	98.917,€	3,528.12	72.315,5	3,126.91	£7.E£1,E	2.890,62	1.486,22	9.571,52	48 Cq
	95.912,5	18.745,5	3,150.94	12.876,2	15.486,2	7.246,42	21,990.3	22,162.92	3A 74
	7.825,5	6L.171,E	22.066,2	62.888,2	19.858,2	7.818,52	1.020,12	1.771,12	Pd 9t
	8.£₽1,€	£.100,£	14.458,41	2,692.05	47.969,2	27,723.6	7.870,02	1.912,02	45 Rh
	2,964.5	2,836.0	2,683.23	15.455,2	2,558.55	8.959,12	4.021,91	2.972,91	44 Ru
	762,2	7,674	2,538	2,420	7,424	50,619	18,250.8	1.78£,81	oT £4

28.682,2

2,163.0

2,293.16

2,165.89

£.809,91

18,622.5

£.47£,71

0.152,61

45.674,71

1.218,81

45 Mo

9N It

2,623,5

8.194,2

2,518.3

0.786,2

18.496,2

4.7257.4

Table 1-2. Energies of x-ray emission lines (continued).

MØ	ИŢ	ч	г у л	ΓαΣ	$\Gamma \alpha_l$	КØ	Κα ²	Κα ^j	Element
1,131	£.084,7	2.843.2	4.884,8	5,816.6	7.248,2	6.750,74	6.106,04	41,542.2	uA 69
1,185	8.287,7	8.201,7	2.817,8	6,025.0	2.720,8	£69'8₽	6.80€,24	2.966,24	PO 149
1,240	201,8	L'99E'L	846'9	0.852,6	8.272,8	286,08	1.447,84	9.184,44	QT 20
1,293	8.814,8	L.858,T	L. T. 42, T	L.TZ4,8	2.264,8	611,28	45,207.8	t [.] 866'St	99 Dy
84£,1	L\$L'8	116'L	£.222,7	£.676,8	8.617,8	LL8'ES	L'669'9t	L'945'Lt	oH L9
904'1	680'6	0.681,8	6.018,7	0.206,8	L'846'9	189'55	1.122,84	L.721,94	68 Er
1,462	974'6	894'8	101,8	1.551,7	6.671,7	LIS'LS	9.277,e4	9.147,08	WL 69
1,521.4	1.087,6	8.827,8	8,104,8	£.78£,7	9.214,7	075,62	0.485,18	6.888,28	9.X 0.L
1,581.3	4.641,01	6.840,6	0.607,8	6.400,7	5.259,7	61,283	0.296,22	8.690,48	nJ I7
9.449,1	8.212,01	£.74E,9	7.220,6	9.448,7	0.668,7	63,234	4.116,42	2.067,88	JH 7L
017,1	2.268,01	8.128,9	1.545,9	6.780,8	1.941,8	65,223	LL7'95	7£\$'L\$	73 Ta
trsll'I	6.282,11	5.136,6	86.278,9	2.255,8	9.795,8	6.442,78	L.186,72	42.818,92	M 7/
1,842.5	4.288,11	10,275.2	0.010,01	2.982,8	8,652.5	016,69	6.717,68	6.041,16	75 Re
1,910.2	12,095.3	2.862,01	6.255,01	0.148,8	7.116,8	£1 † '1/	L.384,13	2.000,59	SO 9L
6.676,1	12,512.6	10,920.3	£.807,01	5.660,6	1.271,9	8.092,87	7.982,59	9.268,49	л 77
2,050,5	12,942.0	2.022,11	7.070,11	8.13£,9	6,442.3	8tL'SL	211,29	758,63	14 8L
2,122.9	7.185,51	L.482,11	11,442.3	0.828,0	6.517,6	₹86°LL	5.686,68	L.E08,83	n∀ 6L
2,195.3	1.058,51	1.426,11	11,822.6	9.768,6	8.886,6	80,233	\$68,89	618'04	gH 08
9.072,2	2.162,41	2.172,21	12,213.3	8.271,01	5.892,01	915,28	6.188,07	2.178,27	IT 18

82 Pb	74,969.4	72,804.2	84,936	10,551.5	10,449.5	12,613.7	12,622.6	14,764.4	2,345.5
83 Bi	77,107.9	74,814.8	87,343	10,838.8	10,730.91	13,023.5	12,979.9	15,247.7	2,422.6
84 Po	79,290	76,862	89,800	11,130.8	11,015.8	13,447	13,340.4	15,744	
85 At	81,520	78,950	92,300	11,426.8	11,304.8	13,876		16,251	
86 Rn	83,780	81,070	94,870	11,727.0	11,597.9	14,316		16,770	_
87 Fr	86,100	83,230	97,470	12,031.3	11,895.0	14,770	14,450	17,303	_
88 Ra	88,470	85,430	100,130	12,339.7	12,196.2	15,235.8	14,841.4	17,849	_
89 Ac	90,884	87,670	102,850	12,652.0	12,500.8	15,713	_	18,408	_
90 Th	93,350	89,953	105,609	12,968.7	12,809.6	16,202.2	15,623.7	18,982.5	2,996.1
91 Pa	95,868	92,287	108,427	13,290.7	13,122.2	16,702	16,024	19,568	3,082.3
92 U	98,439	94,665	111,300	13,614.7	13,438.8	17,220.0	16,428.3	20,167.1	3,170.8
93 Np		_	_	13,944.1	13,759.7	17,750.2	16,840.0	20,784.8	_
94 Pu		_	_	14,278.6	14,084.2	18,293.7	17,255.3	21,417.3	_
95 Am	_			14,617.2	14,411.9	18,852.0	17,676.5	22,065.2	_

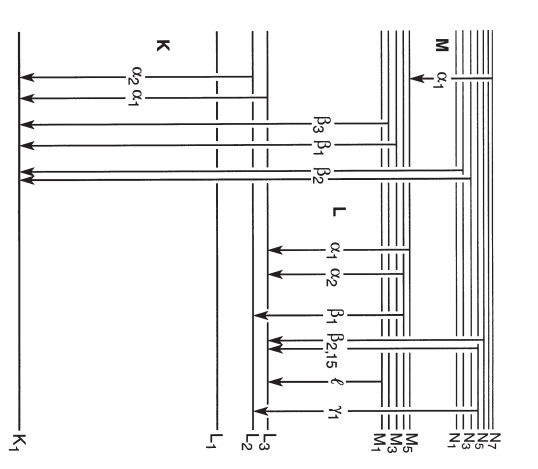


Fig. 1-1. Table 1-3. Transitions that give rise to the emission lines in

Table 1-3. Photon energies and relative intensities of K-, L-, and M-shell lines shown in Fig. 1-1, arranged by increasing energy. An intensity of 100 is assigned to the strongest line in each shell for each element.

Rungy Relative 524.9 8 O $\kappa \alpha_{1,2}$ 151 2851 2891 $L\alpha_{1,2}$ 111 152 2891 $L\alpha_{1,2}$ 111 153 2891 $L\alpha_{1,2}$ 111 153 2891 $L\alpha_{1,2}$ 111 883 2871 $L\beta_{1,2}$ 1891 $L\beta_{1,2}$ $L\beta$,										
Flement Line intensity 556.3 25 Mm Ll 15 868.8 28 Ni Ll l 3 3 Li K $\alpha_{1,2}$ 150 572.8 24 Cr L $\alpha_{1,2}$ 111 883 28 Cr M α_{1} 4 4 Be K $\alpha_{1,2}$ 150 582.8 24 Cr L β_{1} 79 884 30 Zr L β_{1} 6 C K $\alpha_{1,2}$ 150 652.2 26 Cr L β_{1} 10 9292 59 P M α_{1} 6 C K $\alpha_{1,2}$ 147 57 M L β_{1} 77 9498 29 Cr L β_{1} 7 1 S 15 648 25 Mn L β_{1} 77 9498 20 Cr L β_{1} 8 1 S 15 648 25 Mn L β_{1} 10 993 20 Cr L β_{1} 8 1 S 15 46 67 11 10 993 20 Cr L β_{1} 8 1 S 15 17 14	Energy			Relative	524.9	80	$K\alpha_{1,2}$	151	851.5	28 Ni	$L\alpha_{1,2}$	Ξ
$ \begin{array}{cccccccccccccccccccccccccccccccccccc$	(eV)	Element	Line	intensity	556.3	25 Mn		15	868.8	28 Ni	$L\beta_1$	89
$ \begin{array}{cccccccccccccccccccccccccccccccccccc$	54.3	3 Li	$K\alpha_{1,2}$	150	572.8		$L\alpha_{1,2}$	111	883	58 Ce	$M\alpha_1$	100
$ \begin{array}{cccccccccccccccccccccccccccccccccccc$	108.5	4 Be	$K\alpha_{1,2}$	150	582.8		$L\beta_1$	79	884	30 Zn	ロ	7
$ \begin{array}{cccccccccccccccccccccccccccccccccccc$	183.3	5 B	$K\alpha_{1,2}$	151	615.2		I	10	929.2	59 Pr	$M\alpha_1$	100
$ \begin{array}{cccccccccccccccccccccccccccccccccccc$	277	29	$K\alpha_{1,2}$	147	637.4		$L\alpha_{1,2}$	111	929.7	29 Cu	$L\alpha_{1,2}$	Ξ
$ \begin{array}{cccccccccccccccccccccccccccccccccccc$	348.3	21 Sc		21	648.8		$L\beta_1$	77	949.8	29 Cu	$L\beta_1$	65
$ \begin{array}{cccccccccccccccccccccccccccccccccccc$	392.4	7 N	$K\alpha_{1,2}$	150	8.929		$K\alpha_{1,2}$	148	957.2	31 Ga	Ξ	7
$ \begin{array}{cccccccccccccccccccccccccccccccccccc$	395.3	22 Ti		46	8.779		1	10	826	PN 09	$M\alpha_1$	100
$ \begin{array}{cccccccccccccccccccccccccccccccccccc$	395.4	21 Sc	$L\alpha_{1,2}$	111	705.0		$L\alpha_{1,2}$	111	1,011.7	30 Zn	$L\alpha_{1,2}$	111
$ \begin{array}{cccccccccccccccccccccccccccccccccccc$	399.6	21 Sc	$L\beta_1$	77	718.5		Lβ ₁	99	1,034.7	30 Zn	Lβ ₁	9
$ \begin{array}{cccccccccccccccccccccccccccccccccccc$	446.5	23 V	コ	28	742.7		17	6	1,036.2	32 Ge	I	9
22 Ti $L\beta_1$ 79 7914 27Co $L\beta_1$ 76 1,081 62 Sm $M\alpha_1$ 24 Cr Li 17 811.1 29 Cu Li 8 1,097.9 31 Ga $L\alpha_{1,2}$ 23 V $L\alpha_{1,2}$ 111 833 57 La $M\alpha_1$ 100 1,120 33 As Li 23 V $L\beta_1$ 80 848.6 10 Ne $K\alpha_{1,2}$ 150 1,124.8 31 Ga $L\beta_1$	452.2	22 Ti	$L\alpha_{1,2}$	111	776.2		$L\alpha_{1,2}$	111	1,041.0	11 Na	$K\alpha_{1,2}$	150
$ 24 Cr \qquad LI \qquad 17 \qquad \qquad 811.1 29 Cu \qquad LI \qquad 8 \qquad \qquad 1,097.9 31 Ga \\ 23 V \qquad L\alpha_{1,2} \qquad 111 \qquad \qquad 833 57 La \qquad M\alpha_1 \qquad 100 \qquad \qquad 1,120 \qquad 33 As \\ 23 V \qquad L\beta_1 \qquad 80 \qquad \qquad 848.6 10 Ne \qquad K\alpha_{1,2} \qquad 150 \qquad \qquad 1,124.8 31 Ga $	458.4	22 Ti	$L\beta_1$	79	791.4		$L\beta_1$	9/	1,081	62 Sm	$M\alpha_1$	100
23 V $L\alpha_{1,2}$ 111 833 57 La $M\alpha_1$ 100 1,120 33 As 23 V $L\beta_1$ 80 848.6 10 Ne $K\alpha_{1,2}$ 150 1,124.8 31 Ga	500.3	24 Cr	Π	17	811.1		17	∞	1,097.9	31 Ga	$L\alpha_{1,2}$	111
23 V L β_1 80 848.6 10 Ne K $\alpha_{1,2}$ 150 1,124.8 31 Ga	511.3	23 V	$L\alpha_{1,2}$	111	833		$M\alpha_1$	100	1,120	33 As	I	9
	519.2	23 V	$L\beta_1$	80	848.6	10 Ne	$K\alpha_{1,2}$	150	1,124.8	31 Ga	$L\beta_1$	99

Table 1-3. Energies and intensities of x-ray emission lines (continued).

Energy			Relative	1,462	69 Tm	$M\alpha_1$	100	1,740.0	14 Si	$K\alpha_1$	100
(eV)	Element	Line	intensity	1,480.4	35 Br	$L\alpha_{1,2}$	Ξ	1,752.2	37 Rb	$L\beta_1$	28
1,131	63 Eu	$M\alpha_1$	100	1,482.4	37 Rb		5	1,775.4	74 W	$M\alpha_1$	100
1,185	64 Gd	$M\alpha_1$	100	1,486.3	13 Al	$K\alpha_2$	50	1,792.0	40 Zr	I	2
1,188.0	32 Ge	$L\alpha_{1,2}$	111	1,486.7	13 AJ	$K\alpha_1$	100	1,804.7	38 Sr	$L\alpha_2$	Ξ
1,204.4	34 Se	ī	9	1,521.4	70 Yb	$M\alpha_1$	100	1,806.6	38 Sr	$L\alpha_1$	100
1,218.5	32 Ge	$L\beta_1$	09	1,525.9	35 Br	$L\beta_1$	59	1,835.9	14 Si	$K\beta_1$	2
1,240	65 Tb	$M\alpha_1$	100	1,557.4	13 Al	$K\beta_1$	-	1,842.5	75 Re	$M\alpha_1$	100
1,253.6	12 Mg	$K\alpha_{1,2}$	150	1,581.3	71 Lu	$M\alpha_1$	100	1,871.7	38 Sr	$L\beta_1$	58
1,282.0	33 As	$L\alpha_{1,2}$	111	1,582.2	38 Sr	Π	5	1,902.2	41 Nb	1	5
1,293	66 Dy	$M\alpha_1$	100	1,586.0	36 Kr	$L\alpha_{1,2}$	111	1,910.2	76 Os	$M\alpha_1$	100
1,293.5	35 Br	Ξ	S	1,636.6	36 Kr	$L\beta_1$	57	1,920.5	39 Y	$L\alpha_2$	=
1,317.0	33 As	$L\beta_1$	09	1,644.6	72 Hf	$M\alpha_1$	100	1,922.6	39 Y	$L\alpha_1$	100
1,348	67 Ho	$M\alpha_1$	100	1,685.4	39 Y	Ξ	5	1,979.9	77 Ir	$M\alpha_1$	100
1,379.1	34 Se	$L\alpha_{1,2}$	111	1,692.6	37 Rb	$L\alpha_2$	Ξ	1,995.8	39 Y	$L\beta_1$	57
1,386	36 Kr		S	1,694.1	37 Rb	$L\alpha_1$	100	2,012.7	15 P	$K\alpha_2$	20
1,406	68 Er	$M\alpha_1$	100	1,709.6	73 Ta	$M\alpha_1$	100	2,013.7	15 P	$K\alpha_1$	100
1,419.2	34 Se	$L\beta_1$	65	1,739.4	14 Si	$K\alpha_2$	20	2,015.7	42 Mo	Π	S

			41 NO LP2,15 3	4		11 2,367.0	$L\alpha_2$ 11 2,367.0
	4	, El 4	45 Rh Ll 4	7	7	100 2,376.5	$L\alpha_1$ 100 2,376.5
	53	o Lβ ₁ 53	$42 \text{ Mo} \text{L}\beta_1 \qquad 53$	~	4	4	$M\alpha_1$ 100 2,394.8
	11	: Lo ₂ 11	43 Tc Lo ₂ 11	2,420 43 Tc $L\alpha_2$ 11			
_	1 100	$M\alpha_1$ 100		83 Bi	83 Bi	83 Bi	100 2,422.6 83 Bi
_	100	: $L\alpha_1$ 100		43 Tc	43 Tc	54 2,424 43 Tc	54 2,424 43 Tc
	2	$^{\circ}$ L γ_1 2	_	41 Nb	41 Nb	3 2,461.8 41 Nb I	15 P $K\beta_1$ 3 2,461.8 41 Nb 1
	5	Κβ ₁ 5		16 S	16 S	16 S	11 2,464.0 16 S
				46 Pd	46 Pd	100 2,503.4 46 Pd	41 Nb $L\alpha_1$ 100 2,503.4 46 Pd
S	,15	ο Lβ _{2,15}			42 Mo	100 2,518.3 42 Mo	100 2,518.3 42 Mo
54				43 Tc	43 Tc	43 Tc	Lβ _{2,15} 1 2,538 43 Tc
Ξ			44 Ru $L\alpha_2$	44 Ru	44 Ru	4 2,554.3 44 Ru	4 2,554.3 44 Ru
100		$_1$ L α_1		44 Ru	44 Ru	52 2,558.6 44 Ru	Lβ ₁ 52 2,558.6 44 Ru
20	6.			17 Cl	17 Cl	100 2,620.8 17 Cl	$M\alpha_1$ 100 2,620.8 17 Cl
100		$K\alpha_1$	17 Cl Κα ₁	17 CI	17 CI	11 2,622.4 17 CI	11 2,622.4 17 CI
33			42 Mo Ly ₁	42 Mo	42 Mo	100 2,623.5 42 Mo	100 2,623.5 42 Mo
4				47 Ag	47 Ag	47 Ag	2 2,633.7 47 Ag
7	SI,	: Lβ _{2,15}			43 Tc	50 2,674 43 Tc	50 2,674 43 Tc
54			44 Ru Lβ ₁		44 Ru	100 2,683.2 44 Ru	100 2,683.2 44 Ru
Ξ		1 Las	45 Rh Los		2.692.0	100	100 2,692.0

Table 1-3. Energies and intensities of x-ray emission lines (continued).

Energy			Relative	3,487.2	49 In	Lβ ₁	28	3,937.6	53 I	$L\alpha_1$	100
(eV)	Element	Line	intensity	3,519.6	47 Ag	$L\gamma_1$	9	3,954.1	56 Ba	Π	4
3,143.8	45 Rh	$L\gamma_1$	5	3,528.1	48 Cd	$L\beta_{2,15}$	15	4,012.7	20 Ca	$K\beta_{1,3}$	13
3,150.9		$L\beta_1$	99		19 K	$K\beta_{1,3}$	11	4,029.6	52 Te	$L\beta_1$	61
3,170.8	92 U	$M\alpha_1$	100	3,595.3	51 Sb	$L\alpha_2$	11	4,086.1	21 Sc	$K\alpha_2$	20
3,171.8	46 Pd	Lβ _{2,15}	12	3,604.7	51 Sb	$L\alpha_1$	100	4,090.6	21 Sc	$K\alpha_1$	100
3,188.6	51 Sb		4	3,636	54 Xe	ī	4	4,093	54 Xe	$L\alpha_2$	Π
3,190.5	18 Ar	$K\beta_{1,3}$	10	3,662.8	50 Sn	$L\beta_1$	09	4,100.8	51 Sb	$L\beta_{2,15}$	17
3,279.3	49 In	$L\alpha_2$	11	3,688.1	20 Ca	$K\alpha_2$	20	4,109.9	54 Xe	$L\alpha_1$	100
3,286.9	49 In	$L\alpha_1$	100	3,691.7	20 Ca	$K\alpha_1$	100	4,124	57 La	Π	4
3,311.1	19 K	$K\alpha_2$	90	3,713.8	49 In	$L\beta_{2,15}$	15	4,131.1	50 Sn	$L\gamma_1$	7
3,313.8	19 K	$K\alpha_1$	100	3,716.9	48 Cd	Γ_{γ_1}	9	4,220.7	53 I	$L\beta_1$	61
3,316.6	48 Cd	$L\beta_1$	58	3,758.8	52 Te	$L\alpha_2$	==	4,272.2	55 Cs	$L\alpha_2$	Ξ
3,328.7	46 Pd	$L\gamma_1$	9	3,769.3	52 Te	$L\alpha_1$	100	4,286.5	55 Cs	$L\alpha_1$	100
3,335.6	52 Te	I	4	3,795.0	55 Cs	17	4	4,287.5	58 Ce	コ	4
3,347.8	47 Ag	$L\beta_{2,15}$	13	3,843.6	51 Sb	$L\beta_1$	19	4,301.7	52 Te	$L\beta_{2,15}$	18
3,435.4	50 Sn	$L\alpha_2$	111	3,904.9	50 Sn	$L\beta_{2,15}$	16	4,347.8	51 Sb	$L\gamma_1$	∞
3,444.0	50 Sn	$L\alpha_1$	100	3,920.8	49 In	$L\gamma_1$	9	4,414	54 Xe	$L\beta_1$	09
3,485.0	53 I	Π	4	3,926.0	53 I	$L\alpha_2$	11	4,450.9	56 Ba	$L\alpha_2$	Ξ

$L\gamma_1$ 9	1 4	α_2 111	Lβ _{2,15} 21	α_1 100	$L\beta_1$ 60	1 4	4 الا	α_2 11	α_1 100	Lβ _{2,15} 21	α_2 50	α_1 100	1 4	.B _{1,3} 15	β_1 61	α_2 111	6 لل	α_1 100	
56 Ba L	65 Tb L			62 Sm L						59 Pr L								64 Gd L	T 1100
5,531.1		5,609.0		5,636.1		5,743.1		5,816.6	5,845.7	5,850	5,887.6	5,898.8	5,943.4	5,946.7	5,961	6,025.0	6,052	6,057.2	1 000
100	4	=	100	8	09	20	4	11	100	61	8	4	21	20	=	100	15	100	į
Κα ₁	7	$L\alpha_2$	$L\alpha_1$	Γ_{γ_1}	Γβ1	$L\beta_{2,15}$		$\Gamma \alpha_2$	$L\alpha_1$	$L\beta_1$	$L\gamma_1$	Π	$L\beta_{2,15}$	$K\alpha_2$	$L\alpha_2$	$K\alpha_1$	$K\beta_{1,3}$	$\Gamma \alpha_1$	
23 V	62 Sm	59 Pr	59 Pr	54 Xe	57 La	56 Ba	63 Eu	PN 09	PN 09	58 Ce	55 Cs	64 Gd	57 La	24 Cr	61 Pm	24 Cr	23 V	61 Pm	4
4,952.2	4,994.5	5,013.5	5,033.7	5,034	5,042.1	5,156.5	5,177.2	5,207.7	5,230.4	5,262.2	5,280.4	5,362.1	5,383.5	5,405.5	5,408	5,414.7	5,427.3	5,432	
4	15	100	50	19	100	∞	19	4	==	100	20	~	4	Ξ	09	100	15	20	c a
=	Кβ _{1,3}	$\Gamma \alpha_1$	$K\alpha_2$	Lβ _{2.15}	$K\alpha_1$	$L\gamma_1$	$L\beta_1$	I	$L\alpha_2$	$L\alpha_1$	Lβ _{2,15}	Γγ1	I	$L\alpha_2$	$L\beta_1$	$L\alpha_1$	Кβ _{1,3}	Lβ _{2,15}	
59 Pr	21 Sc	56 Ba	22 Ti	53 I	22 Ti	52 Te	55 Cs			57 La	54 Xe	53 I	61 Pm	58 Ce	56 Ba	58 Ce	22 Ti	55 Cs	
4,453.2	4,460.5	4,466.3	4,504.9	4,507.5	4,510.8	4,570.9	4,619.8	4,633.0	4,634.2	4,651.0	4,714	4,800.9	4,809	4,823.0	4,827.5	4,840.2	4,931.8	4,935.9	10110

Table 1-3. Energies and intensities of x-ray emission lines (continued).

Energy			Relative	6,713.2	64 Gd	Lβ1	62	7,367.3	70 Yb	$L\alpha_2$	=
(eV)	Element	Line	intensity	6,719.8	67 Ho	$L\alpha_1$	100	7,387.8	74 W	Π	2
6,152	68 Er	Π	4	6,752.8	71 Lu	17	4	7,415.6	70 Yb	$L\alpha_1$	100
6,205.1	62 Sm	$L\beta_1$	19	6,843.2	63 Eu	Lβ _{2,15}	21	7,460.9	28 Ni	$K\alpha_2$	51
6,238.0	65 Tb	$L\alpha_2$	==	6,892	61 Pm	$L\gamma_1$	10	7,478.2	28 Ni	$K\alpha_1$	100
6,272.8	65 Tb	$L\alpha_1$	100	6,905.0	68 Er	$L\alpha_2$	11	7,480.3	63 Eu	$L\gamma_1$	10
6,322.1	59 Pr	$L\gamma_1$	6	6,915.3	27 Co	$K\alpha_2$	51	7,525.3	67 Ho	$L\beta_1$	64
6,339	61 Pm	$L\beta_2$	21	6,930.3	27 Co	$K\alpha_1$	100	7,603.6	75 Re	I	5
6,341.9	69 Tm	I	4	6,948.7	68 Er	$L\alpha_1$	100	7,604.9	71 Lu	$L\alpha_2$	Ξ
6,390.8	26 Fe	$K\alpha_2$	20	9.656,9	72 Hf	Π	5	7,635.7	66 Dy	Lβ ₂	20
6,403.8	26 Fe	$K\alpha_1$	100	8/6'9	65 Tb	$L\beta_1$	61	7,649.4	27 Co	$K\beta_{1,3}$	17
6,456.4	63 Eu	$L\beta_1$	62	7,058.0	26 Fe	$K\beta_{1,3}$	17	7,655.5	71 Lu	$L\alpha_1$	100
6,457.7		$L\alpha_2$	11	7,102.8	64 Gd	$L\beta_{2,15}$	21	7,785.8	64 Gd	$L\gamma_1$	Ξ
6,490.4		$K\beta_{1,3}$	17	7,133.1	MT 69	Γα2	11	7,810.9	68 Er	$L\beta_1$	64
6,495.2	66 Dy	$L\alpha_1$	100	7,173.1	73 Ta	17	5	7,822.2	76 Os	I	5
6,545.5	70 Yb	Π	4	7,178.0	62 Sm	$L\gamma_1$	10	7,844.6	72 Hf	$L\alpha_2$	Ξ
6,587.0	62 Sm	$L\beta_{2,15}$	21	7,179.9	mT 69	$L\alpha_1$	100	7,899.0	72 Hf	$L\alpha_1$	100
6,602.1	PN 09	$L\gamma_1$	10		66 Dy	$\Gamma \beta_1$	62	7,911	67 Ho	Lβ _{2,15}	20
6,679.5	67 Ho	$L\alpha_2$	11	7,366.7	65 Tb	$L\beta_{2,15}$	21	8,027.8	29 Cu	$K\alpha_2$	51

77 Ir	Π	5	8,721.0	80 Hg	I	5	9,442.3	78 Pt	$\Gamma \alpha_1$	100
nO 6	Kα	100	8,747	67 Ho	$L\gamma_1$	===	9,572.0	$30 \mathrm{Zn}$	$K\beta_{1,3}$	17
73 Ta	Loz	Ξ	8,758.8	70 Yb	Lβ _{2,15}	20	9,628.0		$L\alpha_2$	Ξ
MT 69	ΓβΊ	64	8,841.0	26 Os	$L\alpha_2$	11	9,651.8	-	Lβ ₂	20
5 Tb	Γγ	=	8,905.3	29 Cu	Кβ _{1,3}	17	9,672.4		Lβ1	29
3 Ta	Γα	100	8,911.7	•	Γα1	100	9,713.3	79 Au	$L\alpha_1$	100
58 Er	Lβ _{2.15}	20	8,953.2	81 TI	ī	9	9,780.1	70 Yb	$L\gamma_1$	12
28 Ni	Кβ _{1,3}	17	9,022.7	72 Hf	Lβ ₁	29	9,855.3	32 Ge	$K\alpha_2$	51
78 Pt		5	9,048.9	71 Lu	Lβ ₂	19	9,886.4	32 Ge	$K\alpha_1$	100
74 W	$L\alpha_2$	Ξ	680'6	68 Er	$L\gamma_1$	11	9.897.6	80 Hg	$L\alpha_2$	11
74 W	$L\alpha_1$	100	9,099.5	77 Ir	$L\alpha_2$	11	9,961.5	74 W	$L\beta_2$	21
70 Yb	Γβ1	99	9,175.1	77 Ir	$L\alpha_1$	100	8,988.8	80 Hg	$L\alpha_1$	100
56 Dy	$L\gamma_1$	11	9,184.5	82 Pb	Π	9	10,010.0	75 Re	$L\beta_1$	99
mL 69	Lβ _{2.15}	20	9,224.8	31 Ga	$K\alpha_2$	51	10,143.4	71 Lu	$L\gamma_1$	12
79 Au	Π	5	9,251.7	31 Ga	$K\alpha_1$	100	10,172.8	81 Tl	$L\alpha_2$	Ξ
75 Re	$L\alpha_2$	Ξ	9,343.1	73 Ta	L_{β_1}	29	10,260.3	31 Ga	$K\beta_3$	5
30 Zn	Kα ₂	51	9,347.3	72 Hf	$L\beta_2$	20	10,264.2	31 Ga	$K\beta_1$	99
30 Zn	$K\alpha_1$	100	9,361.8	78 Pt	$L\alpha_2$	11	10,268.5	81 TI	$L\alpha_1$	100
75 Re	$\Gamma \alpha_1$	100	9,420.4	83 Bi	コ	9	10,275.2	75 Re	$L\beta_2$	22
71 Lu	$L\beta_1$	99	9,426	mT 69	$L\gamma_1$	12	10,355.3	76 Os	$L\beta_1$	29

Table 1-3. Energies and intensities of x-ray emission lines (continued).

_			Kelative	11,420.0		71					
l	Element	Line	intensity	11,285.9	74 W	$L\gamma_1$	13	12,613.7	82 Pb	$L\beta_1$	99
10,449.5 8	82 Pb	Lα ₂	=	11,442.3	79 Au	$L\beta_1$	29	12,622.6	82 Pb	$L\beta_2$	25
10,508.0	33 As	$K\alpha_2$	51	11,584.7	79 Au	$L\beta_2$	23	12,649	36 Kr	$K\alpha_1$	100
10,515.8 7	72 Hf	$L\gamma_1$	12	11,618.3	92 U	Π	7	12,652	34 Se	$K\beta_2$	-
10,543.7 3	33 As	$K\alpha_1$	100	11,685.4	75 Re	$L\gamma_1$	13	12,809.6	90 Th	$L\alpha_2$	=
10,551.5 8	82 Pb	$\Gamma \alpha_1$	100	11,720.3	33 As	$K\beta_3$	9	12,942.0	78 Pt	$L\gamma_1$	13
10,598.5 7	sO 9/	$L\beta_2$	22	11,726.2	33 As	$K\beta_1$	13	12,968.7	90 Th	$L\alpha_1$	100
10,708.3	77 Ir	$L\beta_1$	99	11,822.6	80 Hg	$L\beta_1$	<i>L</i> 9	12,979.9	83 Bi	$L\beta_2$	25
10,730.9	83 Bi	$L\alpha_2$	11	11,864	33 As	$K\beta_2$	1	13,023.5	83 Bi	$L\beta_1$	29
10,838.8 8	83 Bi	$L\alpha_1$	100	11,877.6	35 Br	$K\alpha_2$	52	13,284.5	35 Br	$K\beta_3$	7
10,895.2	73 Ta	L_{γ_1}	12	11,924.1	80 Hg	$L\beta_2$	24	13,291.4	35 Br	$K\beta_1$	14
10,920.3 7	77 Ir	Lβ ₂	22	11,924.2	35 Br	$K\alpha_1$	100	13,335.8	37 Rb	$K\alpha_2$	52
10,978.0 3	32 Ge	$K\beta_3$	9	12,095.3	26 Os	$L\gamma_1$	13	13,381.7	79 Au	$L\gamma_1$	13
10,982.1 3	32 Ge	$K\beta_1$	09	12,213.3	81 Tl	$L\beta_1$	29	13,395.3	37 Rb	$K\alpha_1$	100
11,070.7	78 Pt	Lβ ₁	29	12,271.5	81 TI	$L\beta_2$	25	13,438.8	92 U	$L\alpha_2$	Ξ
11,118.6	90 Th	ī	9	12,489.6	34 Se	Kβ ₃	9	13,469.5	35 Br	$K\beta_2$	1
11,181.4 3	34 Se	$K\alpha_2$	52	12,495.9	34 Se	$K\beta_1$	13	13,614.7	92 U	$L\alpha_l$	100
11,222.4 3	34 Se	$K\alpha_1$	100	12,512.6	77 Ir	$L\gamma_1$	13	13,830.1	80 Hg	$L\gamma_1$	14

23	100	∞	15	3	53	15	100	∞	16	4	53	100	∞	16	53	4	100	∞
$K\alpha_2$	$K\alpha_{l}$	$K\beta_3$	$K\beta_1$	$K\beta_2$	$K\alpha_2$	$L\gamma_1$	$K\alpha_1$	$K\beta_3$	$K\beta_1$	$K\beta_2$	$K\alpha_2$	$K\alpha_{1} \\$	$K\beta_3$	$K\beta_1$	$K\alpha_2$	$K\beta_2$	$K\alpha_1$	Kβ,
44 Ru	44 Ru	42 Mo	42 Mo	42 Mo	45 Rh	92 U	45 Rh	43 Tc	43 Tc	43 Tc	46 Pd	46 Pd	44 Ru	44 Ru	47 Ag	44 Ru	47 Ag	45 Rh
19,150.4	19,279.2	19,590.3	19,608.3	19,965.2	20,073.7	20,167.1	20,216.1	20,599	20,619	21,005	21,020.1	21,177.1	21,634.6	21,656.8	21,990.3	22,074	22,162.9	22,698.9
69	26	52	100	∞	15	33	61	52	100	∞	15	33	53	100	∞	15	33	16
Γβ ₁	$L\beta_2$	$K\alpha_2$	$K\alpha_1$	$K\beta_3$	$K\beta_1$	Kβ ₂	$L\beta_1$	$K\alpha_2$	$K\alpha_1$	$K\beta_3$	$K\beta_1$	$K\beta_2$	$K\alpha_2$	$K\alpha_1$	$K\beta_3$	$K\beta_1$	$K\beta_2$	Γγ
90 Th	92 U	41 Nb	41 Nb	39 Y	39 Y	39 Y	92 U	42 Mo	42 Mo	40 Zr	40 Zr	40 Zr	43 Tc	43 Tc	41 Nb	41 Nb	41 Nb	90 Th
16,202.2	16,428.3	16,521.0	16,615.1	16,725.8	16,737.8	17,015.4	17,220.0	17,374.3	17,479.3	17,654	17,667.8	17,970	18,250.8	18,367.1	18,606.3	18,622.5	18,953	18,982.5
52	7	14	100	14	2	14	52	7	100	14	2	14	26	52	100	7	14	3
$K\alpha_2$	$K\beta_3$	Кβ	$K\alpha_1$	$L\gamma_1$	$K\beta_2$	$L\gamma_1$	$K\alpha_2$	Kβ3	$K\alpha_1$	Kβ1	$K\beta_2$	$L\gamma_1$	$L\beta_2$	$K\alpha_2$	$K\alpha_1$	Кβз	$K\beta_1$	Kβ,
38 Sr	36 Kr	36 Kr	38 Sr	81 TI	36 Kr	82 Pb	39 Y	37 Rb	39 Y	37 Rb	37 Rb	83 Bi	90 Th	40 Zr	40 Zr	38 Sr	38 Sr	38 Sr
14,097.9	14,104	14,112	14,165.0	14,291.5	14,315	14,764.4	14,882.9	14,951.7	14,958.4	14,961.3	15,185	15,247.7	15,623.7	15,690.9	15,775.1	15,824.9	15,835.7	16,084.6

Table 1-3. Energies and intensities of x-ray emission lines (continued).

Energy				102070	51 Ch	Va	100	20 072 9	55 Ce	Ko.	100
3			Relative	7.655,07	00.10	1704	100	90,276,00)	134	100
(eV)	Element	Line	intensity	26,643.8	48 Cd	$K\beta_2$	4	30,995.7	52 Te	$K\beta_1$	18
22,723.6	45 Rh	$K\beta_1$	16	27,201.7	52 Te	$K\alpha_2$	54	31,700.4	52 Te	$K\beta_2$	5
22,984.1	48 Cd	$K\alpha_2$	53	27,237.7	49 In	$K\beta_3$	6	31,817.1	56 Ba	$K\alpha_2$	54
23,172.8	45 Rh	$K\beta_2$	4	27,275.9	49 In	$K\beta_1$	17	32,193.6	56 Ba	$K\alpha_1$	100
23,173.6	48 Cd	$K\alpha_1$	100	27,472.3	52 Te	$K\alpha_1$	100	32,239.4	53 I	$K\beta_3$	6
23,791.1	46 Pd	$K\beta_3$	∞	27,860.8	49 In	$K\beta_2$	2	32,294.7	53 I	$K\beta_1$	18
23,818.7	46 Pd	$K\beta_1$	16	28,317.2	53 I	$K\alpha_2$	54	33,034.1	57 La	$K\alpha_2$	54
24,002.0	49 In	$K\alpha_2$	53	28,444.0	50 Sn	Kβ3	6		53 I	$K\beta_2$	S
24,209.7	49 In	$K\alpha_1$	100	28,486.0	50 Sn	$K\beta_1$	17		57 La	$K\alpha_1$	100
24,299.1	46 Pd	$K\beta_2$	4	28,612.0	53 I	$K\alpha_1$	100	33,562	54 Xe	$K\beta_3$	6
24,911.5	47 Ag	Kβ ₃	6	29,109.3	50 Sn	$K\beta_2$	5	33,624		$K\beta_1$	18
24,942.4	47 Ag	$K\beta_1$	16	29,458	54 Xe	$K\alpha_2$	54	34,278.9		$K\alpha_2$	55
25,044.0	50 Sn	$K\alpha_2$	53	29,679.2	51 Sb	$K\beta_3$	6	34,415	54 Xe	$K\beta_2$	5
25,271.3	50 Sn	$K\alpha_1$	100	29,725.6	51 Sb	$K\beta_1$	18	34,719.7	58 Ce	$K\alpha_1$	100
25,456.4	47 Ag	$K\beta_2$	4	29,779	54 Xe	$K\alpha_1$	100	34,919.4	55 Cs	Kβ ₃	6
26,061.2	48 Cd	Kβ ₃	6	30,389.5	51 Sb	$K\beta_2$	5	34,986.9	55 Cs	$K\beta_1$	18
26,095.5	48 Cd	$K\beta_1$	17	30,625.1	55 Cs	$K\alpha_2$	54	35,550.2	59 Pr	$K\alpha_2$	55
26,110.8	51 Sb	$K\alpha_2$	54	30,944.3	52 Te	$K\beta_3$	6	35,822	55 Cs	$K\beta_2$	9

$K\beta_1$ 19	$K\alpha_1$ 100	$K\alpha_2$ 56	Kβ ₂ 6	Kβ ₃ 10	$K\beta_1$ 20	$K\alpha_1$ 100	$K\alpha_2$ 57	Κβ ₂ 7	Кβ ₃ 10	$K\beta_1$ 20	$K\alpha_1$ 100	$K\alpha_2$ 57	Κβ ₂ 7	Кβ ₃ 10	$K\beta_1$ 20	$K\alpha_1$ 100	Kα ₂ 57	7 2
63 Eu	67 Ho	68 Er	63 Eu	64 Gd	64 Gd	68 Er	mT 69	64 Gd	65 Tb	65 Tb	mT 69	70 Yb	65 Tb	66 Dy	66 Dy	70 Yb	71 Lu	U 77
47,037.9	47,546.7	48,221.1	48,256	48,555	48,697	49,127.7	49,772.6	49,959	50,229	50,382	50,741.6	51,354.0	51,698	51,957	52,119	52,388.9	52,965.0	271.53
100	9	10	19	99	100	9	10	99	19	100	9	99	10	19	100	9	99	10
$K\alpha_1$	$K\beta_2$	$K\beta_3$	$K\beta_1$	$K\alpha_2$	$K\alpha_1$	$K\beta_2$	$K\beta_3$	$K\alpha_2$	$K\beta_1$	$K\alpha_1$	$K\beta_2$	$K\alpha_2$	Kβ ₃	$K\beta_1$	$K\alpha_1$	$K\beta_2$	$K\alpha_2$	77.0
63 Eu	59 Pr	PN 09	PN 09	64 Gd	64 Gd	PN 09	61 Pm	65 Tb	61 Pm	65 Tb	61 Pm	66 Dy	62 Sm	62 Sm	66 Dy	62 Sm	67 Ho	62 E.
41,542.2	41,773	42,166.5	42,271.3	42,308.9	42,996.2	43,335	43,713	43,744.1	43,826	44,481.6	44,942	45,207.8	45,289	45,413	45,998.4	46,578	46,699.7	2 600 24
100	10	18	55	9	100	10	19	55	100	9	10	19	55	100	9	10	19	73
$K\alpha_1$	Kβ3	$K\beta_1$	$K\alpha_2$	$K\beta_2$	$K\alpha_1$	Kβ ₃	$K\beta_1$	$K\alpha_2$	$K\alpha_1$	$K\beta_2$	$K\beta_3$	$K\beta_1$	$K\alpha_2$	$K\alpha_1$	$K\beta_2$	Kβ3	$K\beta_1$	N~
59 Pr	56 Ba	56 Ba	PN 09	56 Ba	PN 09	57 La	57 La	61 Pm	61 Pm	57 La	58 Ce	58 Ce	62 Sm	62 Sm	58 Ce	59 Pr	59 Pr	63 En
36,026.3	36,304.0	36,378.2	36,847.4	37,257	37,361.0	37,720.2	37,801.0	38,171.2	38,724.7	38,729.9	39,170.1	39,257.3	39,522.4	40,118.1	40,233	40,652.9	40,748.2	40 901 9

Table 1-3. Energies and intensities of x-ray emission lines (continued).

Energy			Relative	59,370	70 Yb	Kβ ₁	21	66,989.5	79 Au	$K\alpha_2$	59
(eV)	Element	Line	intensity	59,717.9		$K\alpha_2$	28	066,990	73 Ta	$K\beta_2$	7
53,711	67 Ho	Kβ3	=	086'09		$K\beta_2$	7	67,244.3	74 W	$K\beta_1$	22
53,877	67 Ho	$K\beta_1$	20	61,050	71 Lu	Kβ3	11	68,803.7	79 Au	$K\alpha_1$	100
54,069.8	71 Lu	$K\alpha_1$	100	61,140.3	75 Re	$K\alpha_1$	100	68,895	80 Hg	$K\alpha_2$	59
54,611.4	72 Hf	$K\alpha_2$	57	61,283	71 Lu	$K\beta_1$	21	68,994	75 Re	$K\beta_3$	12
55,293	67 Ho	$K\beta_2$	7	61,486.7	76 Os	$K\alpha_2$	58	290,69	74 W	$K\beta_2$	∞
55,494	68 Er	$K\beta_3$	11	62,970	71 Lu	$K\beta_2$	7	69,310	75 Re	$K\beta_1$	22
55,681	68 Er	$K\beta_1$	21	62,980	72 Hf	Κβ3	=	70,819	80 Hg	$K\alpha_1$	100
55,790.2	72 Hf	$K\alpha_1$	100	63,000.5	76 Os	$K\alpha_1$	100	70,831.9	81 TI	$K\alpha_2$	09
56,277	73 Ta	$K\alpha_2$	57	63,234	72 Hf	$K\beta_1$	22	71,077	76 Os	$K\beta_3$	12
57,210	68 Er	$K\beta_2$	7	63,286.7	77 Ir	$K\alpha_2$	58	71,232	75 Re	$K\beta_2$	∞
57,304	mT 69	$K\beta_3$	11	64,895.6	77 Ir	$K\alpha_1$	100	71,413	76 Os	$K\beta_1$	23
57,517	mL 69	$K\beta_1$	21	64,948.8	73 Ta	$K\beta_3$	=	72,804.2	82 Pb	$K\alpha_2$	09
57,532	73 Ta	$K\alpha_1$	100	64,980	72 Hf	Kβ ₂	7	72,871.5	81 Tl	$K\alpha_1$	100
57,981.7	74 W	$K\alpha_2$	28	65,112	78 Pt	$K\alpha_2$	58	73,202.7	77 Ir	$K\beta_3$	12
29,090	mL 69	$K\beta_2$	7	65,223	73 Ta	$K\beta_1$	22	73,363	76 Os	$K\beta_2$	∞
59,140	70 Yb	$K\beta_3$	11	66,832	78 Pt	$K\alpha_1$	100	73,560.8	77 Ir	$K\beta_1$	23
59,318.2	74 W	$K\alpha_1$	100	66,951.4	74 W	$K\beta_3$	11	74,814.8	83 Bi	$K\alpha_2$	09

,969.4	82 PB	KO.	100	87,118	81 11	мр ₃	71	66,68	30 III	NO ₂	70
368	78 Pt	$K\beta_3$	12	82,515	80 Hg	Kβ ₂	8	93,350	90 Th	$K\alpha_1$	100
,575	77 Ir	$K\beta_2$	8	82,576	81 TI	$K\beta_1$	23	94,665	92 U	$K\alpha_2$	62
,748	78 Pt	Kβ ₁	23	84,450	82 Pb	Kβ3	12	98,439	92 U	$K\alpha_1$	100
,107.9	83 Bi	$K\alpha_1$	100	84,910	81 TI	Kβ ₂	∞	104,831	90 Th	$K\beta_3$	12
,580	79 Au	Kβ ₃	12	84,936	82 Pb	$K\beta_1$	23	105,609	90 Th	$K\beta_1$	24
77,850	78 Pt	$K\beta_2$	~	86,834	83 Bi	Kβ ₃	12	108,640	90 Th	$K\beta_2$	6
,984	79 Au	$K\beta_1$	23	87,320	82 Pb	$K\beta_2$	8	110,406	92 U	$K\beta_3$	13
,822	80 Hg	Kβ ₃	12	87,343	83 Bi	$K\beta_1$	23	111,300	92 U	$K\beta_1$	24
,150	79 Au	$K\beta_2$	8	89,830	83 Bi	$K\beta_2$	6	114,530	92 U	$K\beta_2$	6
.253	80 Hg	KB,	23								

1.3 FLUORESCENCE YIELDS FOR K, L, AND M SHELLS

Jeffrey B. Kortright

Fluorescence yields for the K, L, and M shells for the elements $3 \le Z \le 110$ are plotted in Fig. 1-2. The data are based on Ref. 1 for $Z \le 100$, and on Ref. 2 for Z > 100 for K and L shells. These yields represent the probability of a core hole in the K or L shells being filled by a radiative process, in competition with nonradiative processes. Auger processes are the only nonradiative processes competing with fluorescence for the K shell and

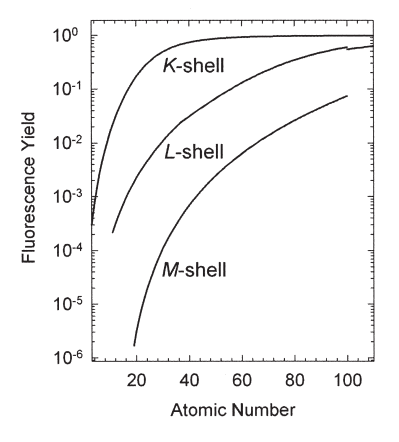


Fig. 1-2. Fluorescence yields for K, L, and M shells for $3 \le Z \le 110$. The plotted curves for the L and M shells represent average subshell effective yields.

 L_3 subshell holes. Auger and Coster-Kronig nonradiative processes complete with fluorescence to fill L_1 and L_2 subshell holes. Only one curve is presented for the three L subshells, representing the average of the L_1 , L_2 , and L_3 effective fluorescence yields. Likewise the M shell curve represents and average over subshells. See Refs. 1 and 2 for details and citations to the theoretical and experimental work upon which Fig. 1-2 is based. Widths of K and L fluorescence lines can be found in Ref. 3.

- J. H. Hubbell, P. N. Trehan, N. Singh, B. Chand, D. Mehta, M. L. Garg, R. R. Garg, S. Singh, and S. Puri, "A Review, Bibliography, and Tabulation of K, L, and Higher Atomic Shell X-Ray Fluorescence Yields," J. Phys. Chem. Ref. Data 23, 339 (1994).
- M. O. Krause, "Atomic Radiative and Radiationless Yields for K and L Shells," J. Phys. Chem. Ref. Data 8, 307 (1979).
- M. O. Krause and J. H. Oliver, "Natural Widths of Atomic K and L Levels, Ka X-Ray Lines and Several KLL Auger Lines," J. Phys. Chem. Ref. Data 8, 329 (1979).

1.4 PRINCIPAL AUGER ELECTRON ENERGIES

Figure 1-3 has been reproduced by permission of Physical Electronics, Inc., and is taken from Ref. 1. For each element, dots indicate the energies of principal Auger peaks, the predominant ones represented by the heavier dots. The families of Auger transitions are denoted by labels of the form WXY, where W is the shell in which the original vacancy occurs, X is the shell from which the W vacancy is filled, and Y is the shell from which the Auger electron is ejected. The listed references should be consulted for detailed tabulations and for shifted values in several common compounds.

- K. D. Childs, B. A. Carlson, L. A. Vanier, J. F. Moulder, D. F. Paul, W. F. Stickle, and D. G. Watson, in C. L. Hedberg, Ed., Handbook of Auger Electron Spectroscopy (Physical Electronics, Eden Prairie, MN, 1995).
- J. F. Moulder, W. F. Stickle, P. E. Sobol, and K. D. Bomben, Handbook of X-Ray Photoelectron Spectroscopy (Physical Electronics, Eden Prairie, MN, 1995).
- 3. D. Briggs, *Handbook of X-Ray and Ultraviolet Photoelectron Spectroscopy* (Heyden, London, 1977).

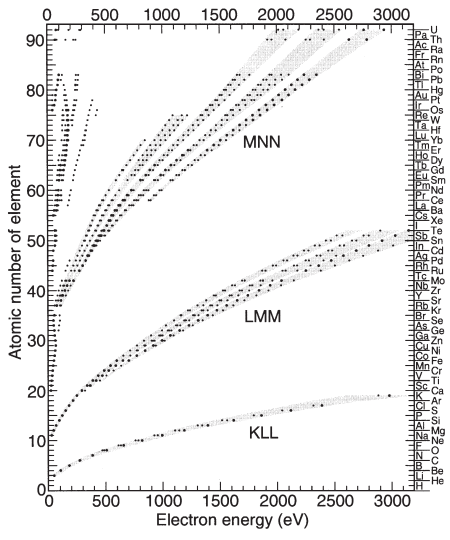


Fig. 1-3. Auger electron energies for the elements. Points indicate the electron energies of the principal Auger peaks for each element. The larger points represent the most intense peaks. (Reproduced by permission of Physical Electronics, Inc.)

1.5 SUBSHELL PHOTOIONIZATION CROSS SECTIONS

Ingolf Lindau

The atomic subshell photoemission cross sections plotted in Fig. 1-4 have been calculated for isolated atoms by Yeh and Lindau [1,2]. The calculations were done with a one-electron central-field frozen-core model using first-order perturbation theory. No single model accurately predicts the photoionization process of all orbitals for all elements from the VUV to 1.5 keV. The complexity of the physics of different atomic orbitals makes it impossible for any single rule to describe all of them. The accuracy of the model used has been discussed in detail by Cooper and Manson [3–5].

- J.-J. Yeh and I. Lindau, "Atomic Subshell Photoionization Cross Sections and Asymmetry Parameters: 1 < Z < 103," At. Data Nucl. Data Tables 32, 1 (1985).
- J.-J. Yeh, Atomic Calculations of Photoionization Cross Sections and Asymmetry Parameters (Gordon and Breach, Langhorne, PA, 1993).
- 3. J. W. Cooper, Phys. Rev. 128, 681 (1962).
- S. T. Manson and J. W. Cooper, *Phys. Rev.* 165, 126 (1968).
- S. T. Manson, Adv. Electron. Electron Phys. 41, 73 (1976).

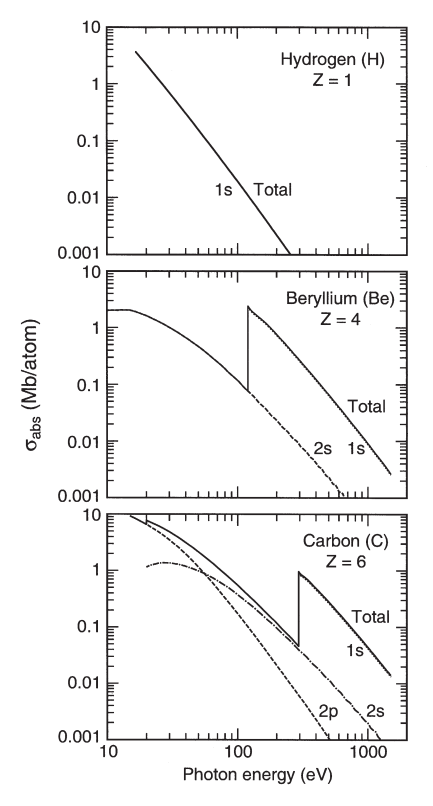


Fig. 1-4. Plots of atomic subshell photoemission cross sections, calculated for isolated atoms.

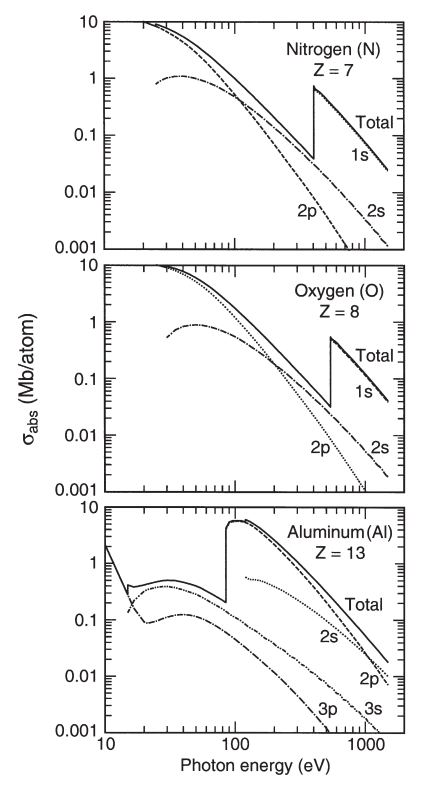


Fig. 1-4. Subshell photoemission cross sections (continued).

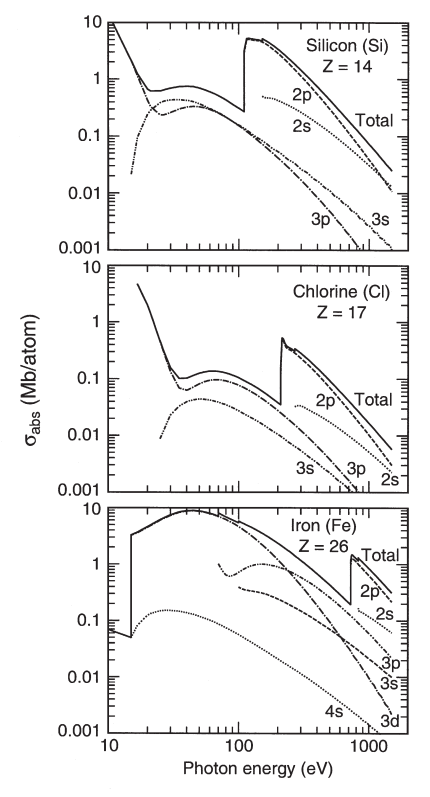


Fig. 1-4. Subshell photoemission cross sections (continued).

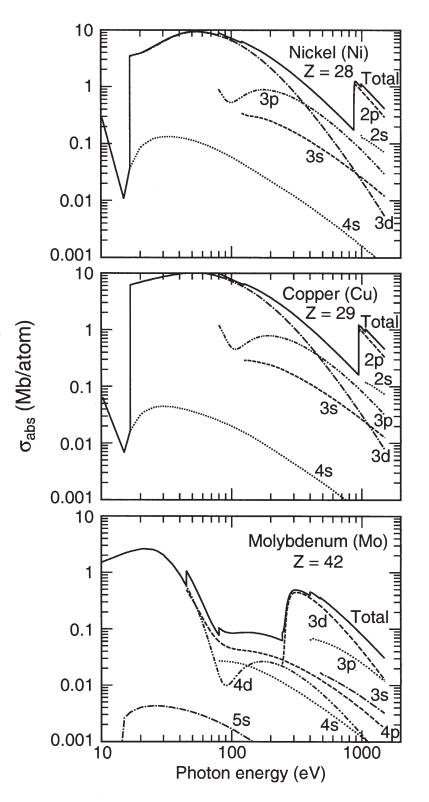


Fig. 1-4. Subshell photoemission cross sections (continued).

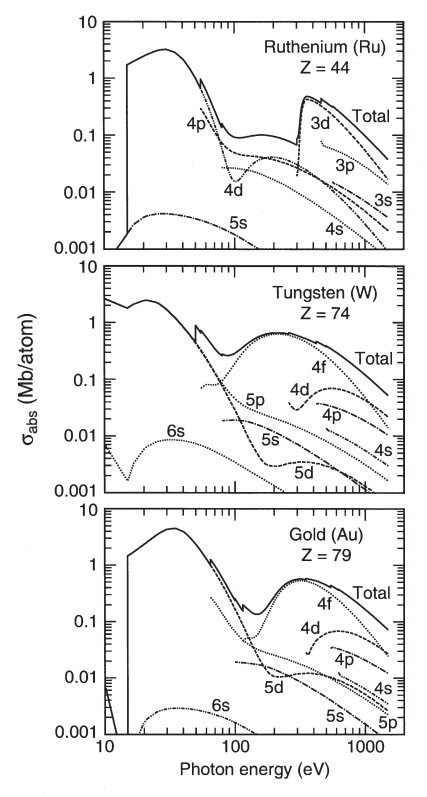


Fig. 1-4. Subshell photoemission cross sections (continued).

1.6 MASS ABSORPTION COEFFICIENTS

Eric M. Gullikson

Mass absorption coefficients have been tabulated for elements $Z \le 92$, based on both measured values and theoretical calculations [see B. L. Henke, E. M. Gullikson, and J. C. Davis, "X-Ray Interactions: Photoabsorption, Scattering, Transmission, and Reflection at E = 50-30,000 eV, Z = 1-92," At. Data Nucl. Data Tables 54, 181 (1993); for updated values, see http://www.cxro.lbl.gov/optical_constants/]. The mass absorption coefficient μ (cm²/g) is related to the transmitted intensity through a material of density ρ (g/cm³) and thickness d by

$$I = I_0 e^{-\mu \rho d} \qquad . \tag{1}$$

Thus, the linear absorption coefficient is μ_ℓ (cm⁻¹) = $\mu\rho$. For a pure material, the mass absorption coefficient is directly related to the total atomic absorption cross section σ_a (cm²/atom) by

$$\mu = \frac{N_{\rm A}}{A} \sigma_{\rm a} \quad , \tag{2}$$

where N_A is Avogadro's number and A is the atomic weight. For a compound material, the mass absorption coefficient is obtained from the sum of the absorption cross sections of the constituent atoms by

$$\mu = \frac{N_{\rm A}}{MW} \sum_{i} x_i \sigma_{ai} \quad , \tag{3}$$

where the molecular weight of a compound containing x_i atoms of type i is $MW = \sum_i x_i A_i$. This approximation, which neglects interactions among the atoms in the material, is generally applicable for photon energies above about 30 eV and sufficiently far from absorption edges.

In Fig. 1-5, the mass absorption coefficient is plotted for 15 elements over the photon energy range 10–30,000 eV. In much of this range, the absorption coefficient is dominated by photoabsorption. However, for H, Be, C, N, and O, Compton (inelastic) scattering is significant at the higher energies. In these cases, the total cross section is shown as a solid curve and the photoabsorption cross section as a separate dashed curve.

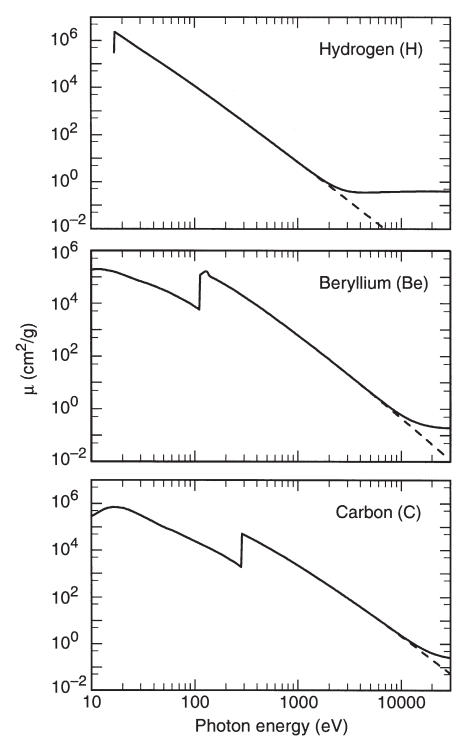


Fig. 1-5. Plots of mass absorption coefficients for several elements in their natural forms. For H, Be, C, N, and O, the photoabsorption cross section is shown as a dashed curve.

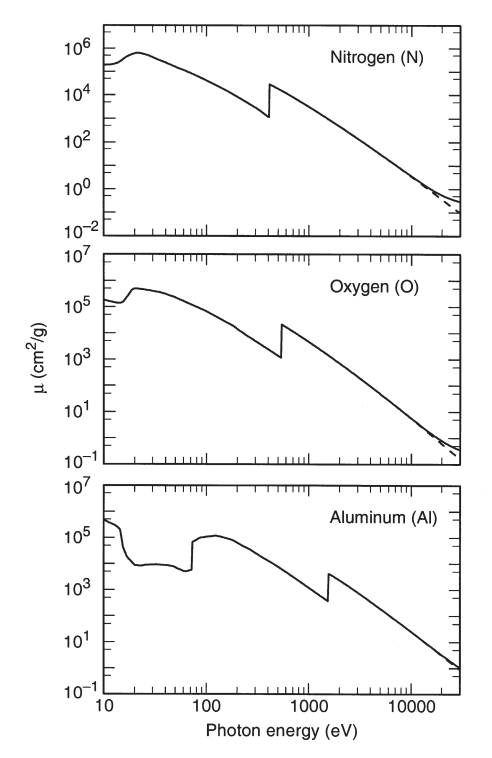


Fig. 1-5. Mass absorption coefficients (continued).

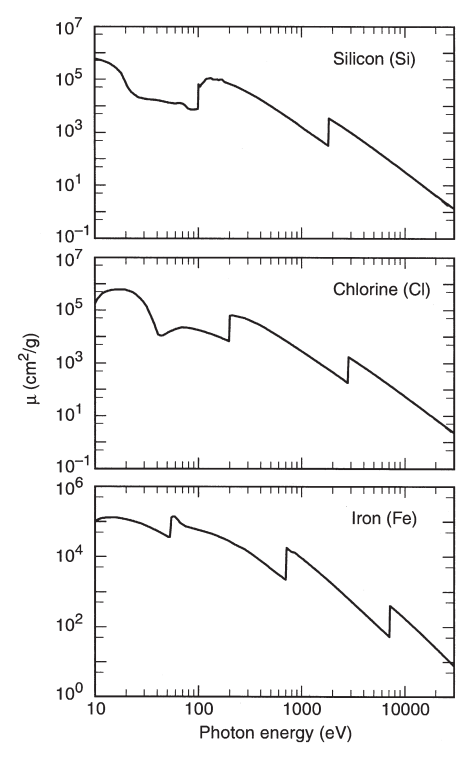


Fig. 1-5. Mass absorption coefficients (continued).

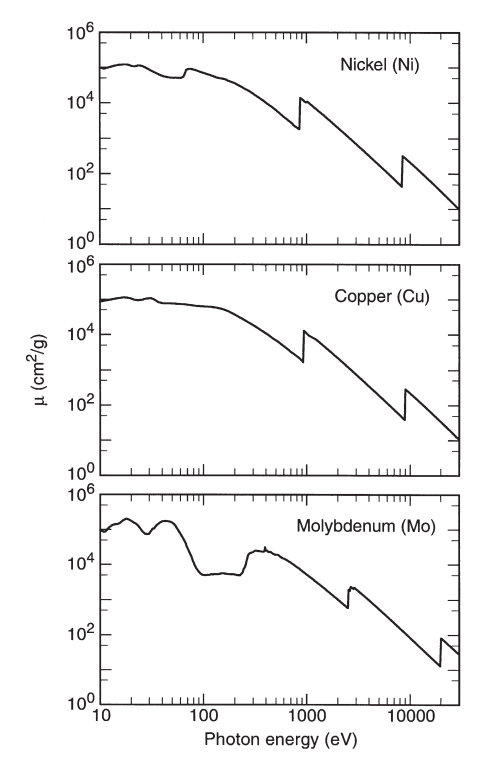


Fig. 1-5. Mass absorption coefficients (continued).

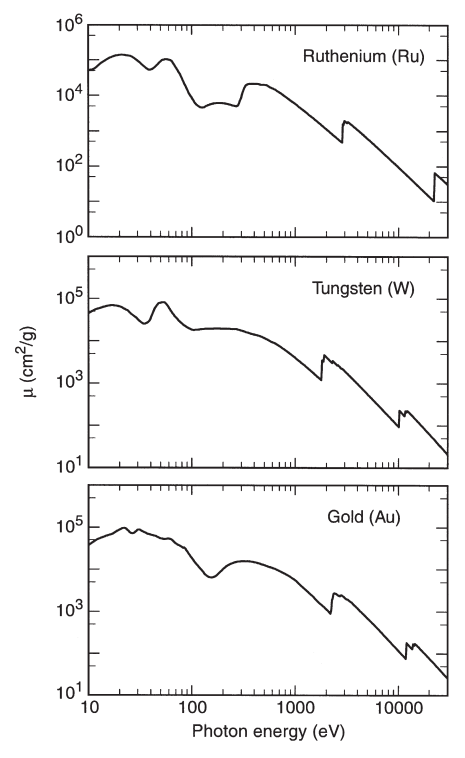


Fig. 1-5. Mass absorption coefficients (continued).

1.7 ATOMIC SCATTERING FACTORS

Eric M. Gullikson

The optical properties of materials in the photon energy range above about 30 eV can be described by the atomic scattering factors. The index of refraction of a material is related to the scattering factors of the individual atoms by

$$n = 1 - \delta - i\beta = 1 - \frac{r_e}{2\pi} \lambda^2 \sum_i n_i f_i(0)$$
 , (1)

where r_e is the classical electron radius, λ is the wavelength, and n_i is the number of atoms of type i per unit volume. The parameters δ and β are called the refractive index decrement and the absorption index, respectively. The complex atomic scattering factor for the forward scattering direction is

$$f(0) = f_1 + if_2$$
 (2)

The imaginary part is derived from the atomic photoabsorption cross section:

$$f_2 = \frac{\sigma_a}{2r_e\lambda} \quad . \tag{3}$$

The real part of the atomic scattering factor is related to the imaginary part by the Kramers-Kronig dispersion relation:

$$f_1 = Z^* + \frac{1}{\pi r_e hc} \int_0^\infty \frac{\varepsilon^2 \sigma_{\rm a}(\varepsilon)}{E^2 - \varepsilon^2} d\varepsilon \qquad . \tag{4}$$

In the high-photon-energy limit, f_1 approaches Z^* , which differs from the atomic number Z by a small relativistic correction:

$$Z^* \approx Z - (Z/82.5)^{2.37}$$
 (5)

On the following pages, Fig. 1-6 presents the scattering factors for 15 elements in their natural forms. Complete tables are given in B. L. Henke, E. M. Gullikson, and J. C. Davis, "X-Ray Interactions: Photoabsorption, Scattering, Transmission, and Reflection at E = 50 - 30,000 eV, Z = 1 - 92," At. Data Nucl. Data Tables 54, 181 (1993).

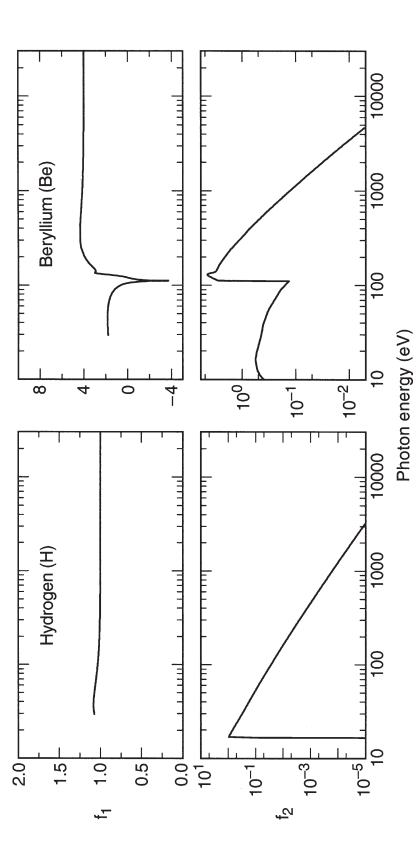


Fig. 1-6. Plots of scattering factors for several elements in their natural forms.

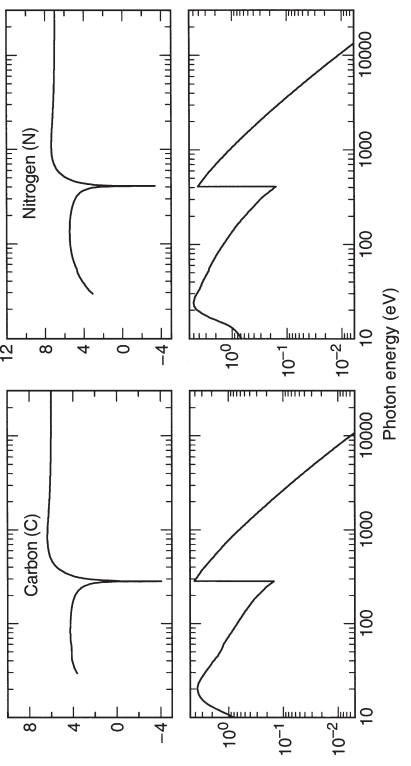
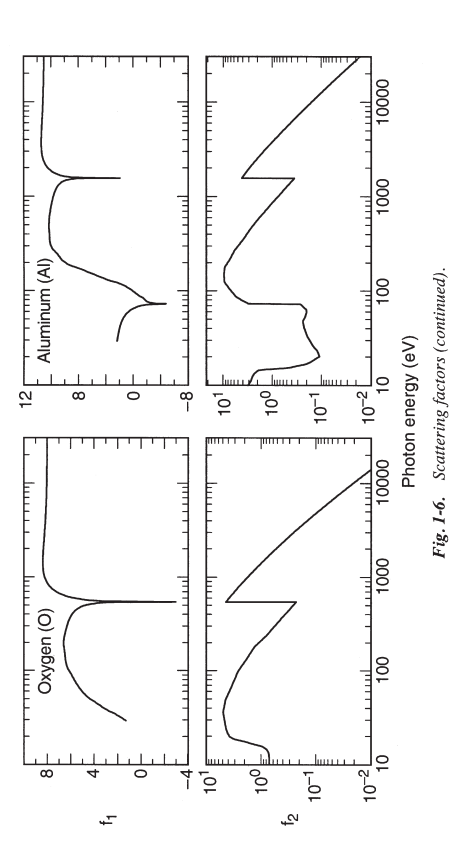


Fig. 1-6. Scattering factors (continued).



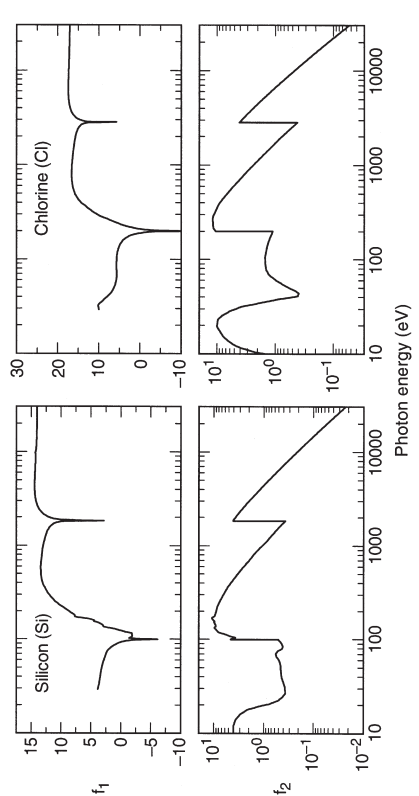
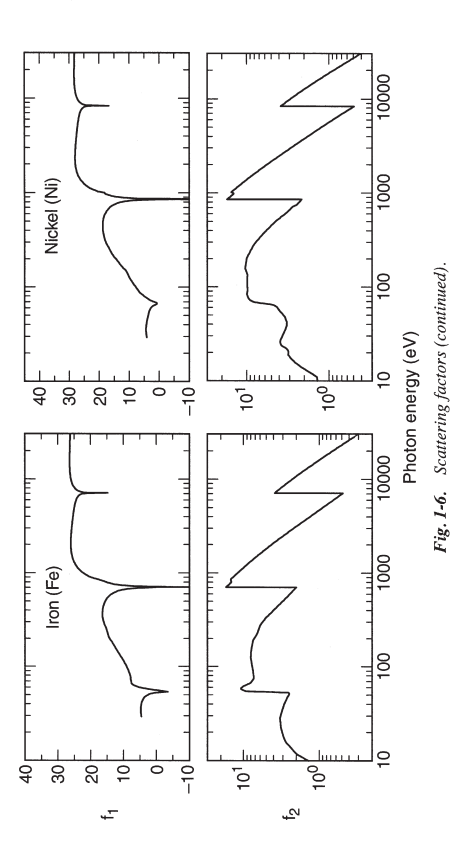


Fig. 1-6. Scattering factors (continued).



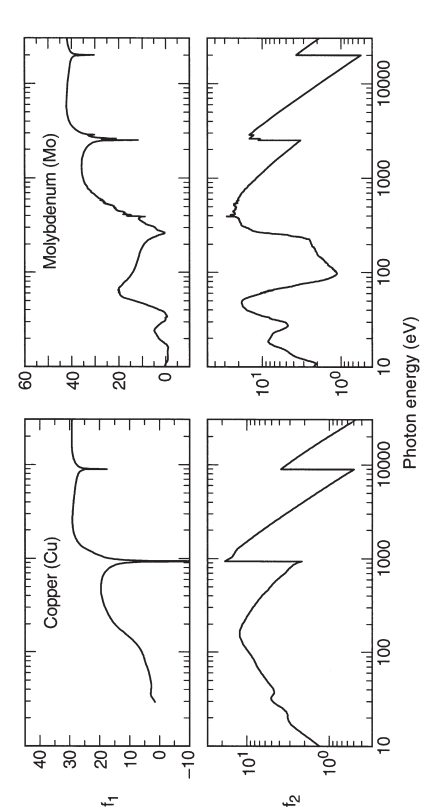
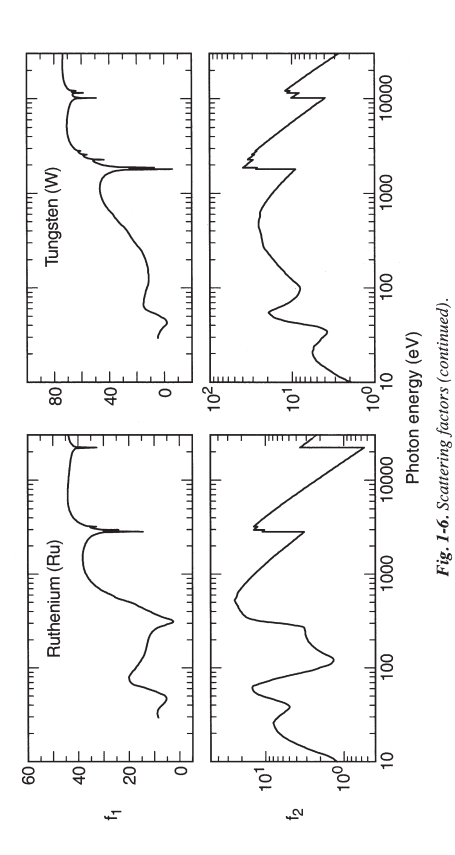


Fig. 1-6. Scattering factors (continued).



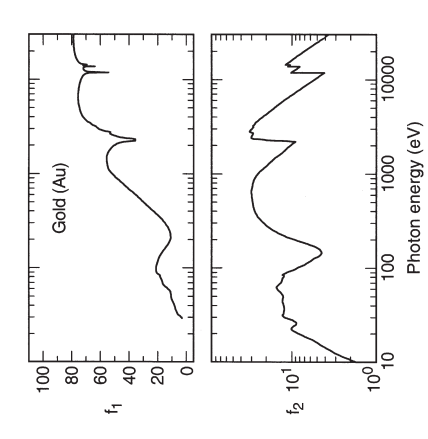


Fig. 1-6. Scattering factors (continued).

1.8 ENERGY LEVELS OF FEW-ELECTRON IONIC SPECIES

James H. Scofield

Table 1-4 presents ionization energies for selected few-electron ions with $6 \le Z \le 54$. Table 1-5 gives the energies of the resonant 2p transitions in hydrogen- and heliumlike ions. The energy values in this section have been generated using the relativistic Hartree-Fock code of I. P. Grant and collaborators [1] with a correction term of the form A + B/(Z - O) added to bring about agreement with the experimental values known for low atomic numbers. Nuclear size effects, radiative corrections, and the Breit interaction accounting for retardation and the magnetic electron-electron interaction are included in the calculations. The hydrogenic values are uncorrected as they come from the code, but to the accuracy given here, they agree with more detailed calculations. The values in Table 1-4 for Co-, Ni-, and Cu-like ions are based on data from C. E. Moore [2], J. Sugar and A. Musgrove [3], and others referenced therein.

- I. P. Grant, B. J. McKenzie, P. H. Norrington, D. F. Mayers, and N. C. Pyper, "An Atomic Multiconfigurational Dirac-Fock Package," Comput. Phys. Commun. 21, 207 (1980).
- C. E. Moore, Ionization Potentials and Ionization Limits Derived from the Analysis of Optical Spectra, NBS Pub. NSRDS-NBS 34 (1970).
- J. Sugar and A. Musgrove, "Energy Levels of Zinc, Zn I through Zn XXX," J. Phys. Chem. Ref. Data 24, 1803 (1995).

with the number of electrons in the ion before ionization and with the symbol for the neutral atom with Ionization energies, in electron volts, for selected few-electron ionic species. Each column is labeled the same number of electrons. Table 1-4.

Element	1 (H)	2 (He)	3 (Li)	4 (Be)	10 (Ne)	11 (Na)	12 (Mg)	27 (Co)	28 (Ni)	29 (Cu)
29	490.0	392.1	64.49	47.89						
7 N	667.1	552.1	97.89	77.48						
80	871.4	739.3	138.11	113.90						
9 F	1103.1	953.9	185.18	157.15						
10 Ne	1362.2	1195.8	239.09	207.26	21.564					
11 Na	1648.7	1465.1	299.86	264.21	47.286	5.139				
12 Mg	1962.7	1761.8	367.5	328.0	80.143	15.035	7.646			
13 AI	2304.2	2086.0	442.0	398.7	119.99	28.447	18.828			
14 Si	2673.2	2437.7	523.4	476.3	166.42	45.12	33.64			
15 P	3070	2816.9	611.7	8.099	220.31	65.02	51.50			
16 S	3494	3224	707.0	652.1	281.00	88.05	72.59			
17 CI	3946	3658	809.2	750.5	348.5	114.20	96.84			
18 Ar	4426	4121	918.4	855.8	422.8	143.46	124.24			
19 K	4934	4611	1034.6	0.896	503.9	175.82	154.75			
20 Ca	5470	5129	1157.7	1087.3	591.9	211.28	188.38			
21 Sc	6034	5675	1288.0	1213.6	9.989	249.84	225.13			
22 Ti	9626	6249	1425.3	1346.9	788.2	291.50	264.98			
23 V	7246	6851	1569.7	1487.3	9.968	336.3	307.9			
24 Cr	7895	7482	1721.2	1634.8	1011.8	384.2	354.0			
25 Mn	8572	8141	1879.9	1789.5	1133.8	435.2	403.2			
26 Fe	9278	8828	2045.8	1951.3	1262.7	489.3	455.6			

	7.73	17.96	30.7	45.72	62.3	81.7	103.0	125.9	150.7	177.3	205.9	236.2	268.5	302.6	338.5	376.3	416.0	457.5	500.9	546.2	593.3	642.3	693.2	746.1	800.8	857.4
į	20.70	39.72	63.4	90.5	121.2	155.4	192.8	233.4	277.1	324.1	374.0	427.4	483.8	541.7	8.509	671.4	740.1	811.8	9.988	964.5	1045.4	1129.1	1215.3	1306.3	1399.3	1495.4
7.86	18.17	59.57	86.0	115.9	149.2	185.5	225.4	268.2	314.2	363.3	413.6	471	530	592	929	724	795	698	946	1026	1109	1196	1285	1377	1472	1571
511.0	631.4	696.4	764.5	835.8	910.3	988.1	1069.1	1153.3	1240.8	1331.5	1425.6	1523.0	1623.7	1727.8	1835.2	1946.1	2060.3	2178.0	2299.2	2423.9	2552.1	2683.9	2819.2	2958.1	3101	3247
546.6	0700	737.3	807.3	880.4	8296	1036.3	1119.1	1205.2	1294.5	1387.2	1483.1	1582.4	1684.9	1790.9	1900.3	2013.0	2129.2	2248.9	2372.0	2498.6	2628.8	2762.5	2899.8	3041	3185	3334
1398.3	1690.2	1846.4	2009.4	2179.3	2356.0	2539.6	2730.1	2927.4	3132	3343	3561	3786	4017	4256	4502	4754	5014	5280	5553	5834	6121	6415	6717	7025	7340	7663
2120.4	2480.7	2671.1	2869.4	3075	3288	3509	3737	3973	4216	4467	4726	4993	5268	5550	5841	6140	6447	6762	7086	7418	7758	8107	8465	8832	9207	1656
2218.9	2587.0	2782.0	2984.4	3194	3412	3637	3869	4109	4357	4612	4876	5147	5426	5713	8009	6312	6623	6943	7271	2097	7953	8307	8670	9041	9421	9810
9544	11063	11865	12696	13557	14448	15367	16317	17296	18306	19345	20415	21516	22648	23810	25004	26230	27487	28776	30097	31451	32837	34257	35710	37196	38716	40271
10012	11568	12389	13239	14119	15029	15968	16937	17936	18965	20025	21115	22237	23389	24572	25787	27033	28312	29623	30966	32341	33750	35192	36668	38177	39721	41300
27 Co	29 Cu	30 Zn	31 Ga	32 Ge	33 As	34 Se	35 Br	36 Kr	37 Rb	38 Sr	39 Y	40 Zr	41 Nb	42 Mo	43 Tc	44 Ru	45 Rh	46 Pd	47 Ag	48 Cd	49 In	50 Sn	51 Sb	52 Te	53 I	54 Xe

Table 1-5. Transition energies, in electron volts, for transitions from the n=2 states to the n=1 ground state of H- and He-like ions.

5 B 6 C 7 N 8 O 9 F 10 Ne 11 Na	2p _{1/2} 255.17 367.5 500.3 653.5 827.3 1021.5	2p _{3/2} 255.20 367.5 500.4 653.7	2p ³ P ₁ 202.78 304.3	2p ¹ P ₁ 205.37
6 C 7 N 8 O 9 F 10 Ne	367.5 500.3 653.5 827.3	367.5 500.4	304.3	
7 N 8 O 9 F 10 Ne	500.3 653.5 827.3	500.4		
8 O 9 F 10 Ne	653.5 827.3			307.8
9 F 10 Ne	827.3	653.7	426.3	430.7
10 Ne			568.7	574.0
	1001.5	827.6	731.5	737.8
11 Na	1021.5	1022.0	914.9	922.1
	1236.3	1237.0	1118.8	1126.9
12 Mg	1471.7	1472.7	1343.2	1352.3
13 AI	1727.7	1729.0	1588.3	1598.4
14 Si	2004.3	2006.1	1853.9	1865.1
15 P	2301.7	2304.0	2140.3	2152.6
16 S	2619.7	2622.7	2447.3	2460.8
17 Cl	2958.5	2962.4	2775.1	2789.8
18 Ar	3318	3323	3124	3140
19 K	3699	3705	3493	3511
20 Ca	4100	4108	3883	3903
21 Sc	4523	4532	4295	4316
22 Ti	4966	4977	4727	4750
23 V	5431	5444	5180	5205
24 Cr	5917	5932	5655	5682
25 Mn	6424	6442	6151	6181
26 Fe	6952	6973	6668	6701
27 Co	7502	7526	7206	7242
28 Ni	8073	8102	7766	7806
29 Cu	8666	8699	8347	8392
30 Zn	9281	9318	8950	8999
31 Ga	9917	9960	9575	9628
32 Ge	10575	10624	10221	10280
33 As	11255	11311	10889	10280
34 Se	11958	12021	11579	11652
35 Br	12682	12753	12292	12372
36 Kr	13429	13509	13026	13114
37 Rb	14199	14288	13783	13114
38 Sr	14990	15090	14562	14669
39 Y	15805	15916	15364	15482
40 Zr	16643	16765	16189	16318
41 Nb	17503	17639	17036	17178
42 Mo	18387	18537	17907	18062
42 MO	19294	19459	18800	18971
44 Ru	20224	20406	19717	
44 Ru 45 Rh	20224	21377	20658	19904 20861
45 Kn 46 Pd	22156	22374	20658	
46 Pd 47 Ag	23157	23396	21622	21843
47 Ag 48 Cd				22851
48 Ca 49 In	24183	24444	23621	23884
49 In 50 Sn	25233 26308	25518 26617	24657 25717	24942 26027

SECTION 2

SYNCHROTRON RADIATION

2.1A CHARACTERISTICS OF SYNCHROTRON RADIATION

Kwang-Je Kim

Synchrotron radiation occurs when a charge moving at relativistic speeds follows a curved trajectory. In this section, formulas and supporting graphs are used to quantitatively describe characteristics of this radiation for the cases of circular motion (bending magnets) and sinusoidal motion (periodic magnetic structures).

We will first discuss the ideal case, where the effects due to the angular divergence and the finite size of the electron beam—the emittance effects—can be neglected.

A. BENDING MAGNETS

The angular distribution of radiation emitted by electrons moving through a bending magnet with a circular trajectory in the horizontal plane is given by

$$\frac{d^{2}g_{B}(\omega)}{d\theta d\psi} = \frac{3\alpha}{4\pi^{2}} \gamma^{2} \frac{\Delta \omega I}{\omega e} y^{2} (1 + X^{2})^{2}$$

$$\times \left[K_{2\beta}^{2}(\xi) + \frac{X^{2}}{1 + X^{2}} K_{1\beta}^{2}(\xi) \right].$$
(1)

where

T_B = photon flux (number of photons per second)

 θ = observation angle in the horizontal plane

 ψ = observation angle in the vertical plane

 α = fine-structure constant

 γ = electron energy/ $m_e c^2$ (m_e = electron mass, c = velocity of light)

 ω = angular frequency of photon ($\varepsilon = \hbar \omega$ = energy of photon)

I = beam current

e = electron charge = 1.602×10^{-19} coulomb

 $y = \omega l \omega_c = \varepsilon l \varepsilon_c$

 a_c = critical frequency, defined as the frequency that divides the emitted power into equal halves,

 $=3\gamma^3c/2\rho$

 $\rho={
m radius}$ of instantaneous curvature of the electron trajectory (in practical units,

 $\rho[m] = 3.3 E[GeV]/B[T])$

E = electron beam energy

B = magnetic field strength

 $\varepsilon_{c} = \hbar \omega_{c}$ (in practical units, ε_{c} [keV] = 0.665 E^{2} [GeV] B[T])

 $X = \gamma \psi$ $\xi = y(1 + X^2)^{3/2/2}$

The subscripted K's are modified Bessel functions of the second kind. In the horizontal direction ($\psi = 0$), Eq. (1) becomes

$$\frac{d^{2} \mathcal{I}_{\mathbf{B}}}{d \theta d \psi}\Big|_{\psi = 0} = \frac{3\alpha}{4\pi^{2}} \gamma^{2} \frac{\Delta \omega}{\omega} \frac{I}{e} H_{2}(y), \tag{2}$$

where

$$H_2(y) = y^2 K_{2/3}^2(y/2)$$
 (3)

In practical units [photons· s^{-1} · mr^{-2} ·(0.1% bandwidth)⁻¹],

$$\frac{d^2 \mathcal{F}_{\rm B}}{d\theta d\psi}\Big|_{w=0} = 1.327 \times 10^{13} E^2 [\text{GeV}] I[\text{A}] H_2(y).$$

The function $H_2(y)$ is shown in Fig. 2-1.

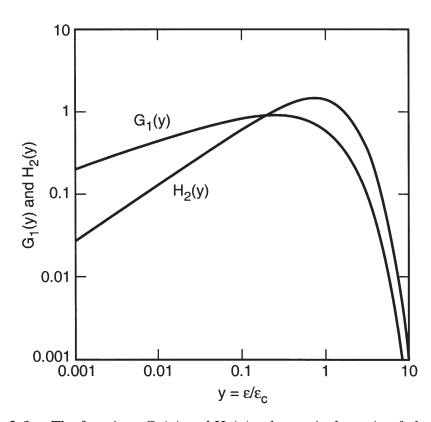


Fig. 2-1. The functions $G_1(y)$ and $H_2(y)$, where y is the ratio of photon energy to critical photon energy.

The distribution integrated over ψ is given by

$$\frac{d \, \mathcal{F}_{\mathbf{B}}}{d\theta} = \frac{\sqrt{3}}{2\pi} \alpha \gamma \frac{\Delta \omega}{\omega} \frac{I}{e} G_{1}(y),\tag{4}$$

where

$$G_1(y) = y \int_y^\infty K_{5/3}(y') dy'$$
 (5)

In practical units [photons \cdot s⁻¹ \cdot mr⁻¹ \cdot (0.1% bandwidth)⁻¹],

$$\frac{d^{9}B}{d\theta} = 2.457 \times 10^{13} E[\text{GeV}]I[A]G_{1}(y).$$

The function $G_1(y)$ is also plotted in Fig. 2-1.

Radiation from a bending magnet is linearly polarized when observed in the bending plane. Out of this plane, the polarization is elliptical and can be decomposed into its horizontal and vertical components. The first and second terms in the last bracket of Eq. (1) correspond, respectively, to the intensity of the horizontally and vertically polarized radiation. Figure 2-2 gives the normalized intensities of these two components, as functions of emission angle, for different energies. The square root of the ratio of these intensities is the ratio of the major and minor axes of the polarization ellipse. The sense of the electric field rotation reverses as the vertical observation angle changes from positive to negative.

Synchrotron radiation occurs in a narrow cone of nominal angular width $\sim 1/\gamma$ To provide a more specific measure of this angular width, in terms of electron and photon energies, it is convenient to introduce the effective rms half-angle $\sigma_{h\nu}$ as follows:

$$\frac{d\mathcal{F}_{B}}{d\theta} \frac{d^{2}\mathcal{F}_{B}}{d\theta d\psi}\Big|_{\psi=0} = \sqrt{2\pi} \,\sigma_{\psi},\tag{6}$$

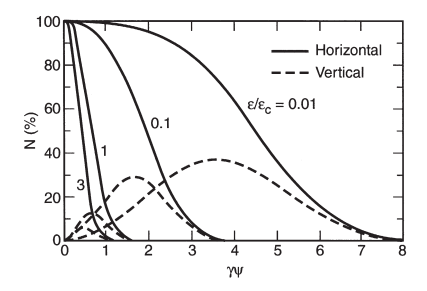


Fig. 2-2. Normalized intensities of horizontal and vertical polarization components, as functions of the vertical observation angle ψ, for different photon energies. (Adapted from Ref. 1.)

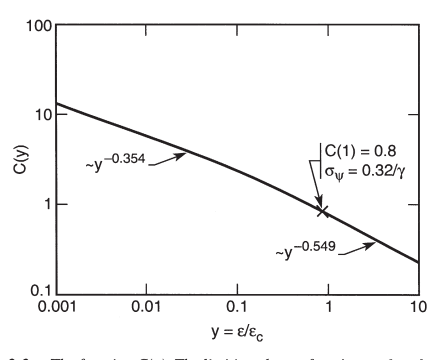


Fig. 2-3. The function C(y). The limiting slopes, for $\mathscr{E}_{\mathcal{C}} << 1$ and $\mathscr{E}/\mathscr{E}_{\mathcal{C}}$ >> 1, are indicated.

where σ_{ψ} is given by

$$\sigma_{\psi} = \frac{2}{\gamma \sqrt{2\pi}} C(y) = 0.408 \frac{C(y)[\text{mr}]}{E[\text{GeV}]} \quad . \tag{7}$$

The function C(y) is plotted in Fig. 2-3. In terms of σ_{ψ} , Eq. (2) may now be rewritten as

$$\frac{d^2 \mathcal{F}_{\rm B}}{d\theta d\psi}\Big|_{\psi=0} = \frac{d\mathcal{F}_{\rm B}}{d\theta} \frac{1}{\sigma_{\psi} \sqrt{2\pi}}.$$
 (2a)

B. PERIODIC MAGNETIC STRUCTURES

In a wiggler or an undulator, electrons travel through a periodic magnetic structure. We consider the case where the magnetic field *B* varies sinusoidally and is in the vertical direction:

$$B(z) = B_0 \cos(2\pi z/\lambda_u) \quad , \tag{8}$$

where z is the distance along the wiggler axis, B_0 the peak magnetic field, and λ_u the magnetic period. Electron motion is also sinusoidal and lies in

the horizontal plane. An important parameter characterizing the electron motion is the deflection parameter K given by

$$K = eB_0 \lambda_1 / 2\pi mc = 0.934 \lambda_1 \text{ [cm] } B_0 \text{[T]} \quad . \tag{9}$$

In terms of K, the maximum angular deflection of the orbit is $\delta = K/\gamma$. For $K \leq 1$, radiation from the various periods can exhibit strong interference phenomena, because the angular excursions of the electrons are within the nominal $1/\gamma$ radiation cone; in this case, the structure is referred to as an undulator. In the case K >> 1, interference effects are less important, and the structure is referred to as a wiggler.

B.1 Wiggler radiation

In a wiggler, K is large (typically ≥ 10) and radiation from different parts of the electron trajectory adds incoherently. The flux distribution is then given by 2N (where N is the number of magnet periods) times the appropriate formula for bending magnets, either Eq. (1) or Eq. (2). However, ρ or B must be taken at the point of the electron's trajectory tangent to the direction of observation. Thus, for a horizontal angle θ ,

$$\varepsilon_c(\theta) = \varepsilon_{cmax} \sqrt{1 - (\theta / \delta)^2}$$
, (10)

where

$$\varepsilon_{\text{cmax}} = 0.665 E^2 [\text{GeV}] B_0 [\text{T}]$$

When ψ = 0, the radiation is linearly polarized in the horizontal plane, as in the case of the bending magnet. As ψ increases, the direction of the polarization changes, but because the elliptical polarization from on half-period of the motion combines with the elliptical polarization (of opposite sense of rotation) from the next, the polarization remains linear.

B.2 Undulator radiation

In an undulator, K is moderate (≤ 1) and radiation from different periods interferes coherently, thus producing sharp peaks at harmonics of the fundamental (n = 1). The wavelength of the fundamental on axis ($\theta = \psi = 0$) is given by

$$\lambda_{l} = \frac{(1 + K^{2}/2)}{2 v^{2}} \lambda_{u} \tag{11}$$

$$\lambda_{\rm l}[{\rm \mathring{A}}] = \frac{13.056~\lambda_{\rm u}[{\rm cm}]}{E^2[{\rm GeV}]}~(1+~K^2/2)$$

The corresponding energy, in practical units, is

$$\varepsilon_{l}[\text{keV}] = 0.950 \frac{E^{2}[\text{GeV}]}{(1 + K^{2}/2)\lambda_{u}[\text{cm}]} .$$

The relative bandwidth at the nth harmonic is

$$\frac{\Delta \lambda}{\lambda} \cong \frac{\Delta \omega}{\omega} \cong \frac{1}{nN} \quad (n = 1, 2, 3, ...) \quad . \tag{12}$$

On axis the peak intensity of the nth harmonic is given by

$$\frac{d^2 \mathcal{F}_n}{d \theta d \psi} \Big|_{0} = \alpha N^2 \gamma^2 \frac{\Delta \omega}{\omega} \frac{I}{e} F_n(K) \quad (n = 1,3,5,...)$$

$$= 0 \quad (n = 2,4,6,.., (13))$$

where

$$F_n(K) = \frac{K^2 n^2}{(1 + K^2/2)^2} \left\{ J_{\frac{n-1}{2}} \left[\frac{nK^2}{4(1 + K^2/2)} \right] - J_{\frac{n+1}{2}} \left[\frac{nK^2}{4(1 + K^2/2)} \right] \right\}^2.$$
 (14)

Here, the J's are Bessel functions. The function $F_n(K)$ is plotted in Fig. 2-4. In practical units [photons·s $^{-1}$ ·mr $^{-2}$ ·(0.1% bandwidth) $^{-1}$], Eq. (13) becomes

$$\frac{d^2 \mathcal{I}_n}{d \theta d \psi} \bigg|_0 = 1.744 \times 10^{14} N^2 E^2 [\text{GeV}] I[\text{A}] F_n(K).$$

The angular distribution of the nth harmonic is concentrated in a narrow cone whose half-width is given by

$$\sigma_{\gamma'} \cong \sqrt{\frac{\lambda_n}{L}} = \frac{1}{\gamma} \sqrt{\frac{(1 + K^2/2)}{2Nn}} \quad . \tag{15}$$

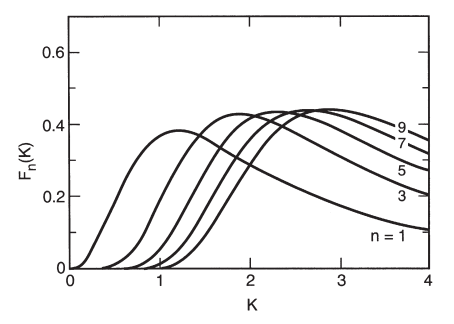


Fig. 2-4. The function $F_n(K)$ for different values of n, where K is the deflection parameter.

Here L is the length of the undulator $(L = N\lambda_u)$. Additional rings of radiation of the same frequency also appear at angular distances

$$\theta_{n,\ell} = \frac{1}{\gamma} \sqrt{\frac{\ell}{n} (1 + K^2/2)}$$
 $(\ell = 1, 2, 3, ...)$. (16)

The angular structure of undulator radiation is illustrated in Fig. 2-5 for the limiting case of zero beam emittance.

We are usually interested in the central cone. An approximate formula for the flux integrated over the central cone is

$$\mathcal{F}_{n} = \pi \alpha N \frac{\Delta \omega}{\omega} \frac{I}{e} Q_{n}(K), \tag{17}$$

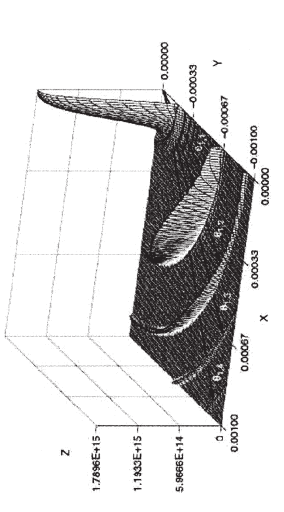
or, in units of photons \cdot s⁻¹ \cdot (0.1% bandwidth)⁻¹,

$$\mathcal{I}_n = 1.431 \times 10^{14} NQ_n I[A].$$

The function $Q_n(K) = (1 + K^2/2)F_n/n$ is plotted in Fig. 2-6. Equation (13) can also be written as

correspond to the observation angles • and • (in radians), respectively, The angular distribution of fundamental (n = 1) undulator radiation calculation were N = 14, K = 1.87, • $_{u} = 3.5$ cm, and E = 1.3 GeV. for the limiting case of zero beam emittance. The x and y axes and the z axis is the intensity in photons·s-1·A-1·(0.1 mr)-2·(1% bandwidth)-'. The undulator parameters for this theoretical Fig. 2-5.

Figure courtesy of R. Tatchyn, Stanford University.)



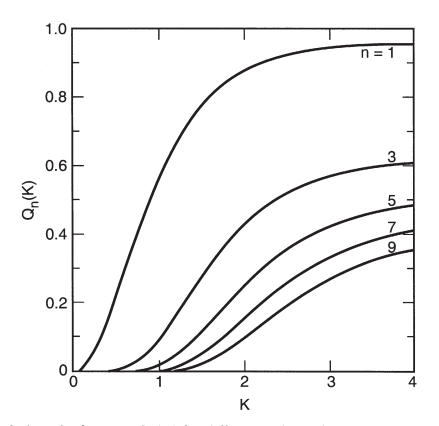


Fig. 2-6. The function $Q_n(K)$ for different values of n.

$$\left. \frac{d^2 \mathcal{F}_n}{d\theta d\psi} \right|_0 = \frac{\mathcal{F}_n}{2\pi\sigma_{r'}^2}.$$
 (13a)

Away from the axis, there is also a change in wavelength: The factor $(1 + K^2/2)$ in Eq. (11) must be replaced by $[1 + K^2/2]$

+ γ^2 $(\theta^2 + \hat{\psi}^2)$]. Because of this wavelength shift with emission angle, the angle-integrated spectrum consists of peaks at λ_n superposed on a continuum. The peak-to-continuum ratio is large for $K \ll 1$, but the continuum increases with K, as one shifts from undulator to wiggler conditions.

B.3 Power

The total power radiated by an undulator or wiggler is

$$P_{\rm T} = \frac{N}{6} Z_0 I e^{\frac{2\pi c}{\lambda_{\rm B}}} \gamma^2 K^2 \quad , \tag{18}$$

where $Z_0 = 377$ ohms, or, in practical units,

$$P_{\rm T}[kW] = 0.633 E^2[\text{GeV}] B_0^2[\text{T}] L[m] I[A]$$

The angular distribution of the radiated power is

$$\frac{d^2P}{d\theta d\psi} = P_{\rm T} \frac{21\gamma^2}{16\pi K} G(K) f_K(\gamma \theta, \gamma \psi) \quad , \tag{19}$$

or, in units of W·mr-2,

$$\frac{d^2P}{d\theta dw} = 10.84B_0[T]E^4 [\text{GeV}]I[A]NG(K)f_K(\gamma\theta,\gamma\psi) .$$

The behavior of the angular function $f_K(\gamma\theta,\gamma\psi)$, which is normalized as $f_K(0,0)=1$, is shown in Fig. 2-7. The function G(K), shown in Fig. 2-8, quickly approaches unity as K increases from zero.

C. EMITTANCE EFFECTS

Electrons in storage rings are distributed in a finite area of transverse phase space—position × angle. We introduce the rms beam sizes σ_x (horizontal) and σ_y (vertical), and beam divergences σ_x (horizontal) and σ_y : (vertical). The quantities $\varepsilon_x = \sigma_x \sigma_x$ and $\varepsilon_y = \sigma_y \sigma_y$ are known as the horizontal and vertical emittances, respectively. In general, owing to the finite emittances of real electron beams, the intensity of the radiation observed in the forward direction is less than that given by Eqs. (2a) and (13a). Finite emittances can be taken into account approximately by replacing these equations by

$$\frac{d^2 \mathcal{F}_{\rm B}}{d\theta d\psi}\bigg|_{\psi=0} = \frac{d\mathcal{F}_{\rm B}}{d\theta} \frac{1}{\sqrt{2\pi \left(\sigma_{\psi}^2 + \sigma_{\psi'}^2\right)}}$$
(20)

and

$$\frac{d^2 \mathcal{F}_n}{d\theta d\psi}\bigg|_0 = \frac{\mathcal{F}_n}{2\pi \sqrt{(\sigma_{r'}^2 + \sigma_{x'}^2)(\sigma_{r'}^2 + \sigma_{y'}^2)}}$$
(21)

for bends and undulators, respectively. For bending magnets, the electron beam divergence effect is usually negligible in the horizontal plane.

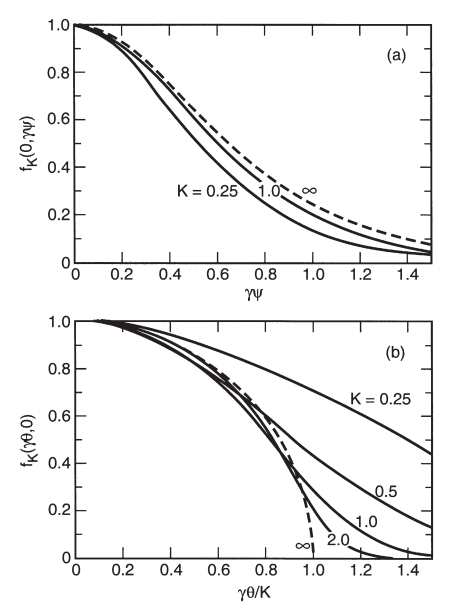


Fig. 2-7. The angular function $f_{K'}$ for different values of the deflection parameter K, (a) as a function of the vertical observation angle ψ when the horizontal observation angle $\theta=0$ and (b) as a function of θ when $\psi=0$.

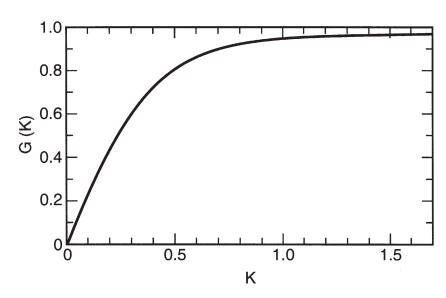


Fig. 2-8. The function G(K).

D. SPECTRAL BRIGHTNESS AND TRANSVERSE COHERENCE

For experiments that require a small angular divergence and a small irradiated area, the relevant figure of merit is the beam brightness \mathcal{B} , which is the photon flux per unit phase space volume, often given in units of photons·s⁻¹·mr⁻²·mm⁻²·(0.1% bandwidth)⁻¹. For an undulator, an approximate formula for the peak brightness is

$$\mathcal{B}_{n}(0,0) = \frac{\mathcal{F}_{n}}{(2\pi)^{2} \sigma_{Tx} \sigma_{Ty} \sigma_{Tx'} \sigma_{Ty'}},$$
(22)

where, for example,

$$\sigma_{Tx} = \sqrt{\sigma_{\bar{\chi}}^2 + \sigma_{\bar{r}}^2}$$
,
 $\sigma_{Tx'} = \sqrt{\sigma_{x'}^2 + \sigma_{x'}^2}$,
$$(23)$$

and where the single-electron radiation from an axially extended source of finite wavelength is described by

$$\sigma_r = \frac{1}{4\pi} \sqrt{\lambda L}$$
 , (24)
 $\sigma_{r'} = \sqrt{\lambda / L}$.

Brightness is shown in Fig. 2-9 for several sources of synchrotron radiation, as well as some conventional x-ray sources.

That portion of the flux that is transversely coherent is given by

$$\mathcal{F}_{c} = \mathcal{B}_{n} \left(\frac{\lambda}{2}\right)^{2} = \frac{\mathcal{F}_{n} \lambda^{2}}{(4\pi)^{2} \sigma_{Tx} \sigma_{Ty} \sigma_{Ty'} \sigma_{Ty'}}.$$
 (25)

A substantial fraction of undulator flux is thus transversely coherent for a low-emittance beam satisfying $\varepsilon_\chi \varepsilon_\gamma \lesssim (\lambda/4\pi)^2$.

E. LONGITUDINAL COHERENCE

Longitudinal coherence is described in terms of a coherence length

$$\ell_{\rm c} = \lambda^2 / \Delta \lambda \quad . \tag{26}$$

For an undulator, the various harmonics have a natural spectral purity of $\Delta \lambda / \lambda = 1/nN$ [see Eq. (12)]; thus, the coherence length is given by

$$\ell_c = nN\lambda$$
 , (27)

which corresponds to the relativistically contracted length of the undulator. Thus, undulator radiation from low-emittance electron beams $[\varepsilon_x \varepsilon_y \leq (\lambda/4\pi)^2]$ is transversely coherent and is longitudinally coherent within a distance described by Eq. (27). In the case of finite beam emittance or finite angular acceptance, the longitudinal coherence is reduced because of the change in wavelength with emission angle. In this sense, undulator radiation is partially coherent. Transverse and longitudinal coherence can be enhanced when necessary by the use of spatial and spectral filtering (i.e., by use of apertures and monochromators, respectively).

The references listed below provide more detail on the characteristics of synchrotron radiation.

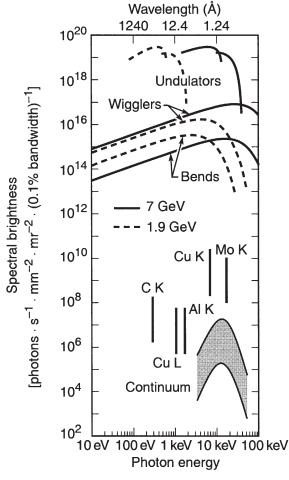


Fig. 2-9. Spectral brightness for several synchrotron radiation sources and conventional x-ray sources. The data for conventional x-ray subes should be taken as rough estimates only, since brightness depends strongly on such parameters as operating voltage and take-off angle. The indicated two-order-of-magnitude ranges show the approximate variation that can be expected among stationary-anode tubes (lower end of range), rotating-anode tubes (middle), and rotating-anode tubes with microfocusing (upper end of range). The envelope of spectral brightness curves for today's third-generation synchrotron facilities is somewhat higher than the curves above due to increased average current (due to "top up" mode) and decreased electron beam emittance.

REFERENCES

- G. K. Green, "Spectra and Optics of Synchrotron Radiation," in Proposal for National Synchrotron Light Source, Brookhaven National Laboratory, Upton, New York, BNL-50595 (1977).
- H. Winick, "Properties of Synchrotron Radiation," in H. Winick and S. Doniach, Eds., Synchrotron Radiation Research (Plenum, New York, 1979), p. 11.
- S. Krinsky, "Undulators as Sources of Synchrotron Radiation," IEEE Trans. Nucl. Sci. NS-30, 3078 (1983).
- D. F. Alferov, Yu. Bashmakov, and E. G. Bessonov, "Undulator Radiation," Sov. Phys. Tech. Phys. 18, 1336 (1974).
- K.-J. Kim, "Angular Distribution of Undulator Power for an Arbitrary Deflection Parameter K," Nucl. Instrum. Methods Phys. Res. A246, 67 (1986).
- K.-J. Kim, "Brightness, Coherence, and Propagation Characteristics of Synchrotron Radiation," *Nucl. Instrum. Methods Phys. Res.* A246, 71 (1986).
- K.-J. Kim, "Characteristics of Synchrotron Radiation," in *Physics of Particle Accelerators*, AIP Conf. Proc. 184 (Am. Inst. Phys., New York, 1989), p. 565.
- D. Attwood, Soft X-Rays and Extreme Ultraviolet Radiation: Principles and Applications (Cambridge Univ. Press, Cambridge, 1999); see especially Chaps. 5 and 8.

2.1B. FREE ELECTRON LASERS (FELS) AT EXTREME ULTRAVIOLET AND X-RAY WAYELENGTHS

Yanwei Liu

As fourth-generation radiation facilities, FELs can generate very short duration, spatially coherent beams at short wavelengths. The lack of suitable mirrors prevents x-ray FELs from using a cavity oscillator. Instead, x-ray FELs are based on the Self Amplified Spontaneous Emission (SASE) process in a very long undulator [1]. The long undulator allows interaction between the radiated electric field and the electron beam to the extent that the light field can effectively modulate the energy of the electrons, forcing them into microbunches separated by one wavelength of the radiation (see Fig. 2-10). This microbunching process results in coherently radiating electrons and selfamplification of the light field, producing extremely bright, spatially coherent radiation. As the SASE process starts from shot noise, the x-ray FEL beams generally contain multiple spikes in their time structure, and thus have a complicated temporal phase and somewhat limited temporal coherence. Future FELs will likely use a seed pulse to improve temporal coherence.

Fully operational x-ray FELs include FLASH at DESY (Deutsches Elektronen-Synchrotron, Hamburg, Germany) and LCLS (Linac Coherent Light Source, Stanford, CA, USA). FLASH started user operation in August 2005, with a fundamental wavelength ranging from 6.5 nm (starting 2007) to 47 nm [2]. In April 2009, LCLS realized lasing in the hard x-ray region, with saturation at a wavelength of 1.5 Å [3]. X-ray FELs under construction worldwide include the SCSS at Japan, FERMI in Italy, the European XFEL, and others.

Examples of FEL Electron Beam and Photon Beam Characteristics at FLASH and LCLS

	FLASH	LCLS
Electron beam energy	0.2-1 GeV	13.6 GeV
Undulator period	2.73 cm	3 cm
Undulator length	30 m	112 m
Wavelength (fundamental)	6.5–47 nm	1.5 Å
Pulse energy	100 μJ	1.1 mJ
Peak power	5 GW	15 GW
Pulse duration	10-50 fs	75 fs
Peak brightness [phs/(s mrad² mm² 0.1% BW)]	$10^{29} - 10^{30}$	$10^{32} - 10^{33}$

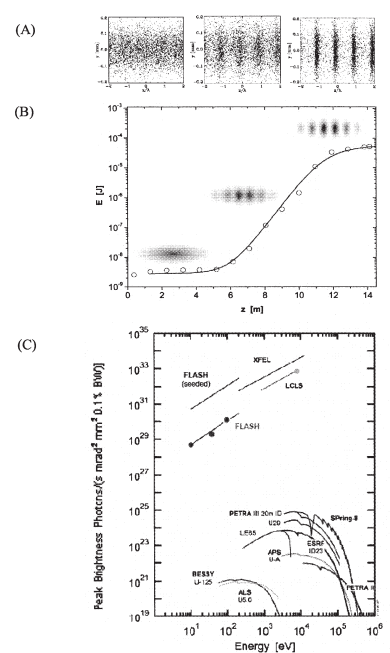


Figure 2-10. (A) Simulation of the electron microbunching process and (B) the exponential growth of FEL output energy due to microbunching (following S. Reiche and K.-J. Kim). (C) FEL beams have very short pulse duration and full spatial coherence, with peak brightness many orders of magnitude higher than 3rd generation synchrotron facilities [4, modified].

List of Some X-Ray FEL Facilities (operational and under construction)

FLASH at DESY (Deutsches Elektronen-Synchrotron), Hamburg, Germany http://flash.desy.de/

LCLS (Linac Coherent Light Source) at Stanford, CA, USA http://lcls.slac.stanford.edu/

SCSS (Spring-8 Compact SASE Source) http://www-xfel.spring8.or.jp/

FERMI@Elettra, Trieste, Italy www.elettra.trieste.it/FERMI/

European XFEL http://xfel.desy.de/

REFERENCES

- C. Pellegrini and S. Reiche, "The development of X-ray Free-Electron Lasers," IEEE J. of Selected Topics in Quantum Electronics, 10, 1393-1404 (2004).
- FLASH brochure, available at http://flash.desy.de/sites/site_vuvfel/content/e395/e2188/F LASH-Broschrefrs_web.pdf
- P. Emma, "First lasing of the LCLS X-ray FEL at 1.5 Å." for the LCLS Commissioning Team; SLAC, Stanford, CA 94309, USA. Available at http://ssrl.slac.stanford.edu/lcls/commissioning/documents /th3pbi01.pdf
- H. Weise et al., "The TTF/VUV-FEL (FLASH) as the prototype for the European XFEL project." Proceedings of LINAC 2006, Knoxville, TN, USA

2.2 HISTORY OF SYNCHROTRON RADIATION

Arthur I. Robinson

Synchrotron radiation generated by relativistic electrons in circular accelerators is only a little more than 60 years old. The first observation—literally, since it was visible light that was generated—came at the General Electric Research Laboratory in Schenectady, New York, on April 24, 1947. In the six decades since, synchrotron radiation in the x-ray and ultraviolet spectral regions has become a premier research tool for the study of matter in all its varied manifestations, as facilities around the world have evolved to provide this light in ever more useful forms.

A. BACKGROUND

Both scientists and society have long recognized the exceptional importance of x-rays, beginning immediately after their discovery in 1895. The first Nobel Prize in Physics ever awarded went to Röntgen in 1901 "in recognition of the extraordinary services he has rendered by the discovery of the remarkable rays subsequently named after him." By the time synchrotron radiation was observed almost 50 years later, the scientific use of x-rays was well established. Some highlights include the following:

- 1909: Barkla and Sadler discover characteristic x-ray radiation (1917 Nobel Prize to Barkla)
- 1912: von Laue, Friedrich, and Knipping observe x-ray diffraction (1914 Nobel Prize to von Laue)
- 1913: Bragg, father and son, build an x-ray spectrometer (1915 Nobel Prize)
- 1913: Moseley develops quantitative x-ray spectroscopy and Moseley's Law
- 1916: Siegbahn and Stenstrom observe emission satellites (1924 Nobel Prize to Siegbahn)
- 1921: Wentzel observes two-electron excitations
- 1922: Meitner discovers Auger electrons
- · 1924: Lindh and Lundquist resolve chemical shifts

- 1927: Coster and Druyvesteyn observe valence-core multiplets
- 1931: Johann develops bent-crystal spectroscopy

B. DISCOVERY OF SYNCHROTRON RADIATION

In the 1920s, physicists began contemplating magneticinduction electron accelerators (betatrons) as machines to produce intense beams of x-rays by directing the accelerated beam onto a suitable target. Ivanenko and Pomeranchuk in the Soviet Union published calculations in 1944 showing that energy losses due to radiating electrons would limit the energy obtainable in a betatron. Subsequent theoretical work proceeded independently in the Soviet Union and in the U.S., where by 1945 Schwinger had worked out in considerable detail the classical (i.e., nonquantum) theory of radiation from accelerated relativistic electrons. After GE began testing a 100-MeV betatron in 1944, Blewett suggested a search for the radiation losses, which he expected to be significant at this energy. Although quantitative measurements reported in 1946 of the shrinking electron-orbit radius with energy were in accord with predicted losses, there was no direct observation of synchrotron radiation, owing to an opaque coating on the tube in which the electrons circulated

Advances on another accelerator front led to the 1947 visual observation of synchrotron radiation at GE, where Pollack assembled a team to build a 70-MeV electron synchrotron to test the idea of phase stability in accelerators, independently proposed by McMillan in the U.S. and Veksler in the Soviet Union. Fortunately for the future of synchrotron radiation, the coating on the doughnut-shaped electron tube was transparent, which allowed a technician to look around the shielding with a mirror and see a bright arc of light, which the GE group quickly realized was actually coming from the electron beam. Their subsequent measurements launched the experimental investigation of the spectral and polarization properties of the radiation. Characterization measurements were also carried out in the 1950s at a 250-MeV synchrotron at the Lebedev Institute in Moscow.

The next big step came with the 1956 experiments of Tomboulian and Hartman, who were granted a two-week run at the 320-MeV electron synchrotron at Cornell. However,

despite the advantages of synchrotron radiation that were detailed by the Cornell scientists and the interest their work stimulated, it was not until 1961 that an experimental program using synchrotron radiation got under way when the National Bureau of Standards (now National Institute of Standards and Technology) modified its 180-MeV electron synchrotron to allow access to the radiation.

C. THE FIRST GENERATION

Under Madden and Codling, measurements began at the new NBS facility (Synchrotron Ultraviolet Radiation Facility or SURF) to determine the potential of synchrotron radiation for standards and as a source for spectroscopy in the ultraviolet. Their findings further stimulated the growing interest in synchrotron radiation. Establishment of SURF began the first generation of synchrotron radiation facilities. If SURF headed the first generation, it was not by much, as activity was also blossoming in both Europe and Asia. At the Frascati laboratory near Rome, researchers began measuring absorption using a 1.15-GeV synchrotron. In 1962 scientists in Tokyo formed the INS-SOR (Institute for Nuclear Studies-Synchrotron Orbital Radiation) group and by 1965 were measuring soft x-ray absorption spectra of solids using light from a 750-MeV synchrotron. The trend toward higher energies and shorter wavelengths took a big leap with the use of the 6-GeV Deutsches Elektronen-Synchrotron (DESY) in Hamburg, which provided synchrotron radiation at wavelengths in the x-ray region down to 0.1 Å.

While the number of synchrotrons with budding synchrotron radiation facilities was growing, the next major advance came with the development of storage rings, the basis for all of today's synchrotron sources. In the 1950s, the Midwest Universities Research Association was formed to develop a proposal for a high-current accelerator for particle physics. As part of the project, Mills and Rowe designed a 240-MeV storage ring as a test bed for advanced accelerator concepts. Politics intervened, however, and funding disappeared. Instead, supported by the U.S. Air Force Office of Scientific Research, the University of Wisconsin took on the responsibility of completing the storage ring, known as Tantalus I, and operating it for synchrotron radiation research. The first spectrum was

measured in 1968. With Tantalus I, the superiority of the electron storage ring as a source of synchrotron radiation became evident.

A surge of interest in storage rings soon followed. In 1971 synchrotron radiation work began on the 540-MeV ACO storage ring at the Orsay laboratory in France. NBS converted its synchrotron into a 250-MeV storage ring (SURF II) in 1974. The same year, the INS-SOR group in Tokyo began commissioning a 300-MeV storage ring, generally considered the first machine designed from the start specifically for the production of synchrotron radiation. The first storage ring in the multi-GeV class to provide x-rays to a large community of synchrotron radiation users was the 2.5-GeV SPEAR ring at the Stanford Linear Accelerator Center under the auspices of the Stanford Synchrotron Radiation Project in 1974. Other large storage rings to which synchrotron radiation capabilities were added early on include DORIS at the DESY laboratory, VEPP-3 at the Institute for Nuclear Physics in Novosibirsk, DCI at Orsay, and CESR at Cornell (the CHESS facility).

D. THE SECOND GENERATION: DEDICATED SOURCES

Parasitic operation at high-energy physics facilities often meant a severely limited output of synchrotron radiation, thereby motivating a demand for storage rings designed for and dedicated to the production of synchrotron radiation. The Synchrotron Radiation Source (SRS) at the Daresbury Laboratory in the UK was the first of the resulting "second generation" of sources. Experiments began at the new facility in 1981. That same year in the U.S., construction of the National Synchrotron Light Source (NSLS) at the Brookhaven National Laboratory was completed and commissioning began. The NSLS complex included separate 700-MeV and 2.5-GeV storage rings for production of UV radiation and x-rays, respectively. During this same period, the University of Wisconsin Synchrotron Radiation Center built a new 1-GeV storage ring named Aladdin, which superseded the old Tantalus I. In Japan the Photon Factory was completed in 1982 at the KEK laboratory in Tsukuba; in Berlin the BESSY facility began serving users in 1982 with an 800-MeV storage ring; and at Orsay LURE (Laboratoire pour l'Utilisation du Rayonnement Electromagnétique) began operating an 800-MeV storage ring, SuperACO, in 1984.

Elsewhere, some of the first-generation facilities gradually evolved toward second-generation status by means of upgrades and agreements to dedicate a fraction and sometimes all of the yearly machine operations to synchrotron radiation as the high-energy physics frontier advanced. The Stanford Synchrotron Radiation Laboratory at SLAC and HASYLAB (Hamburger Synchrotronstrahlungslabor) at DESY are prime examples.

E. BRIGHTNESS

As the clamor for facilities dedicated to synchrotron radiation expanded in the 1970s, users increasingly appreciated that spectral brightness, or brilliance, was often more important than flux alone for many experiments. As the flux density in phase space, brightness is an invariant quantity, so that no optical technique can improve it. The cure therefore is proper design of the source, the electron beam in the storage ring. As planning for NSLS progressed, Chasman and Green designed what has become the prototype magnet lattice (a so-called double-bend achromat) for storage rings with a low emittance (product of beam size and divergence) and hence a light source with high brightness. The Chasman-Green lattice and variations are the basis for most of today's synchrotron sources.

Undulators provide a way to take maximum advantage of the intrinsic brightness of the synchrotron radiation source. They produce one or a few spectrally narrow peaks (a fundamental and harmonics) in a beam that is highly collimated in both the horizontal and the vertical directions. Wigglers are similar to undulators but produce a continuous spectrum with a higher flux and a spectrum that extends to shorter wavelengths than bend magnets. Together, wigglers and undulators are called insertion devices because they are placed in the otherwise empty straight sections that connect the curved arcs of large storage rings.

The undulator concept traces back to the 1947 theoretical work of Ginzburg in the Soviet Union. Motz and coworkers experimentally verified the idea in 1953 by building an undulator and using it to produce radiation from the millimeterwave to the visible range in experiments with a linear accelerator at Stanford University. The next step came in the 1970s

with the installation of undulators in storage rings at the Lebedev Institute in Moscow and the Tomsk Polytechnic Institute. Undulators became practical devices for producing synchrotron radiation in storage rings in 1981 when Halbach at the Lawrence Berkeley Laboratory and coworkers constructed a device based on permanent magnets and successfully tested it at SSRL. Parallel work was also under way in Novosibirsk. A decade after the initial suggestion by Robinson, a wiggler was installed in 1966 at the Cambridge Electron Accelerator to enhance beam storage. In 1979 a wiggler comprising just seven electromagnet poles at SSRL was the first to be used for producing synchrotron radiation. Nowadays, wigglers may be permanent-magnet devices following the Halbach design or be based on high-field superconductors that shift the spectrum to the shortest wavelengths.

F. THE THIRD GENERATION: OPTIMIZED FOR BRIGHTNESS

Synchrotron users recognized that a new generation of storage rings with a still lower emittance and long straight sections for insertion devices would permit achieving even higher brightness and with it a considerable degree of spatial coherence. Following the NSLS two-ring model, third-generation facilities specialize in either hard x-rays or vacuum-ultraviolet radiation and soft x-rays. The European Synchrotron Radiation Facility (ESRF) in Grenoble was the first of the third-generation hard x-ray sources to operate, coming on line for experiments by users with a 6-GeV storage ring and a partial complement of commissioned beamlines in 1994. The ESRF was followed by the Advanced Photon Source at Argonne National Laboratory (7 GeV) in late 1996 and by SPring-8 (8 GeV) in Harima Science Garden City in Japan in late 1997.

Among the soft x-ray sources, the Advanced Light Source at Berkeley (1.9 GeV) began its scientific program in early 1994, as did the Synchrotrone Trieste (2.0 GeV) in Italy, followed by the Synchrotron Radiation Research Center (1.3 GeV) in Hsinchu, Taiwan, and the Pohang Light Source (2.0 GeV) in Korea. Many other soft x-ray facilities have been and are being constructed around the world. Addition of superconducting bend magnets to the storage-ring lattice in these smaller machines, as the Advanced Light Source has

done, will allow them to extend their spectral coverage to higher photon energies without sacrificing performance at lower photon energies. At the same time, storage rings at SSRL (SPEAR3) and HASYLAB (DORIS III) have been reconfigured to push them into the third-generation regime.

Following on the success of the third-generation sources, a newer round of third-and-a-half-generation facilities with still higher brightness has come into operation. Added to an often higher beam energy (typically 2.5 to 3 GeV) and circumference and advanced insertion devices (such as narrow gaps and the coming use of superconducting technology), these machines are filling in the spectral gap between the high- and low-energy facilities. Examples include the Swiss Light Source at the Paul Scherrer Institut in Switzerland; Soleil in Saclay, France; Diamond at the CCLRC Rutherford Appleton Laboratory in the UK; the Canadian Light Source at the University of Saskatchewan, Canada; the Australian Synchrotron in Melbourne; and the Shanghai Synchrotron Radiation Facility in China.

Even more advanced storage rings are also on the horizon. The PETRA III machine (6 GeV) now in operation at HASYLAB takes advantage of its 2.3-km circumference to reach an ultralow emittance. Construction has started on NSLS-II at Brookhaven on an ultrahigh-performance medium energy machine (3 GeV). Other similar projects have been proposed at locations around the world.

G. NEXT: THE FOURTH GENERATION

Plans to develop a new generation—the fourth—of synchrotron radiation sources with vastly enhanced performance are now reaching fruition. With the fourth generation, the accelerator technology shifts from storage rings to linear accelerators. In the x-ray and ultraviolet spectral regions now served by synchrotron radiation facilities, the technologies fall into two broad classes: free electron lasers (FELs) and energy recovery linacs (ERLs).

FELs differ from conventional lasers in that they use the electron beam as the lasing medium rather than a gas or a solid. To date, FELs available at longer wavelengths have been based on a high-precision insertion device and an optional optical cavity formed by mirrors. Current and future generations of

FELs will access shorter wavelengths by use of a single-pass configuration, in which the laser energy builds during the passage of each individual electron bunch, without the use of an optical cavity. The FEL can generate fully coherent light, can have peak brightnesses up to one billion times higher than that of ordinary synchrotron light, and can produce ultrashort pulses of 10 fs or shorter, properties that facilitate time-resolved investigations of extremely rapid processes. (See Section 2.1b for a fuller discussion of FELs.)

FLASH at HASYLAB is the first free-electron laser for VUV and soft x-ray radiation, having begun user operation in 2005. Currently it covers a wavelength range from 6.5 nm to about 50 nm with pulse durations between 10 fs and 50 fs. The Linac Coherent Light Source at SLAC is now undergoing commissioning and is the first facility designed specifically to produce hard x rays in the 1-Å range in 100-fs pulses. Many other projects, some including more advanced concepts to further improve performance or broaden the range of parameters available, are under way or under study in Asia, Europe, and the USA.

An Energy Recovery Linac (ERL) x-ray source takes advantage of recent advances in superconducting linear accelerators and in high-brightness electron sources. ERLs have the potential to generate synchrotron radiation with an average brightness about 1000 times greater than that of today's storage rings, together with ultrashort pulses, suitable for studying the dynamics of materials on extremely rapid time scales, and with intense x-ray nanoprobe beams to study samples that are spatially inhomogeneous on a nanometer scale or are simply ultra-tiny, also on the nanoscale.

While both ERLs and XFELS will be able to produce very fast x-ray pulses, the two sources are quite distinct in the timing of these pulses: ERLs are being designed to produce pulse times up to a billion times a second, whereas the first XFELs will produce bigger pulses with the capability of temporal as well as spatial coherence, but at a far lower repetition rate. In the meantime, the technology is advancing extremely rapidly, and advanced concepts may blur the distinction between these two extremes.

2.3 SYNCHROTRON RADIATION FACILITIES

Herman Winick and David Attwood

The number of synchrotron radiation facilities is growing rapidly. As a result, the Internet is the most reliable source of up-to-date information on facilities around the world. A very useful site is www.lightsources.org. A list of present facilities and their websites follows.

Advanced Light Source Barkelay CA www	
	www.isa.au.dk
	www.als.lbl.gov
Advanced Photon Source, Argonne, IL	www.aps.anl.gov
ALBA - Consortium for the Exploitation of the	www.cells.es
Synchrotron Light Laboratory, Barcelona, Spain	
ANKA-Angstromquelle Karlsruhe, Germany www	www.anka-online.de
Australian Synchrotron, Melbourne, Australia www	www.synchrotron.vic.gov.au
Beijing Synchrotron Radiation Facility, Beijing, China ww	www.ihep.ac.cn/bsrf/english
BESSY, Berlin, Germany www	www.bessy.de
Canadian Light Source, Saskatoon, Saskatchewan, www	www.lightsource.ca
Canada	
Center for Advanced Microstructures and Devices, www	www.camd.lsu.edu
Baton Rouge, LA	
Cornell High Energy Synchrotron Sources, Cornell, NY www	www.chess.cornell.edu
Dafne, Frascati, Italy www	www.lnf.infn.it
Deutsches Elektronen-Synchrotron, Hamburg, Germany www	www-hasylab.desy.de
Diamond Light Source, Didcot, Oxfordshire, England www	www.diamond.ac.uk
Dortmund Electron Test Accelerator, Dortmund, www	www.delta.uni-dortmund.de
Germany	
Electron Stretcher Accelerator, Bonn, Germany http	http://www-elsa.physik.uni-bonn.de/elsa-facility_en.html
Elettra Synchrotron Light Laboratory, Trieste, Italy www	www.elettra.trieste.it
an Synchrotron Radiation Facility, Grenoble,	www.esrf.fr
France	

Facility	Website
Hiroshima Synchrotron Radiation Center, Hiroshima,	www.hsrc.hiroshima-u.ac.jp
Indus, Indore, India	www.cat.ernet.in/technology/accel/indus/index.html
Laboratorio Nacional de Luz Sincrotron, Campinas, Brazil	www.lnls.br
Linear Coherent Light Source, Stanford CA	http://lcls.slac.stanford.edu/
MAX-lab, Lund, Sweden	www.maxlab.lu.se
Metrology Light Source, Berlin, Germany	www.ptb.de/mls/
National Synchrotron Light Source, Upton, NY	www.nsls.bnl.gov
National Synchrotron Radiation Laboratory, Hefei,	www.ustc.edu.cn/en/srl.htm
China	
NewSUBARU, Nishi-Harima, Hyogo, Japan	www.lasti.himeji-tech.ac.jp/NS/Index.html
Petra III	http://hasylab.desy.de/facilities/petra_iii/index_eng.html
Photon Factory, Tsukuba, Japan	http://pfwww.kek.jp
Pohang Light Source, Pohang, Korea	http://pal.postech.ac.kr
MIRRORCLE - Ritsumeikan, Kusatsu, Japan	www.ritsumei.ac.jp/se/d11/index-e.html
SAGA-Light Source, Kyushu Synchrotron Light	http://www.saga-ls.jp/?page=206
Research Center, Japan	
SESAME, Amman, Jordan	www.sesame.org.jo
Shanghai Synchrotron Radiation Facility, Shanghai,	http://ssrf.sinap.ac.cn/english/1/Introduction.htm
Siberia-2. Kurchatov Institute, Moscow, Russia	www.kiae.ru
Singapore Synchrotron Light Source, Singapore	www.nus.edu.sg/NUSinfo/SSLS

Facility	Website
SOLEIL, Saint-Aubin, France	www.synchrotron-soleil.fr
SPring-8, Nishi-Harima, Hyogo, Japan	www.spring8.or.jp
Stanford Synchrotron Radiation Lightsource,	www-ssrl.slac.stanford.edu
Stanford, CA	
SURF, NIST, Gaithersburg, MD	http://physics.nist.gov/MajResFac/SURF/SURF.html
Swiss Light Source, Villigen, Switzerland	http://sls.web.psi.ch/view.php/about/index.html
Synchrotron Light Research Institute, Nakhon	http://sut2.sut.ac.th
Ratchasima, Thailand	
Synchrotron Radiation Center, Stoughton, WI	www.src.wisc.edu
Synchrotron Radiation Research Center, Hsinchu,	www.srrc.gov.tw/en/main2000.htm
Taiwan	
UVSOR Facility, Myodajji, Okazaki, Japan	www.uvsor.ims.ac.jp
VEPP-3. VEPP-4. Budker INP. Novosibirsk. Russia	http://ssrc.inp.nsk.su

SECTION 3

SCATTERING PROCESSES

3.1 SCATTERING OF X-RAYS FROM ELECTRONS AND ATOMS

Janos Kirz

A. COHERENT, RAYLEIGH, OR ELASTIC SCATTERING

Scattering from single electrons (Thomson scattering) has a total cross section

$$\sigma_{\rm T} = 8\pi r_{\rm e}^2 / 3 = 6.652 \times 10^{-29} \text{ m}^2$$
 , (1)

where r_e is the classical radius of the electron, $e^2/mc^2 = 2.818 \times 10^{-15}$ meter. The angular distribution for unpolarized incident radiation is proportional to $(1 + \cos^2 \theta)$, where θ is the scattering angle. For polarized incident radiation, the cross section vanishes at 90° in the plane of polarization.

Scattering from atoms involves the cooperative effect of all the electrons, and the cross section becomes

$$\sigma_{\rm R} = \pi r_{\rm e}^2 \int_{-1}^{1} |f(\theta)|^2 (1 + \cos^2 \theta) d(\cos \theta) ,$$
 (2)

where $f(\theta)$ is the (complex) atomic scattering factor, tabulated in Section 1.7 of this booklet. Up to about 2 keV, the scattering factor is approximately independent of scattering angle, with a real part that represents the effective number of electrons that participate in the scattering. At higher energies, the scattering factor falls off rapidly with scattering angle. For details see Ref. 1.

B. COMPTON SCATTERING

In relativistic quantum mechanics, the scattering of x-rays by a free electron is given by the Klein-Nishina formula. If we assume unpolarized x-rays and unaligned electrons, this formula can be approximated as follows for x-ray energies below 100 keV:

$$d\sigma_{\text{KN}} / d\Omega = \frac{r_{\text{e}}^2 (1 + \cos^2 \theta)}{2[1 + k(1 - \cos \theta)]^2}$$
, (3)

where $k = E/mc^2$, the photon energy measured in units of the electron rest energy. The total cross section is approximately

$$\sigma_{\text{KN}} = 8\pi r_{\text{e}}^2 \frac{(1+2k+1.2k^2)}{3(1+2k)^2}$$
 (4)

Note that for very low energies $(k \to 0)$, we recover the Thomson cross section. The real difference comes when we deal with atoms. In that case, if the scattering leaves the atom in the ground state, we deal with coherent scattering (see above), whereas if the electron is ejected from the atoms, the scattering is (incoherent) Compton scattering. At high energies, the total Compton cross section approaches $Z\sigma_{KN}$. At low energies and small scattering angles, however, binding effects are very important, the Compton cross section is significantly reduced, and coherent scattering dominates (see Figs. 3-1 and 3-2). For details see Refs. 1 and 2.

The scattered x-ray suffers an energy loss, which (ignoring binding effects) is given by

$$E'/E = 1/[1 + k(1 - \cos \theta)]$$
 (5)

or, in terms of the wavelength shift,

$$\lambda' - \lambda = \lambda_{\rm c} (1 - \cos \theta) \quad , \tag{6}$$

where $\lambda_{\rm C}=h/mc=2.426\times 10^{-12}$ meter. The kinetic energy of the recoil electron is just the energy lost by the photon in this approximation:

$$E_{\rm e} = E \frac{k(1 - \cos \theta)}{1 + k(1 - \cos \theta)} \quad . \tag{7}$$

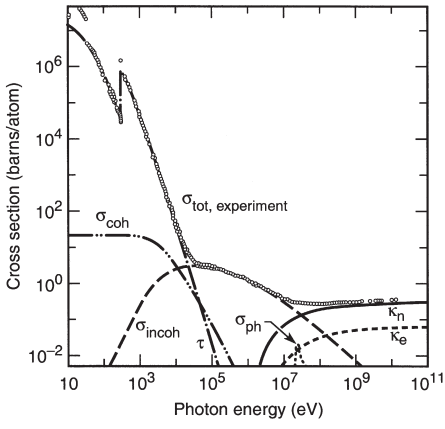


Fig. 3-1. Total photon cross section σ_{tot} in carbon, as a function of energy, showing the contributions of different processes: τ, atomic photo-effect (electron ejection, photon absorption); σ_{coh}, coherent scattering (Rayleigh scattering—atom neither ionized nor excited); σ_{incoh}, incoherent scattering (Compton scattering off an electron); κ_n, pair production, nuclear field; κ_e, pair production, electron field; σ_{ph}, photonuclear absorption (nuclear absorption, usually followed by emission of a neutron or other particle). (From Ref. 3; figure courtesy of J. H. Hubbell.)

REFERENCES

 J. H. Hubbell, W. J. Veigele, E. A. Briggs, R. T. Brown, D. T. Cromer, and R. J. Howerton, "Atomic Form Factors, Incoherent Scattering Functions, and Photon Scattering Cross Sections," J. Phys. Chem. Ref. Data 4, 471 (1975).

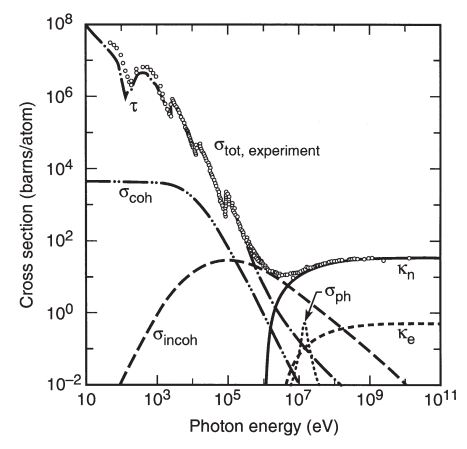


Fig. 3-2. Total photon cross section σ_{tot} in lead, as a function of energy. See Fig. 3-1. (From Ref. 3; figure courtesy of J. H. Hubbell.)

- R. D. Evans, The Atomic Nucleus (Kreiger, Malabar, FL, 1982); R. D. Evans, "The Compton Effect," in S. Flugge, Ed., Handbuch der Physik, vol. 34 (Springer-Verlag, Berlin, 1958), p. 218; W. J. Veigele, P. T. Tracy, and E. M. Henry, "Compton Effect and Electron Binding," Am. J. Phys. 34, 1116 (1966).
- J. H. Hubbell, H. A. Gimm, I. Øverbø, "Pair, Triplet, and Total Atomic Cross Sections (and Mass Attenuation Coefficients) for 1 MeV-100 GeV Photons in Elements Z = 1 to 100," J. Phys. Chem. Ref. Data 9, 1023 (1980).

3.2 LOW-ENERGY ELECTRON RANGES IN MATTER

Piero Pianetta

The electron range is a measure of the straight-line penetration distance of electrons in a solid [1]. Electrons with energies in the kilo-electron volt range, traveling in a solid, are scattered inelastically in collisions with the electrons in the material. For low-Z materials, such as organic insulators, scattering from the valence electrons is the major loss mechanism for incident electron energies from 10 eV to 10 keV. The core levels contribute less than 10% to the electron's energy dissipation for energies between 1 keV and 10 keV [2].

A. CSDA RANGES

For electron energies below 5 keV, the usual Bethe-Bloch formalism is inadequate for calculating the electron energy loss in a solid, and an approach using the dielectric response of the material is used [3]. The complex dielectric function $\varepsilon(k,\omega)$ describes the response of a medium to a given energy transfer $\hbar\omega$ and momentum transfer $\hbar k$. The dielectric function contains contributions from both valence and core electrons. References 4 and 5 describe the steps for calculating $\varepsilon(k,\omega)$ for insulators and metals, respectively. For an electron of energy E, the probability of an energy loss ω per unit distance is given by [2]

$$\tau(E,\hbar\omega) = \frac{1}{\pi a_0 E} \int_{k_-}^{k_+} \frac{dk}{k} \operatorname{Im} \left[\frac{-1}{\varepsilon(k,\omega)} \right] , \qquad (1)$$

where $\hbar k_{\pm} = \sqrt{2m}(\sqrt{E} \pm \sqrt{E - \hbar \omega})$ and $a_0 = \hbar^2 / me^2$. The quantity $\tau(E,\hbar\omega)$ is also known as the differential inverse mean free path, because by integrating it over all allowed energy transfers, the inelastic mean free path (IMFP) is obtained. Furthermore, an integration of $\hbar\omega\tau(E,\hbar\omega)$ over all allowed energy transfers gives the energy loss per unit path length, or stopping power S(E) The stopping power can then be used to calculate the distance it takes to slow an electron down

to a given energy. This distance is called the continuous slowing down approximation range, or CSDA range, because the calculation assumes that the electron slows down continuously from the initial energy E to the final energy, which is usually taken to be 10 eV [2]. The CSDA range $R_0(E)$ is given by

$$R_0(E) = \int_{10\text{eV}}^{E} \frac{dE'}{S(E')}$$
 (2)

The calculations for IMFP and stopping power have been carried out down to 10 eV for a number of materials, including SiO₂ [3]; polystyrene [2]; polyethylene [6]; collodion [7]; and silicon, aluminum, nickel, copper, and gold [5]. The CSDA ranges from 15 eV to 6 keV were then calculated for polystyrene, silicon, and gold by integrating Eq. (2) and are shown in Fig. 3-3. These curves can be used with confidence down to 100 eV. However, comparisons of different available calculations with the meager experimental data below 100 eV indicate that errors as large as 100% may occur at 10 eV. An example of this is shown in the figure, where experimental range data for collodion are given. It is clear that the agreement between the collodion and polystyrene data starts to become reasonable above 100 eV. The differences below 100 eV could equally well be due to problems with the theory or to the increased difficulty of the measurement. Stopping-power calculations for polymethyl methacrylate (PMMA) have been carried out only from 100 eV, so that the CSDA range as defined above could not be calculated [4]. However, data on effective electron ranges of photoelectrons in PMMA at several energies can be found in Ref. 8.

B. ELECTRON INELASTIC MEAN FREE PATHS

A very important aspect of photoelectron spectroscopy, especially with synchrotron radiation, is the ability to effectively tune the surface sensitivity from a few angstroms or a few tens of angstroms in core-level photoemission measurements to a few hundred angstroms in total-electron-yield surface EXAFS experiments. This variation arises from the fact that the IMFP of the photoemitted electrons is a strong function of the electron kinetic energy, which can be tuned by the appropriate choice of photon energy. The definition of the IMFP

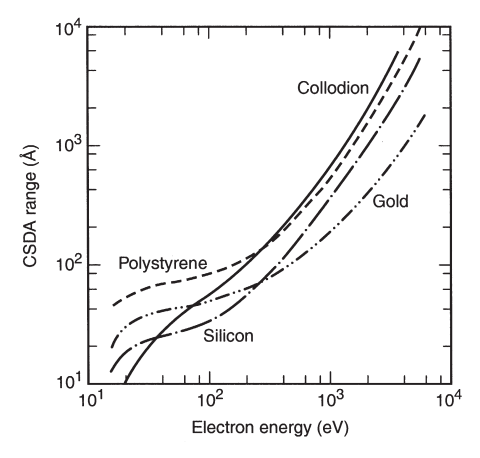


Fig. 3-3. Plot of the CSDA range, as a function of energy, for gold and silicon [5] and for polystyrene, (CgH₈)_n, with a density of 1.05 g/cm³ [2]. The measured electron range in collodion with a density of 1 g/cm³ is also plotted [7].

[9] is the average distance traveled by an electron between inelastic collisions. Although the exact relationship between the IMFP and kinetic energy depends on the detailed electronic structure of the element or compound of interest, the general features are similar for all elements, starting at large values for kinetic energies below 10–15 eV, dropping to a minimum value of 5–10 Å at kinetic energies between 30 and 100 eV, and then rising monotonically above 100 eV.

Since the surface sensitivity is determined by the depth perpendicular to the surface from which electrons can escape, it is best defined using the mean escape depth (MED), which is related to the IMFP by

$$\Delta = \lambda_i \cos \alpha \quad , \tag{3}$$

where Δ is the MED, λ_i is the IMFP, and α is the emission angle of the electrons relative to the surface normal. However, it should be noted that elastic scattering effects within the solid could increase the MED as much as a factor of two at electron emission angles greater than 60°, depending on the angle of incidence of the incoming x-rays and the particular core level being studied [9,10]. Therefore, the standard technique of increasing the surface sensitivity by working at glancing emission angles using Eq. (3) must be qualified to take these effects into account. In addition, both angle-dependent cross sections and photoelectron diffraction effects can result in anisotropic emission from the solid that can also cause errors in the interpretation of the MEDs in solids. Because of these complications, graphs of the IMFPs, rather than the MEDs, versus electron kinetic energy will be presented here to give a measure of the surface sensitivity. The reader is referred to Ref. 9 when more complicated experimental conditions need to be considered

Using the formalism developed by Penn that uses optical data to determine the IMFP of a material [11], Tanuma et al. have calculated the IMFPs for a large number of elements and compounds for kinetic energies up to 2000 eV [12-14]. Figure 3-4 shows IMFP curves for Ag, Al, Na, PMMA, Si, and SiO₂. These materials are representative of a fairly wide variety of materials for kinetic energies between 200 and 2000 eV. For example, the IMFPs for Ni, Ta, W, Pt, and Au all hover around the values given here for Ag; Cr, Fe, and Cu fall between Al and Ag. Likewise, C falls between Si and SiO2, whereas GaAs overlies the PMMA curve for much of this energy range. The behavior below 200 eV is more complex, because the IMFPs are strongly dependent on the details of the electronic structure. Figure 3-5 shows the region below 250 eV for Al. Ag. GaAs. Na, PMMA, and Si. Silicon dioxide is not shown here because it overlaps the PMMA curve in this range, whereas GaAs does not. Although the calculations below 50 eV may not be reliable, owing to limitations in the theory, the values are plotted at these low energies to show the general behavior of the IMFPs in this region, as well as the location of the minima for the different materials. Calculations for additional materials

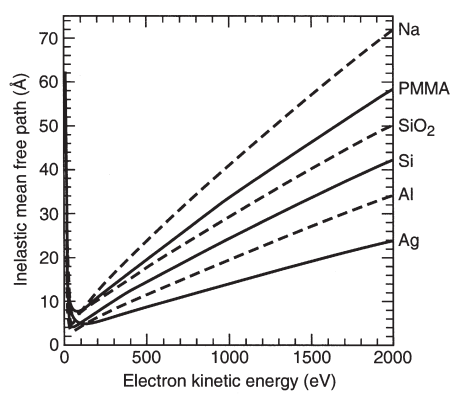


Fig. 3-4. Inelastic mean free paths for electron kinetic energies up to 2000 eV, for Ag, Al, Na, PMMA, Si, and SiO₂.

can be found in the literature as follows: (i) elements from C to Bi [12]; (ii) III-V and II-VI compound semiconductors, alkali halides, Si₃N₄, and several oxides [13]; and (iii) organic compounds [14]. Calculations are being presented here because they provide the most complete and consistent set of values for the IMFPs. References 9 and 10 give the historical background for both the theory and the experimental work in this field and show that it is difficult to generalize much of the experimental data in the literature, owing to the experiment-specific effects described above, as well as uncertainties in sample preparation. Seah and Dench [15] were the first to classify the material dependence of the IMFPs and presented data for kinetic energies up to 10 keV. A good example of the care that is needed in determining IMFPs is given in Ref. 8, which is a study of the Si/SiO2 system. Finally, it should be mentioned that spin-dependent effects on the IMFP have also been observed in ferromagnetic materials [17].

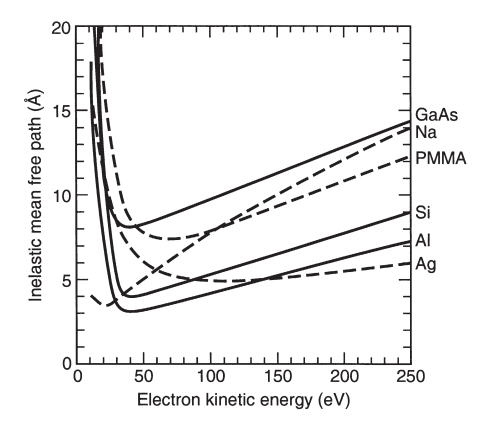


Fig. 3-5. Detail of the inelastic mean free paths in the kinetic energy range below 250 eV, for Ag, Al, GaAs. Na. PMMA. and Si.

REFERENCES

- T. E. Everhart and P. H. Hoff, "Determination of Kilovolt Electron Energy Dissipation vs Penetration Distance in Solid Materials," J. Appl. Phys. 42, 5837 (1971).
- J. C. Ashley, J. C. Tung, and R. H. Ritchie, "Inelastic Interactions of Electrons with Polystyrene: Calculations of Mean Free Paths, Stopping Powers, and CSDA Ranges," *IEEE Trans. Nucl. Sci.* NS-26, 1566 (1978).
- J. C. Ashley and V. E. Anderson, "Interaction of Low Energy Electrons with Silicon Dioxide," *J. Elect. Spectrosc.* 24, 127 (1981).
- J. C. Ashley, "Inelastic Interactions of Low Energy Electrons with Organic Solids: Simple Formulae for Mean Free Paths and Stopping Powers," *IEEE Trans. Nucl. Sci.* NS-27, 1454 (1980).

- J. C. Ashley, C. J. Tung, R. H. Ritchie, and V. E. Anderson, "Calculations of Mean Free Paths and Stopping Powers of Low Energy Electrons (< 10 keV) in Solids Using a Statistical Model," *IEEE Trans. Nucl. Sci.* NS-23, 1833 (1976).
- J. C. Ashley, "Energy Losses and Elastic Mean Free Path of Low Energy Electrons in Polyethylene," *Radiat. Res.* 90, 433 (1982).
- A. Cole, "Absorption of 20 eV to 50 keV Electron Beams in Air and Plastic," Radiat. Res. 38, 7 (1969).
- R. Feder, E. Spiller, and J. Topalian, "X-Ray Lithography," *Polymer Eng. Sci.* 17, 385 (1977).
- C. J. Powell, A. Jablonski, I. S. Tilinin, S. Tanuma, and D. R. Penn, "Surface Sensitivity of Auger-Electron Spectroscopy and X-Ray Photoelectron Spectroscopy," *J. Elect. Spectrosc.* 98–99, 1 (1999).
- A. Jablonski and C. J. Powell, "Relationships between Electron Inelastic Mean Free Paths, Effective Attenuation Lengths, and Mean Escape Depths," *J. Elect. Spectrosc.* 100, 137 (1999).
- D. R. Penn, "Electron Mean-Free-Path Calculations Using a Model Dielectric Function," *Phys. Rev. B* 35, 482 (1987).
- S. Tanuma, C. J. Powell, and D. R. Penn, "Calculations of Electron Inelastic Mean Free Paths. II. Data for 27 Elements over the 50–2000 eV Range," Surf. Interface Anal. 17, 911 (1991).
- S. Tanuma, C. J. Powell, and D. R. Penn, "Calculations of Electron Inelastic Mean Free Paths. III. Data for 15 Inorganic Compounds over the 50–2000 eV Range." Surf. Interface Anal. 17, 927 (1991).
- S. Tanuma, D. J. Powell, and D. R. Penn, "Calculations of Electron Inelastic Mean Free Paths. V. Data for 14 Organic Compounds over the 50–2000 eV Range," Surf. Interface Anal. 21, 165 (1991).
- M. P. Seah and W. A. Dench, "Quantitative Electron Spectroscopy of Surfaces: A Standard Data Base for Electron Inelastic Mean Free Paths in Solids," Surf. Interface Anal. 1, 2 (1979).

- F. J. Himpsel, F. R. McFeely, A. Taleb-Ibrahimi, and J. A. Yarmoff, "Microscopic Structure of the SiO₂/Si Interface," *Phys. Rev. B* 38, 6084 (1988).
- H. Hopster, "Spin Dependent Mean-Free Path of Low-Energy Electrons in Ferromagnetic Materials," J. Elect. Spectrosc. 98-99, 17 (1999).

SECTION 4

OPTICS AND DETECTORS

4.1 MULTILAYERS AND CRYSTALS

James H. Underwood

A. MULTILAYERS

Multilayered structures consisting of alternating layers of highand low-Z materials, with individual layers having thicknesses of the order of nanometers, can be fabricated using sputtering or evaporation on suitable smooth substrates. These structures act as multilayer interference reflectors for x-rays, soft x-rays, and extreme ultraviolet (EUV) light. Their high reflectivity and moderate energy bandwidth (10 < $E/\Delta E$ < 100) make them a valuable addition to the range of optical components useful in instrumentation for EUV radiation and x-rays with photon energies from a few hundred eV to tens of keV. Multilayer reflectors have a wide range of applications in the EUV region, where normalincidence multilayer reflectors allow the construction of space telescopes and of optics for EUV lithography. Multilayers are useful as mirrors and dispersive elements on synchrotron radiation beamlines. They may be used to produce focal spots with micrometer-scale sizes and for applications such as fluorescent microprobing, microdiffraction, and microcrystallography.

Ordinary mirrors are useful in the EUV and x-ray regions when operated at glancing incidence (see Section 4.2). However, at near-normal incidence angles the reflectivity is typically very small. The reason is that the value of the complex refractive index, $n = 1 - \delta - i\beta$, is close to unity for all materials in this region. Although the normal-incidence intensity reflectivity of a surface

might be 10^2 to 10^4 , the corresponding *amplitude* reflectivity, r = (n-1)/(n+1), which is the square root of the intensity reflectivity, will be 1/10 to 1/100. This implies that, if the reflections from 10-100 surfaces could be made to add in phase, a total reflectivity approaching unity could be obtained. This is the multilayer principle. As shown in Fig. 4-1, a multilayer reflector comprises a stack of materials having alternately high and low refractive indices. The thicknesses are adjusted so that the path length difference between reflections from successive layer pairs is equal to one wavelength. Hence, x-ray/EUV multilayers are

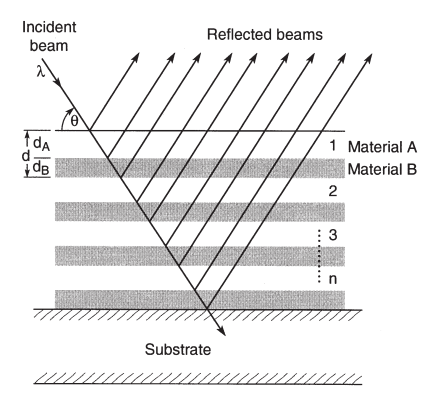


Fig. 4-1. Schematic of a multilayer reflector of n bilayer pairs. The parameters λ, θ, and d are chosen to satisfy the familiar Bragg equation, but the relative thicknesses of the high- and low-Z materials are also critical in optimizing reflectivity. The total reflectivity is the vector sum of the complex reflection coefficients at each interface, with the different path lengths taken into account.

approximately equivalent to the familiar "quarter-wave stacks" of visible-light coating technology. The equivalence is not exact, however, because of the absorption term B, which is usually negligible for visible-light multilayers. This absorption reduces the multilayer reflectivity below unity and requires the design to be optimized for highest reflectivity. This optimization normally requires modeling or simulation of the multilaver. Most thin-film calculation programs, even if designed for the visible region, will perform these calculations if given the right complex values of the refractive index. (An on-line calculation program is available at http://www.cxro.lbl.gov/.) Either elemental materials or compounds can be used to fabricate multilayer reflectors. The performance obtained from a multilayer depends largely on whether there exists a fortuitous combination of materials having the right refractive indices (good contrast, low absorption), whether these materials can be deposited in smooth thin layers, and whether they remain stable (low reactivity, low diffusion) in the deposited state. The roughness of the underlying substrate is also of prime importance; an rms roughness of the same order of magnitude as the layer thicknesses will spoil the performance of most coatings. "Superpolished" substrates, with roughness $\sigma \approx 0.1$ nm, are available. On such substrates, the peak reflectivity of the coatings can approach 80% to 90% of theoretical predictions.

A large variety of multilayers have been fabricated over the years. A database of reported reflectivities has been assembled from surveys taken at the biennial Physics of X-ray Multilayer Structures conferences and can be found at the website listed in Fig. 4-2. The reported near-normal incidence reflectivity is shown in Fig. 4-2 for photon energies below 600 eV. The highest reflectivity (~ 70%) is obtained for the EUV region around 100 eV by multilayers Mo-Si and Mo-Be (see Fig. 4-2). This relatively high reflectivity is the basis for current efforts in the field of EUV lithography. At hard x-ray wavelengths near 10 keV, a commonly used multilayer is made with tungsten as the high-Z material and boron carbide (B₄C) as the low-Z material. A reflectivity of 84% has been achieved with this combination at 8048 eV, the energy of the Cu Ku line (see Fig. 4-3).

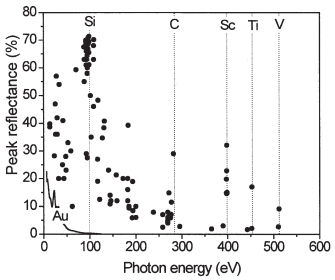


Fig. 4-2. The peak reflectivity achieved for multilayer mirrors at near-normal incidence versus photon energy. The data are based on the results of surveys taken at the biennial Physics of X-Ray Multilayer Structures conferences (maintained at http://www.cxro.lbl.gov/multilayer/survey.html). The normal incidence reflectivity of a gold mirror is shown for reference.

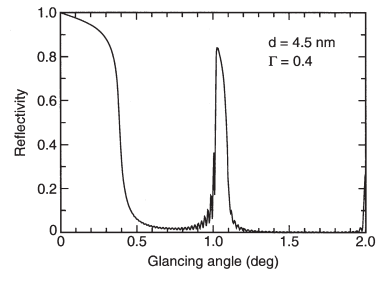


Fig. 4-3. The reflectivity of a tungsten-boron carbide multilayer at 8048 eV. The parameters d and Γ are discussed in the text.

B. CRYSTALS

Dispersion of radiation by a periodic structure is formally equivalent to multiple-beam interferometry. Crystals and multilaver structures produce the N interfering beams by division of the incident amplitude. (Structures periodic across their surface and that produce the N interfering beams by division of the incident wave front are called gratings and are treated in Section 4.3.) The spectrum of the incident radiation is dispersed in angle according to the Bragg equation $n\lambda = 2d \sin \theta$, where n is an integer representing the order of the reflection, λ is the wavelength of the incident radiation, d is the period of the multilaver or crystal structure, and θ is the angle of glancing incidence. For a crystal, d is the lattice spacing, the perpendicular distance between the successive planes of atoms contributing to the reflection. These planes are designated by their Miller indices [(hkl) or, in the case of crystals belonging to the hexagonal group, (hkil). The value of 2d also represents the longest wavelength that the structure can diffract.

For 2d values greater than about 25 Å, the choice of natural crystals is very limited, and those available (such as prochlorite) are likely to be small and of poor quality. Sputtered or evaporated multilayers can be used as dispersing elements at longer wavelengths. (Langmuir-Blodgett films have seen limited use since the development of vacuum-deposited multilayers.)

Table 4-1 is a revision of one compiled by E. P. Bertin [1]. The crystals are arranged in order of increasing 2d spacing.

REFERENCE

 E. P. Bertin, "Crystals and Multilayer Langmuir-Blodgett Films Used as Analyzers in Wavelength-Dispersive X-Ray Spectrometers," in J. W. Robinson, Ed., Handbook of Spectroscom (CRC Press, Cleveland, 1974), vol. 1, p. 238.

specification of (hkl) or 2d are likely to be references to this "cut." The indicated useful wavelength region lies in dispersive element. A question mark (?) indicates that the crystal is developmental and that the indices have not indices {(hkl), or (hkil) for hexagonal crystals} are given for the diffracting planes parallel to the surface of the Data for selected crystals used as dispersive elements in x-ray spectrometers and monochromators. The Miller been ascertained. An asterisk following the indices indicates that literature references to this crystal without Table 4-1.

the 2θ interval between 10° and 140° . The analyzer should be used outside this region in special cases only.

					Oseful	
		Miller	•		wavelength	
No.	Crystal	indices	2d (Å)	Chemical formula	region (A)	Applications, remarks
-	α -Quartz, silicon dioxide (50 $\overline{5}$ 2)	(5052)	1.624	SiO ₂	0.142-1.55	Shortest 24 of any practical crystal. Good for high-Z K-lines excited by 100-kV generators.
2	Lithium fluoride	(422)	1.652	LIF	0.144-1.58	Better than quartz $(50\overline{5}2)$ for the same applications.
3	Corundum, aluminum oxide	(146)	1.660	Al ₂ O ₃	0.145-1.58	Same applications as quartz (5052)
4	Lithium fluoride	(420)	1.801	LiF	0.157-1.72	Similar to LiF (422).
S	Calcite, calcium carbonate	(633)	2.02	CaCO ₃	0.176-1.95	
9	α -Quartz, silicon dioxide (2243)	(2243)	2.024	SiO ₂	0.177-1.96	
7	α -Quartz, silicon dixoide	(3140)	2.3604	SiO ₂	0.205-2.25	Transmission-crystal optics.
œ	α -Quartz, silicon dioxide (22 $\overline{40}$)	(2240)	2.451	SiO ₂	0.213-2.37	

Improves dispersion for V–Ni K-lines and rare earth L-lines.	Diffracted intensity ~2~4X topaz (303) and quartz (203) with the same or better resolution.	Same applications as topaz (303) and LiF (220).		Same applications as topaz (303) and quarz. (2023), with 2-4X their diffracted intensity. Diffracted intensity ~0.4–0.8X Lifr (200).	Transmission-crystal optics (Cauchois, DuMond types).				Lattice period known to high accuracy.		
0.236-2.59	0.240-2.62	0.240-2.62	0.244-2.67	0.248-2.72	0.262-2.86	0.264-2.93	0.269-2.94	0.317-3.47	0.335-3.66	0.337-3.68	0.349-3.82
$Al_2(F,OH)_2SiO_4$	Al ₂ O ₃	SiO ₂	Al ₂ (F,OH) ₂ SiO ₄	LiF	$K_2O\cdot 3Al_2O_3\cdot 6SiO_2\cdot 2H_2O$	CaCO ₃	SiO ₂	SiO ₂	Si	CaF_2	Ge
2.712	2.748	2.749	2.795	2.848	3.00	3.034	3.082	3.636	3.8403117	3.862	4.00
(303)*	(030)	(20 <u>2</u> 3)	(900)	(220)	(331)	(422)	(2131)	(1122)	(220)	(220)	(220)
Topaz, hydrated aluminum fluorosilicate	Corundum, aluminum oxide, sapphire, alumina	α -Quartz, silicon dioxide (20 $\overline{2}$ 3)	Topaz	Lithium fluoride	Mica, muscovite	Calcite, calcium carbonate	α -Quartz, silicon dioxide (21 $\overline{3}$ 1)	α -Quartz, silicon dioxide	Silicon	Fluorite, calcium fluoride	Germanium
6	01	=	12	13	4	15	16	17	18	61	20

Table 4-1. Selected data for crystals (continued).

Applications, remarks	Best general crystal for K K- to Lr L- lines. Highest intensity for largest number of elements of any crystal. Combines high intensity and high dispersion.	Curved, especially doubly curved, optics.	"Prism" cut.	Used in prototype Laue multichannel spectrometer.		Curved, especially doubly curved, optics.		Efflorescent: loses water in vacuum to become Plaster of Paris.	S $K\alpha$ and CI $K\alpha$ in light matrixes. Like LiF (200), good general crystal for S K to Lr L .
Useful wavelength region (Å)	0.351-3.84	0.353-3.86	0.370-4.11	0.398-4.35	0.405-4.43	0.408-4.46	0.428-4.75	0.435-4.76	0.492–5.38
Chemical formula	LiF	ΑΙ	SiO ₂	SiO_2	$Al_2(F,OH)_2SiO_4$	ΥI	SiO2	CaSO ₄ ·2H ₂ O	NaCi
2d (Å)	4.027	4.048	4.246	4.564	4.638	4.676	4.912	4.990	5.641
Miller	(200)*	(200)	(20 <u>2</u> 0)	(1012)	(200)	(111)	(11 <u>2</u> 0)	(003)	(200)
Crystal	Lithium fluoride	Aluminum	α -Quartz, silicon dioxide (20 $\overline{2}$ 0)	α -Quartz, silicon dioxide	Topaz	Aluminum	α-Quartz, silicon dioxide	Gypsum, calcium sulfate dihydrate	Rock salt, sodium chloride
No.	21	22	23	24	25	26	27	28	29

Very precise wavelength measurements. Extremely high degree of crystal perfection with resultant sharp lines.		Very rugged and stable general-purpose crystal. High degree of perfection obtainable.		Very weak second order, strong third order.	Eliminates second order. Useful for intermediate- and low-Z elements where Ge $K\alpha$ emission is eliminated by pulse-height selection.		P $K\alpha$ in low-Z matrixes, especially in calcium. Intensity for P-K K-lines greater than EDDT, but less than PET.	P, S, Cl K -lines, P $K\alpha$ intensity > 5 X -EDDT. Relatively poor resolution but high integrated reflectivity.	Important for K-edge of Si.
0.529-5.79	0.535-5.86	0.547-5.98	0.549-6.00	0.550-6.02	0.570-6.23	0.574-6.28	0.583-6.38	0.585-6.40	0.652-7.23
CaCO ₃	$NH_4H_2PO_4$	Si	KCI	CaF ₂	95	KBr	SiO_2	S	InSb
6.071	6.14	6.2712	6.292	6.306	6.532	6.584	6.687	802'9	7.4806
(200)	(112)	(111)*	(200)	(111)	(111)*	(200)	(1010)	(003)	(111)
Calcite, calcium carbonate	Ammonium dihydrogen phosphate (ADP)	Silicon	Sylvite, potassium chloride	Fluorite, calcium fluoride	Germanium	Potassium bromide	α-Quartz, silicon dioxide	Graphite	Indium antimonide

Table 4-1. Selected data for crystals (continued).

		Miller			Useful wavelength	
No.	Crystal	indices	2d (Å)	Chemical formula	region (Å)	Applications, remarks
40	Ammonium dihydrogen phosphate (ADP)	(200)	7.5	$\mathrm{NH_4H_2PO_4}$	0.654-7.16	Higher intensity than EDDT.
41	Topaz	(000)	8.374	Al ₂ (F,OH) ₂ SiO ₄	0.730-7.99	
42	α -Quartz, silicon dioxide	(1010) *	8.512	SiO ₂	0.742-8.12	Same applications as EDDT and PET; higher resolution, but lower intensity.
43	Pentaerythritol (PET)	(005)	8.742	C(CH ₂ OH) ₄	0.762–8.34	Al, Si, P, S, Cl $K\alpha$. Intensities ~1.5-2X EDDT, ~2.5X KHP. Good general crystal for Al–Sc $K\alpha$. Soft; deteriorates with age and exposure to x-rays.
4	Ammonium tartrate	(3)	8.80	(CHOH) ₂ (COONH ₄) ₂	0.767-8.4	
45	Ethylenediamine-d-tartrate (EDDT, EDdT, EDT)	(020)	8.808	$NH_2 - CH_2 - CH_2 - NH_2$	0.768-8.40	Same applications as PET, but lower intensity, substantially lower thermal expansion coefficient. Rugged and stable.
46	Ammonium dihydrogen phosphate (ADP)	*(101)	10.640	$\mathrm{NH_4H_2PO_4}$	0.928-10.15	Mg $K\alpha$. Same applications as PET, EDDT, but lower intensity.
47	Na β -alumina	(0004)	11.24	$NaAl_{11}O_{17}$	0.980-10.87	
84	Oxalic acid dihydrate	(100)	11.92	(COOH)2·2H2O	1.04-11.37	

\$ 33

57

28

64

20

51

Table 4-1. Selected data for crystals (continued).

No.	Crystal	Miller	2d (Å)	Chemical formula	Useful wavelength region (Å)	Applications, remarks
59	Rubidium hydrogen phthalate (RHP, RbHP, RAP, RbAP)	(100)	26.121	$ m RbHC_8H_4O_4$	2.28–24.92	Diffracted intensity ~3X KHP for Na, Mg, Al $K\alpha$ and Cu $L\alpha$; ~4X KHP for F $K\alpha$; ~8X KHP for O $K\alpha$
09	Potassium hydrogen phthalate (KHP, KAP)	(100)	26.632	$\mathrm{KHC_8H_4O_4}$	2.32–25.41	Good general crystal for all low-Z elements down to O.
19	Octadecyl hydrogen maleate (OHM)	6	63.5	СН ₃ (СН ₂) ₁₇ ООС(СН) ₂ СООН	5.54-60.6	Ultralong-wavelength region down to C $K\alpha$

4.2 SPECULAR REFLECTIVITIES FOR GRAZING-INCIDENCE MIRRORS

Eric M. Gullikson

The specular reflectivity of six common materials is given in Figs. 4-4 and 4-5 for photon energies between 30 eV and 30 keV. The reflectivity for a perfectly smooth surface and for s-polarization is

$$R = |r|^2 = \frac{|k_{iz} - k_{tz}|^2}{|k_{iz} + k_{tz}|^2} , \qquad (1)$$

where

$$k_{iz} = \frac{2\pi}{\lambda} \cos \theta$$
 and $k_{tz} = \frac{2\pi}{\lambda} \sqrt{n^2 - \cos^2 \theta}$

The grazing angle θ is measured from the plane of the mirror surface. The normal components of the incident and transmitted wave vectors are k_{tz} and k_{tz} , respectively. The complex index of refraction n is obtained from the average atomic scattering factor of the material, as described in Section 1.7 and in Ref. 1.

The effect of high-spatial-frequency roughness on the reflection coefficient of an interface can be approximated by the multiplicative factor

$$r = r_0 \exp(-2k_{i7}k_{t7}\sigma^2)$$
 , (2)

where r_0 is the complex reflection coefficient of a perfectly smooth interface and σ is the rms roughness. For updated values of the atomic scattering factors and for on-line reflectivity calculations, see http://www.cxro.lbl.gov/optical_constants/.

REFERENCE

 B. L. Henke, E. M. Gullikson, and J. C. Davis, "X-Ray Interactions: Photoabsorption, Scattering, Transmission, and Reflection at E = 50–30,000 eV, Z = 1–92," At. Data Nucl. Data Tables 54, 181 (1993).

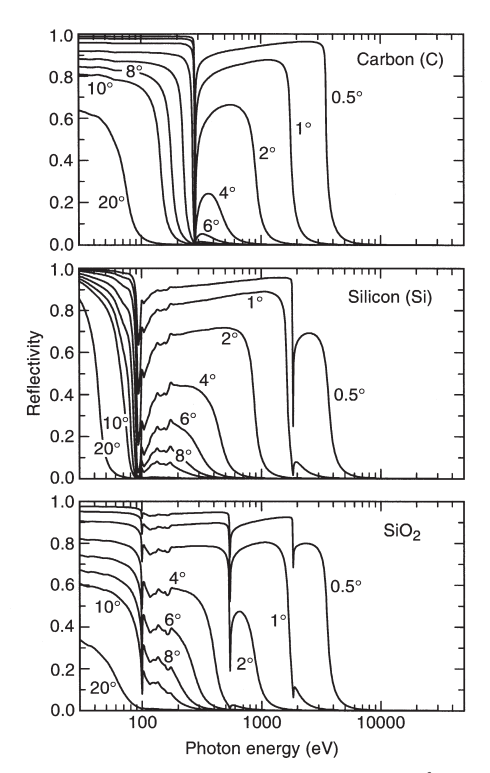


Fig. 4-4. Specular reflectivities of carbon ($\rho = 2.2 \text{ g/cm}^3$), silicon ($\rho = 2.33 \text{ g/cm}^3$), and silicon dioxide ($\rho = 2.2 \text{ g/cm}^3$). The reflectivity is calculated for spolarization at grazing angles of 0.5, 1, 2, 4, 6, 8, 10, and 20 degrees.

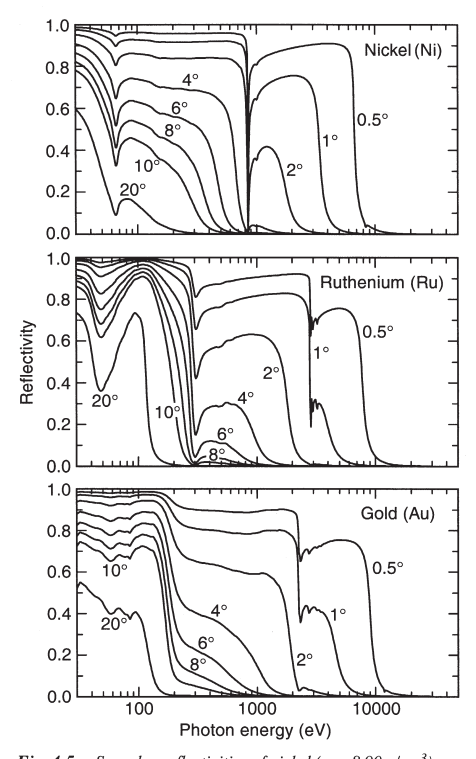


Fig. 4-5. Specular reflectivities of nickel ($\rho = 8.90 \text{ g/cm}^3$), ruthenium ($\rho = 12.41 \text{ g/cm}^3$), and gold ($\rho = 19.3 \text{ g/cm}^3$). The reflectivity is calculated for spolarization at grazing angles of 0.5, 1, 2, 4, 6, 8, 10, and 20 degrees.

4.3 GRATINGS AND MONOCHROMATORS

Malcolm R Howells

A more complete version of this document is available at http:// www.cxro.lbl.gov/. The web version includes additional references to original sources, and values for coefficients given here to fourth order are given there to sixth order.

A. DIFFRACTION PROPERTIES

A.1 Notation and sign convention

We adopt the notation of Fig. 4-6, in which α and β have opposite signs if they are on opposite sides of the normal.

A.2 Grating equation

The grating equation may be written

$$m\lambda = d_0(\sin\alpha + \sin\beta) \quad . \tag{1}$$

The angles α and β are both arbitrary, so it is possible to impose various conditions relating them. If this is done, then for each λ , there will be a unique α and β . The following conditions are used:

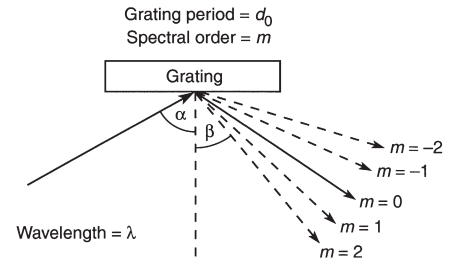


Fig. 4-6. Grating equation notation.

(i) On-blaze condition:

$$\alpha + \beta = 2\theta_{\rm B} \quad , \tag{2}$$

where $\theta_{\rm B}$ is the blaze angle (the angle of the sawtooth). The grating equation is then

$$m\lambda = 2d_0 \sin \theta_{\rm B} \cos(\beta + \theta_{\rm B}) \qquad . \tag{3}$$

(ii) Fixed in and out directions:

$$\alpha - \beta = 2\theta$$
 , (4)

where 2θ is the (constant) included angle. The grating equation is then

$$m\lambda = 2d_0 \cos\theta \sin(\theta + \beta)$$
 (5)

In this case, the wavelength scan ends when α or β reaches 90°, which occurs at the horizon wavelength $\lambda_{\rm H} = 2d_0 \cos^2 \theta$.

- (iii) Constant incidence angle: Equation (1) gives β directly.
- (iv) Constant focal distance (of a plane grating):

$$\frac{\cos \beta}{\cos \alpha} = \text{a constant } c_{\text{ff}}$$
, (6)

leading to a grating equation

$$1 - \left(\frac{m\lambda}{d} - \sin\beta\right)^2 = \frac{\cos^2\beta}{c_{\text{ff}}^2} \quad . \tag{7}$$

Equations (3), (5), and (7) give β (and thence α) for any λ . Examples of the above α - β relationships are (for references see http://www.cxro.lbl.gov/):

- (i) Kunz et al. plane-grating monochromator (PGM), Hunter et al. double PGM, collimated-light SX700 PGM
- (ii) Toroidal-grating monochromators (TGMs), sphericalgrating monochromators (SGMs, "Dragon" system), Seya-Namioka, most aberration-reduced holographic SGMs, variable-angle SGM, PGMs
- (iii) Spectrographs, "Grasshopper" monochromator
- (iv) Standard SX700 PGM and most variants

B. FOCUSING PROPERTIES

The study of diffraction gratings (for references see http://www.cxro.lbl.gov/) goes back more than a century and has included plane, spherical [1], toroidal, and ellipsoidal surfaces and groove patterns made by classical ("Rowland") ruling [2], holography [3,4], and variably spaced ruling [5,6]. In recent years the optical design possibilities of holographic groove patterns and variably spaced rulings have been extensively developed. Following normal practice, we provide an analysis of the imaging properties of gratings by means of the path function F [7]. For this purpose we use the notation of Fig. 4-7, in which the zeroth groove (of width d_0) passes through the grating pole O, while the nth groove passes through the variable point $P(\xi, w, l)$. The holographic groove pattern is taken to be made using two coherent point sources C and D with cylindrical polar coordinates $(r_C, \gamma, z_C), (r_D, \delta, z_D)$ relative to O. The lower (upper) sign in Eq. (9) refers to C and D both real or both virtual (one real and one virtual), for which case the equiphase surfaces are confocal hyperboloids (ellipses) of revolution about CD. Gratings with varied line spacing d(w) are assumed to be ruled according to d(w)

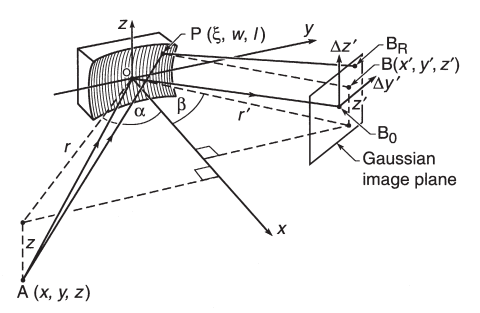


Fig. 4-7. Focusing properties notation.

= $d_0(1 + v_1w + v_2w^2 + ...)$. We consider all the gratings to be ruled on the general surface

$$x = \sum_{ij} a_{ij} w^i l^j$$

and the a_{ii} coefficients are given below.

Ellipse coefficients aii

$$a_{20} = \frac{\cos \theta}{4} \left(\frac{1}{r} + \frac{1}{r'} \right) \qquad a_{12} = \frac{a_{20}A}{\cos^2 \theta}$$

$$a_{30} = a_{20}A \qquad a_{22} = \frac{a_{20}(2A^2 + C)}{2\cos^2 \theta}$$

$$a_{40} = \frac{a_{20}(4A^2 + C)}{4} \qquad a_{04} = \frac{a_{20}C}{8\cos^2 \theta}$$

$$a_{02} = \frac{a_{20}}{2\cos^2 \theta}$$

$$a_{02} = \frac{a_{20}}{\cos^2 \theta}$$

The other a_{ii} 's with $i + j \le 4$ are zero. In the expressions above, r, r', and θ are the object distance, image distance, and incidence angle to the normal, respectively, and

$$A = \frac{\sin \theta}{2} \left(\frac{1}{r} - \frac{1}{r'} \right)$$
, $C = A^2 + \frac{1}{rr'}$.

Toroid coefficients aii

$$a_{20} = \frac{1}{2R} \qquad a_{22} = \frac{1}{4\rho R^2}$$

$$a_{40} = \frac{1}{8R^3} \qquad a_{04} = \frac{1}{8\rho^3}$$

$$a_{02} = \frac{1}{2\rho}$$

Other a_{ij} 's with $i + j \le 4$ are zero. Here, R and ρ are the major and minor radii of the bicycle-tire toroid.

The a_{ij} 's for spheres; circular, parabolic, and hyperbolic cylinders; paraboloids; and hyperboloids can also be obtained from the values above by suitable choices of the input parameters $r,\,r'$, and θ .

Values for the ellipse and toroid coefficients are given to sixth order at http://www.cxro.lbl.gov/.

B.1 Calculation of the path function F

F is expressed as

$$F = \sum_{ijk} F_{ijk} w^i l^j \quad , \tag{8}$$

where

$$F_{ijk} = z^k C_{ijk}(\alpha,r) + z'^k C_{ijk}(\beta,r') + \frac{m\lambda}{d_0} f_{ijk}$$

and the f_{ijk} term, originating from the groove pattern, is given by one of the following expressions:

$$f_{ijk} = \begin{cases} 1 \text{ when } ijk = 100, \ 0 \text{ otherwise} & \text{Rowland} \\ \frac{d_0}{\lambda_0} \left[z_C^k C_{ijk}(\gamma, r_C) \pm z_D^k C_{ijk}(\delta, r_D) \right] \text{ holographic} \\ n_{ijk} & \text{varied line spacing} \end{cases}$$
(9)

The coefficient F_{ijk} is related to the strength of the i,j aberration of the wavefront diffracted by the grating. The coefficients C_{ijk} and n_{ijk} are given below, where the following notation is used:

$$T = T(r,\alpha) = \frac{\cos^2 \alpha}{r} - 2a_{20} \cos \alpha \tag{10a}$$

and

$$S = S(r,\alpha) = \frac{1}{r} - 2a_{02}\cos\alpha \quad . \tag{10b}$$

Coefficients Cijk of the expansion of F

$$\begin{split} C_{011} &= -\frac{1}{r} & C_{020} &= \frac{S}{2} & C_{022} &= -\frac{S}{4r^2} - \frac{1}{2r^3} \\ C_{031} &= \frac{S}{2r^2} & C_{040} &= \frac{4a_{02}^2 - S^2}{8r} - a_{04} \cos \alpha \\ C_{100} &= -\sin \alpha & C_{102} &= \frac{\sin \alpha}{2r^2} \\ C_{111} &= -\frac{\sin \alpha}{r^2} & C_{120} &= \frac{S\sin \alpha}{2r} - a_{12} \cos \alpha \\ C_{200} &= \frac{T}{2} & C_{202} &= -\frac{T}{4r^2} + \frac{\sin^2 \alpha}{2r^3} \\ C_{211} &= \frac{T}{2r^2} - \frac{\sin^2 \alpha}{r^3} & C_{300} &= -a_{30} \cos \alpha + \frac{T\sin \alpha}{2r} \\ C_{220} &= -a_{22} \cos \alpha + \frac{1}{4r} (4a_{20}a_{02} - TS - 2a_{12} \sin 2\alpha) + \frac{S\sin^2 \alpha}{2r^2} \\ C_{400} &= -a_{40} \cos \alpha + \frac{1}{2r} (4a_{20}^2 - T^2 - 4a_{30} \sin 2\alpha) + \frac{T\sin^2 \alpha}{2r^2} \end{split}$$

The coefficients for which $i \le 4, j \le 4, k \le 2, i + j + k \le 4, j + k = \text{even are included here.}$

Coefficients niik of the expansion of F

$$\begin{array}{ll} n_{ijk}=0 & {\rm for} & j,k\neq 0 \\ \\ n_{100}=1 & n_{300}=\frac{v_1^2-v_2}{3} \\ \\ n_{200}=\frac{-v_1}{2} & n_{400}=\frac{-v_1^3+2v_1v_2-v_3}{4} \end{array}$$

Values for C_{ijk} and n_{ijk} are given to sixth order at http://www.cxro.lbl.gov/.

B.2 Determination of the Gaussian image point

By definition the principal ray AOB_0 arrives at the Gaussian image point $B_0(r_0', \beta_0, z_0')$ in Fig. 4-7. Its direction is given by Fermat's principal, which implies $[\partial F/\partial w]_{w=0, l=0} = 0$ and $[\partial F/\partial l]_{w=0, l=0} = 0$, from which

$$\frac{m\lambda}{d_0} = \sin\alpha + \sin\beta_0 \tag{11a}$$

and

$$\frac{z}{r} + \frac{z'_0}{r'_0} = 0 \quad , \tag{11b}$$

which are the grating equation and the law of magnification in the vertical direction. The tangential focal distance r'_0 is obtained by setting the focusing term F_{200} equal to zero and is given by

$$T(r,\alpha) + T(r'_0,\beta_0) =$$

$$\begin{bmatrix} 0 & \text{Rowland} \\ -\frac{m\lambda}{\lambda_0} [T(r_{\text{C}},\gamma) \pm T(r_{\text{D}},\delta)] & \text{holographic} \\ \frac{\nu_1 m\lambda}{d_0} & \text{varied line spacing} \end{bmatrix}$$
(12)

Equations (11) and (12) determine the Gaussian image point B_0 and, in combination with the sagittal focusing condition ($F_{020} = 0$), describe the focusing properties of grating systems under the paraxial approximation. For a Rowland spherical grating the focusing condition, Eq. (12), is

$$\left(\frac{\cos^2\alpha}{r} - \frac{\cos\alpha}{R}\right) + \left(\frac{\cos^2\beta}{r'_0} - \frac{\cos\beta}{R}\right) = 0 \quad , \tag{13}$$

which has important special cases: (i) plane grating, $R = \infty$, implying

$$r_0' = -r\cos^2\alpha/\cos^2\beta = -r/c_{\rm ff}^2$$

so that the focal distance and magnification are fixed if c_{ff} is held constant; (ii) object and image on the Rowland circle, i.e., $r = R\cos\alpha$, $r'_0 = R\cos\beta$, M = 1; and (iii) $\beta = 90^\circ$ (Wadsworth condition). The focal distances of TGMs and SGMs, with or without moving slits, are also determined using Eq. (13).

B.3 Calculation of ray aberrations

In an aberrated system, the outgoing ray will arrive at the Gaussian image plane at a point B_R displaced from the Gaussian image point B_0 by the ray aberrations $\Delta y'$ and $\Delta z'$ (Fig. 4-7). The latter are given by

$$\Delta y' = \frac{r_0'}{\cos \beta_0} \frac{\partial F}{\partial w} \quad , \quad \Delta z' = r_0' \frac{\partial F}{\partial l} \,, \tag{14}$$

where F is to be evaluated for $A = (r, \alpha, z)$ and $B = (r'_0, \beta_0, z'_0)$. By means of the expansion of F, these equations allow the ray aberrations to be calculated separately for each aberration type:

$$\Delta y'_{ijk} = \frac{r'_0}{\cos \beta_0} \, F_{ijk} i w^{i-1} l^j \, , \, \Delta z'_{ijk} = r'_0 F_{ijk} w^i j l^{j-1} \quad . \quad (15)$$

Moreover, provided the aberrations are not too large, they are additive, so that they may either reinforce or cancel.

C. DISPERSION PROPERTIES

Dispersion properties can be summarized by the following relations.

(i) Angular dispersion:

$$\left(\frac{\partial \lambda}{\partial \beta}\right)_{\alpha} = \frac{d\cos\beta}{m} \quad . \tag{16}$$

(ii) Reciprocal linear dispersion:

$$\left(\frac{\partial \lambda}{\partial (\Delta y')}\right)_{\alpha} = \frac{d\cos\beta}{mr'} = \frac{10^{-3} d[\text{Å}]\cos\beta}{mr'[\text{m}]} \text{Å/mm} \quad . \quad (17)$$

(iii) Magnification:

$$M(\lambda) = \frac{\cos \alpha}{\cos \beta} \frac{r'}{r} . \tag{18}$$

(iv) Phase-space acceptance (ε):

$$\varepsilon = N\Delta\lambda_{S1} = N\Delta\lambda_{S2}$$
 (assuming $S_2 = MS_1$), (19)

where N is the number of participating grooves.

D. RESOLUTION PROPERTIES

The following are the main contributions to the width of the instrumental line spread function. An estimate of the total width is the vector sum.

(i) Entrance slit (width S₁):

$$\Delta \lambda_{S1} = \frac{S_1 d \cos \alpha}{mr} \quad . \tag{20}$$

(ii) Exit slit (width S2):

$$\Delta \lambda_{S2} = \frac{S_2 d \cos \beta}{mr'} \quad . \tag{21}$$

(iii) Aberrations (of perfectly made grating):

$$\Delta \lambda_{\rm A} = \frac{\Delta y' d \cos \beta}{mr'} = \frac{d}{m} \left(\frac{\partial F}{\partial w} \right) \quad . \tag{22}$$

(iv) Slope error Δφ (of imperfectly made grating):

$$\Delta \lambda_{\rm SE} = \frac{d(\cos\alpha + \cos\beta)\Delta\phi}{m} \quad . \tag{23}$$

Note that, provided the grating is large enough, diffraction at the entrance slit always guarantees a coherent illumination of enough grooves to achieve the slit-width-limited resolution. In such case a diffraction contribution to the width need not be added to the above.

E. EFFICIENCY

The most accurate way to calculate grating efficiencies is by the full electromagnetic theory [8]. However, approximate scalar-theory calculations are often useful and, in particular, provide a way to choose the groove depth h of a laminar grating. According to Bennett, the best value of the groove-width-to-period ratio r is the one for which the usefully illuminated area of the groove bottom is equal to that of the top. The scalar-theory efficiency of a laminar grating with r = 0.5 is given by Franks et al. as

$$E_0 = \frac{R}{4} \left[1 + 2(1-P)\cos\left(\frac{4\pi h \cos\alpha}{\lambda}\right) + (1-P)^2 \right]$$

$$E_{m} = \begin{cases} \frac{R}{m^{2}\pi^{2}} [1 - 2\cos Q^{+} \cos(Q^{-} + \delta)] & (24) \\ + \cos^{2} Q^{+}] & m = \text{odd} \\ \frac{R}{m^{2}\pi^{2}} \cos^{2} Q^{+} & m = \text{even} \end{cases}$$

where

$$\begin{split} P &= \frac{4h\tan\alpha}{d_0} \quad , \\ Q^\pm &= \frac{m\pi h}{d_0} (\tan\alpha \pm \tan\beta) \quad , \\ \delta &= \frac{2\pi h}{d_0} (\cos\alpha + \cos\beta) \quad , \end{split}$$

and R is the reflectance at grazing angle $\sqrt{\alpha_G \beta_G}$, where

$$\alpha_{\rm G} = \frac{\pi}{2} - |\alpha|$$
 and $\beta_{\rm G} = \frac{\pi}{2} - |\beta|$

REFERENCES

- 1. H. G. Beutler, "The Theory of the Concave Grating," J. Opt. Soc. Am. 35, 311 (1945).
- H. A. Rowland, "On Concave Gratings for Optical Purposes," *Phil. Mag.* 16 (5th series), 197 (1883).
- G. Pieuchard and J. Flamand, "Concave Holographic Gratings for Spectrographic Applications," Final report on NASA contract number NASW-2146, GSFC 283-56,777 (Jobin Yvon, 1972).
- T. Namioka, H. Noda, and M. Seya, "Possibility of Using the Holographic Concave Grating in Vacuum Monochromators," Sci. Light 22, 77 (1973).
- T. Harada and T. Kita, "Mechanically Ruled Aberration-Corrected Concave Gratings," Appl. Opt. 19, 3987 (1980).
- M. C. Hettrick, "Aberration of Varied Line-Space Grazing Incidence Gratings," Appl. Opt. 23, 3221 (1984).
- H. Noda, T. Namioka, and M. Seya, "Geometrical Theory of the Grating," J. Opt. Soc. Am. 64, 1031 (1974).
- R. Petit, Ed., Electromagnetic Theory of Gratings, Topics in Current Physics, vol. 22 (Springer-Verlag, Berlin, 1980). An efficiency code is available from M. Neviere, Institut Fresnel Marseille, faculté de Saint-Jérome, case 262, 13397 Marseille Cedex 20, France (michel.neviere@ fresnel.fr).

4.4 ZONE PLATES

Janos Kirz and David Attwood

A zone plate is a circular diffraction grating. In its simplest form, a transmission Fresnel zone plate lens consists of alternate transparent and opaque rings. The radii of the zone plate edges are given by

$$r_n^2 = nf\lambda + n^2\lambda^2/4 \qquad , \tag{1}$$

where n is the zone number (opaque and transparent zones count separately), λ is the wavelength, and f is the first-order focal length. The zone plate lens can be used to focus monochromatic, uniform plane wave (or spherical wave) radiation to a small spot, as illustrated in Fig. 4.8, or can be used for near-axis point-by-point construction of a full-field image, as illustrated in Fig. 4.9. When used in imaging applications, it obeys the thin-lens formula

$$\frac{1}{p} + \frac{1}{q} = \frac{1}{f} \quad , \tag{2}$$

where p and q are the object and image distances, respectively. Note that the second term on the right-hand side of Eq. (1) is correct only for p < q or p > q, which are the common cases in zone plate applications. Descriptions of the diffractive properties of zone plate lenses, their use in x-ray microscopes, and extensive references to the literature are given elsewhere [1–3].

A zone plate lens is fully specified by three parameters. Most applications are dominated by the choice of photon energy $\hbar \omega$, and thus by λ . Resolution is set in large part by λ and the outer zone width, $\Delta r = r_N - r_{N-1}$. To avoid chromatic blurring, the number of zones, N, must be less than the inverse relative spectral bandwidth, $\lambda \Delta \lambda$. Thus, for many applications, λ , Δr , and N constitute a natural set of zone plate–defining parameters. In terms of these three basic parameters, other zone plate parameters are given by [3]

$$D = 4N\Delta r \tag{3}$$

$$f = 4N(\Delta r)^2 / \lambda \tag{4}$$

$$F^{\#} = \Delta r / \lambda \tag{5}$$

$$NA = \lambda / 2\Delta r \quad . \tag{6}$$

To avoid chromatic blurring requires that

$$N < \lambda / \Delta \lambda$$
 , (7)

where $\Delta\lambda$ is the spectral width of the illuminating radiation. For uniform plane-wave illumination, as in Fig. 4-8, the Rayleigh criterion sets the diffraction-limited (λ , NA) spatial resolution of a perfect lens as

$$Res = \frac{0.610\lambda}{NA} = 1.22 \,\Delta r$$
 , (8)

where $NA = \sin \theta$ is the numerical aperture of the lens in vacuum and θ is the half-angle of the focused radiation. This resolution is obtained over an axial depth of focus given by

$$DOF = \pm \frac{\lambda}{2(NA)^2} . (9)$$

Spatial resolution in the full-field case can be improved somewhat from that given in Eq. (8), depending on both the object itself and the partial coherence of the illumination [4], as set by the parameter

$$\sigma = \frac{(NA)_{\rm c}}{(NA)_{\rm o}} \quad , \tag{10}$$

where $(NA)_c$ refers to the illumination numerical aperture of the condenser, and $(NA)_o$ is that of the zone plate objective lens, as given in Eq. (6).

The efficiency of the simple zone plate in the first order is ideally π^2 , or about 10%. The remainder of the radiation is absorbed (50%) or diffracted in other orders—zero order (25%), negative orders (12.5%), and higher positive orders (2.5%). If opaque zones are replaced by transparent but phase-shifting zones, efficiencies can be substantially improved [5]. To isolate the first order from unwanted orders, zone plate lenses are often made with a central stop, used in conjunction with a somewhat smaller collimating aperture near the focal

region. This is particularly effective in scanning x-ray microscopes [6,7], where the zone plate is used to focus the radiation to a small spot, as in Fig. 4-8. For full-field x-ray microscopes, as suggested by Fig. 4-9, first-order imaging is assisted in a similar manner by stopping the central portion of the illuminating radiation [8].

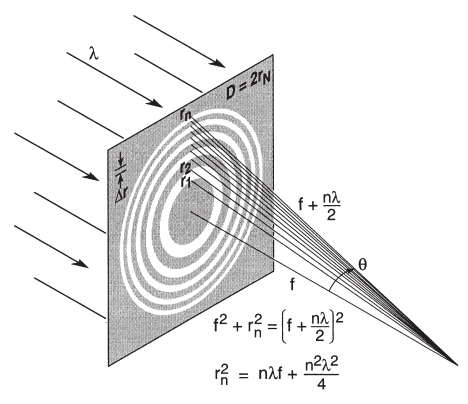


Fig. 4-8. A Fresnel zone plate lens with plane wave illumination, showing only the convergent (+1st) order of diffraction. Sequential zones of radius r_n are specified such that the incremental path length to the focal point is nλ/2. Alternate zones are opaque in the simple transmission zone plate. With a total number of zones, N, the zone plate lens is fully specified. Lens characteristics such as the focal length f, diameter D, and numerical aperture NA are described in terms of λ, N, and Δr, the outer zone width. [Courtesy of Cambridge University Press. Ref. 3.]

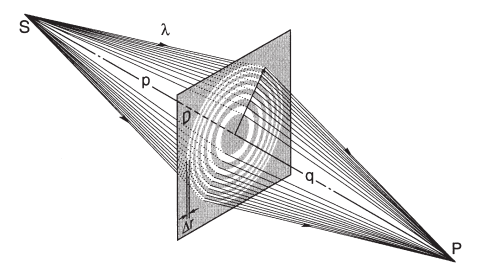


Fig. 4-9. A Fresnel zone plate used as a diffractive lens to form an x-ray image of a source point S in the image plane at P. The lens is shown as having a diameter D and outer zone width Δr. The object and image distances are p and q, respectively. A fullfield image is formed concurrently in this manner. [Courtesy of Cambridge University Press, Ref. 3.]

REFERENCES

- A. G. Michette, Optical Systems for Soft X-Rays (Plenum, London, 1986).
- G. R. Morrison, "Diffractive X-Ray Optics," Chapter 8 in A. G. Michette and C. J. Buckley, Eds., X-Ray Science and Technology (Inst. Phys., London, 1993).
- D. T. Attwood, Soft X-Rays and Extreme Ultraviolet Radiation: Principles and Applications (Cambridge Univ. Press, Cambridge, 1999).
- L. Jochum and W. Meyer-Ilse, "Partially Coherent Image Formation with X-Ray Microscopes," Appl. Opt. 34, 4944 (1995).
- J. Kirz, "Phase Zone Plates for X-Rays and the Extreme UV," J. Opt. Soc. Amer. 64, 301 (1974).
- H. Rarback, D. Shu, S. C. Feng, H. Ade, J. Kirz, I. McNulty, D. P. Kern, T. H. P. Chang, Y. Vladimirsky, N. Iskander, D. Attwood, K. McQuaid, and S. Rothman,

- "Scanning X-Ray Microscopy with 75-nm Resolution," Rev. Sci. Instrum. **59**, 52 (1988).
- C. Jacobsen, S. Williams, E. Anderson, M. Browne, C. J. Buckley, D. Kern, J. Kirz, M. Rivers, and X. Zhang, "Diffraction-limited Imaging in a Scanning Transmission X-Ray Microscope," Opt. Commun. 86, 351 (1991); http://xray1.physics.sunysb.edu/downloads/ stxm_optcom91.pdf.
- B. Niemann, D. Rudolph, and G. Schmahl, "X-Ray Microscopy with Synchrotron Radiation," Appl. Opt. 15, 1883 (1976).

4.5 X-RAY DETECTORS

Albert C. Thompson

A wide variety of x-ray detectors is available, some counting single photons, some providing only measurements of count rate or total flux, others measuring the energy, position, and/or incidence time of each x-ray. Table 4-2 provides typical values for useful energy range, energy resolution, dead time per event, and maximum count rate capability for common x-ray detectors. For special applications, these specifications can often be substantially improved.

Table 4-2. Properties of common x-ray detectors; ΔE is measured as FWHM.

Detector	Energy range (keV)	Δ <i>E/E</i> at 5.9 keV (%)	Dead time/event (µs)	Maximum count rate (s ⁻¹)
Gas ionization (current mode)	0.2–50	n/a	n/a	10 ^{11a}
Gas proportional	0.2-50	15	0.2	10^{6}
Multiwire and microstrip proportional	3–50	20	0.2	10 ⁶ /mm ²
Scintillation [NaI(Tl)]	3-10,000	40	0.25	2×10^6
Energy-resolving semiconductor	1-10,000	2.1	0.5-30	5×10^5
Surface-barrier (current mode)	0.1-20	n/a	n/a	108
Avalanche photodiode	0.1-50	20	0.001	108
CCD	0.1-70	n/a	n/a	n/a
Superconducting	0.1-4	< 0.5	100	5×10^3
Image plate	4-80	n/a	n/a	n/a

^a Maximum count rate is limited by space-charge effects to around 10¹¹ photons/s per cm³.

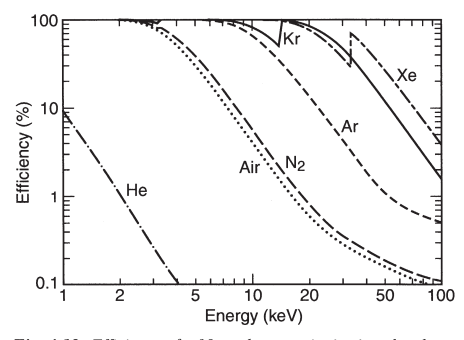


Fig. 4-10. Efficiency of a 10-cm-long gas ionization chamber as a function of energy, for different gases at normal pressure.

A. GAS IONIZATION DETECTORS

Gas ionization detectors are commonly used as integrating detectors to measure beam flux rather than individual photons. A typical detector consists of a rectangular gas cell with thin entrance and exit windows. Inside the detector, an electric field of about 100 V/cm is applied across two parallel plates. Some of the x-rays in the beam interact with the chamber gas to produce fast photoelectrons, Auger electrons, and/or fluorescence photons. The energetic electrons produce additional electron-ion pairs by inelastic collisions, and the photons either escape or are photoelectrically absorbed. The electrons and ions are collected at the plates, and the current is measured with a low-noise current amplifier. The efficiency of the detector can be calculated from the active length of the chamber, the properties of the chamber gas, and the x-ray absorption cross section at the appropriate photon energy. Figure 4-10 shows, for different gases at normal pressure, the efficiency of a 10-cm-long ion chamber as a function of energy. Once the efficiency is known, the photon flux can be estimated from

chamber current and the average energy required to produce an electron-ion pair (Table 4-3)[1].

Element	Energy (eV)
Helium	41
Nitrogen	36
Air	34.4
Neon	30
Argon	25
Krypton	24
Xenon	22

Table 4-3. Average energy required to produce an electron-ion pair in several gases

B. GAS PROPORTIONAL COUNTERS

Gas proportional detectors consist of a small-diameter anode wire in an enclosed gas volume. They are usually used to count single photon events. When a photon interacts in the gas, some gas atoms are ionized, and the electrons are attracted to the positive anode wire. Near the anode wire, the electrons are accelerated by the high electric field, producing a cascade of electrons that result in a large electrical pulse. The output is coupled to a low-noise preamplifier to give usable pulses. The pulse height resolution of the detector (about 20% at 6 keV) can be used for some energy discrimination, and the output counting rate can be as high as 10^6 counts per second.

C. MULTIWIRE AND MICROSTRIP PROPORTIONAL CHAMBERS

Multiwire and microstrip proportional chambers are widely used as position-sensitive detectors of both photons and charged particles. Multiwire chambers use a grid of fine wires spaced about 2 mm apart as the anode plane in a gas proportional chamber. Microstrip detectors use a patterned anode plane. The spatial resolution can be as good as 30 μ m. Gas electron multiplying (GEM) detectors have been

developed that have improved spatial resolution and lower operating voltages [2].

D. SCINTILLATION DETECTORS

Scintillation detectors work by converting x-rays to optical photons in special materials and then detecting the light with a photomultiplier tube or a photodiode. The scintillator materials can be either organic scintillators, single crystals of thalliumactivated sodium iodide [commonly referred to as NaI(T1)]. single crystals of sodium-activated cesium iodide [CsI(Na)], or single crystals of bismuth germanate (BGO). Since the light output is low (about 200-300 eV is required for each optical photon), the energy resolution is also low. Organic scintillators have very poor energy resolution, whereas the NaI(Tl), CsI(Na), and BGO crystals have energy resolutions of about 40% at 10 keV. These detectors can have a time resolution of better than 1 ns and a count rate capability up to 2×10^6 photons per second. For a scintillator thickness of more than 5 mm, for both NaI and CsI, the detection efficiency between 20 and 100 keV is essentially unity.

Gas scintillation detectors combine the operation of gas ionization chambers and photon detectors to give improved performance. Electrons generated from photon or charged-particle interactions in a gas (usually pure xenon or argon with 1% xenon) are accelerated in a high-field (-3 kV/cm) region, where they produce UV scintillation light. This light is usually wave-shifted and then detected by a photomultiplier. These detectors have an energy resolution about two to three times better than conventional proportional chambers.

E. ENERGY-RESOLVING SEMICONDUCTOR DETECTORS

Silicon and germanium detectors can make excellent energy-resolving detectors of single photons (about 150 eV at 5.9 keV). They are basically large, reverse-biased n*-i-p* diodes. When a photon interacts in the intrinsic region, tracks of electron-hole pairs are produced (analogous to electron-positive ion pairs in a counting gas). In the presence of the electric field, these pairs separate and rapidly drift to the detector contacts. The average energy required to generate an

electron-hole pair is 3.6 eV for silicon and 2.98 eV for germanium. To keep the leakage current low, the detector must have very few electrically active impurities. For example, germanium detectors are made from zone-refined crystals that have fewer than 10^{10} electrically active impurities/cm³. They are usually cooled to reduce the thermal leakage current. Recently, silicon drift detectors have become available with an energy resolution of <140 eV and a count rate up to about 5×10^5 per second. To handle the high counting rates available at synchrotrons, multielement arrays of 4-30 elements have been developed for fluorescent EXAFS experiments.

F. CURRENT-MODE SEMICONDUCTOR DETECTORS

Semiconductor diodes are also used in current mode to measure x-ray flux. They have very linear responses and are available with thin entrance windows. Surface-barrier detectors are good beam monitors when used with low-noise current amplifiers. In addition, silicon avalanche detectors are now available in which the silicon is biased so that there is an internal avalanche of electron-hole pairs for each interacting photon. These devices can be used at lower beam intensities in a pulse-counting mode and in current mode at higher photon fluxes. They have excellent time resolution (al ns) but limited energy resolution.

G. CCD DETECTORS

CCD detectors are now used in a variety of ways for x-ray imaging. They are available with up to 4096 x 4096 pixels, with pixel sizes of $12~\mu m \times 12~\mu m$ and readout times of less than 1 s. 1n most scientific applications, CCD detectors are cooled to below $-30^{\circ}\mathrm{C}$ to reduce background noise. In most systems, a thin phosphor screen converts the incident x-rays into optical photons, which the CCD detects. A commonly used phosphor is $\mathrm{Gd_2O_3S(Tb)}$, which has a high efficiency and a light decay time of a few hundred microseconds. When used as a detector for macromolecular crystallography, a large phosphor screen (up to 300 mm²) is usually coupled to a set of up to 9 CCD's with tapered optical fibers [3]. On the other hand, for high-spatial-resolution x-ray imaging, a very thin (5-

to 20- μ m) sapphire scintillation screen is optically coupled with a high-quality microscope lens to give a spatial resolution of less than 1μ m [4]. For imaging with x-rays below 1 keV, direct exposure of back-thinned CCD detectors is used.

H. OTHER X-RAY DETECTORS

X-ray detectors operating at superconducting temperatures (0.1–4 K) have recently been developed; these devices achieve excellent energy resolution (12 eV at 700 eV). They are currently very small and very inefficient for x-rays above 1 keV, and they have maximum count rates of only about $5 \times 10^3 \text{ s}^{-1}$. With further development, however, they may make very useful x-ray spectrometers [5].

Microchannel plate detectors are compact, high-gain electron multipliers, which are often used as efficient electron ro low-energy photon detectors. A typical MCP consists of about 10^7 closely packed lead-glass channels of equal diameter. Typically, the diameter of each channel, which acts as an independent, continuous dynode photomultiplier, is $\sim 10~\mu m$.

Image plate detectors are available that have many of the characteristics of film but with the advantage of excellent dynamic range, efficiency, and large area [6]. They are made with a plate containing a photosensitive material that on exposure to x-rays creates color centers that can be read out in a scanning mode with a laser as a digital image.

For fast timing experiments, silicon Avalanche Detectors are available that have a time resolution of less than 1 ns [7].

For high-speed x-ray imaging experiments, x-ray streak cameras have been developed that have time resolutions of around 350 fs.

Finally, photographic film is also available for quick x-rayimaging experiments; however, because of the need for processing after exposure, it is no longer commonly used for scientific measurements. Special films are available that give improved efficiency, contrast, or resolution.

I. CALIBRATION OF X-RAY BEAM MONITORS

Measurement of the relative intensity of x-ray beams is usually done with a gas ionization chamber or a thin silicon diode in

the beam path. Another technique is to place a thin foil (usually plastic) in the beam and to measure the scattered photons with a scintillation detector. The approximate efficiency of a gas ionization detector can be estimated from its active length and the properties of the chamber gas at the energy of the x-ray beam. However, calibration of these detectors to measure absolute x-ray intensity is more difficult. One calibration technique is to use a well-characterized single-photon detector as a standard and to establish the x-ray flux-to-detector current calibration of the beam monitor at a reduced beam flux where the single-photon counter response is linear. A thick silicon pin diode can also be used for flux measurement [8].

At photon energies below 1000 eV, silicon photodiodes are available that can be used as absolute beam monitors [9].

REFERENCES

- 1. C. Amsler *et al.* (Particle Data Group), Physics Letters **B667**, Table 28.6 (2008).
- F. Sauli, "Gas Detectors: Recent Developments and Future Perspectives," Nucl. Instrum. Methods A419, 26 (2000).
- W. C. Phillips, M. Stanton, A. Stewart, Q. Hua, C. Ingersoll, and R. M. Sweet, "Multiple CCD Detector for Macromolecular X-Ray Crystallography," *J. Appl. Crystallog.* 33, 243 (2000).
- A. Koch, C. Raven, P. Spanne, and A. Snigirev, "X-Ray Imaging with Submicrometer Resolution Employing Transparent Luminescent Screens," J. Opt. Soc. Am. A15, 1940 (1998).
- K. Pretzl, "Cryogenic Calorimeters in Astro and Particle Physics," Nucl. Instrum. Methods A454, 114 (2000).
- Y. Amemiya, "Imaging Plates for Use with Synchrotron Radiation," J. Synch. Rad. 2, 13 (1995).
- L.M.P.Fernandes et al, "Characterization of Large Area Avalanche Photodiodes in X-ray and VUV-Light Detection,"
 - http://arxiv.org/ftp/physics/papers/0702/0702130.pdf

- R.L.Owen, J.M.Holton, C.Schulze-Briese, and E.F.Garman, "Determination of X-ray flux using pin diodes", J. Synchrotron Radiat. 16, 143 (2009).
- E. M Gullikson, R. Korde, L. R. Canfield, and R. E. Vest, "Stable Silicon Photodiodes for Absolute Intensity Measurements in the VUV and Soft X-Ray Regions," J. Elect. Spectrosc. Related Phenom. 80, 313 (1996).

SECTION 5

MISCELLANEOUS

5.1 PHYSICAL CONSTANTS

Table 5-1 was drawn from the recommendations of CODATA (the Committee on Data for Science and Technology). The full 1998 CODATA set of constants may be found at http://physics.nist.gov/cuu/Constants/index.html.

Table 5-1. Physical constants.

Quantity	Symbol, equation	Value	Uncert. (ppb)
speed of light	c (see note *)	299 792 458 m s ⁻¹ (10 ¹⁰ cm s ⁻¹)	exact
Planck constant	h	$6.626\ 068\ 96(33)\times10^{-34}\ J\ s\ (10^{-27}\ erg\ s)$	20
Planck constant, reduced	$\hbar = h/2\pi$	$1.054\ 571\ 628(53)\times10^{-34}\ J\ s = 6.582\ 118\ 99(16)\times10^{-22}\ MeV\ s$	50, 25
electron charge magnitude	9	$4.803\ 204\ 27(12)\times10^{-10}\ esu = 1.602\ 176\ 87(40)\times10^{-19}\ C$	25, 25
conversion constant	ħc	197.326 9631(49) MeV fm (= eV nm)	25
electron mass	me	$0.510998910(13)\text{MeV}/c^2 = 9.10938215(45)\times 10^{-31}\text{kg}$	25, 50
proton mass	m _p	$938.272\ 013(23)\ \text{MeV/}c^2 = 1.672\ 621\ 637(83)\times 10^{-27}\ \text{kg}$	25, 50
		= 1.007 276 466 77(10) $u = 1836.152 672 47(80) m_e$	0.10, 0.43
deuteron mass	P <i>m</i>	1875.612 793 (47) MeV/c ²	25
unified atomic mass unit (u)	(mass ${}^{12}C$ atom)/12 = (1 g)/(N _A mol)	931.494 028(23) MeV/ $c^2 = 1.660$ 538 782(83)×10 ⁻²⁷ kg	25, 50
permittivity of free space	$\varepsilon_0 = 1/(\mu_0 c^2)$	8.854 187 817×10 ⁻¹² F m ⁻¹	exact
permeability of free space	и0	$4\pi \times 10^{-7} \text{ N A}^{-2} = 12.566\ 370\ 614\times 10^{-7} \text{ N A}^{-2}$	exact
fine-structure constant	$\alpha = e^2/4\pi\epsilon_0 \hbar c$	1/137.035 999 679(94)	89.0
classical electron radius	$r_{\rm c} = e^2/4\pi\varepsilon_0 m_{\rm e} c^2$	2.817 940 2894(58)×10 ⁻¹⁵ m	2.1
Bohr radius $(m_{\text{nucleus}} = \infty)$	$a_0 = 4\pi \varepsilon_0 h^2 / m_e e^2 = r_e \alpha^{-2}$	$0.529\ 177\ 208\ 59(36)\times10^{-10}\ \mathrm{m}\ (10^{-8}\ \mathrm{cm})$	89.0
Rydberg energy	$hcR_{\infty} = m_c e^4/2(4\pi \epsilon_0)^2 \hbar^2$	13.605 691 93(34) eV	25
	$=m_{\rm e}c^2\alpha^2/2$		

Thomson cross section	$\sigma_{\Gamma} = 8\pi r_e^2/3$	$0.665245858(27)$ barn (10^{-28} m^2)	4.1
Bohr magneton	$\mu_{\rm B} = e \hbar / 2 m_{\rm e}$	5.788 381 7555(79)×10 ⁻¹¹ MeV T ⁻¹	1.4
nuclear magneton	$\mu_N = e \hbar / 2 m_p$	3.152 451 2326(45)×10 ⁻¹⁴ MeV T ⁻¹	1.4
electron cyclotron freq./field	$\omega_{\rm cycl}^{\rm e}$ /B = e/m _e	1.758 820 150(44)×10 ¹¹ rad s ⁻¹ T ⁻¹	25
proton cyclotron freq./field	$\omega_{\rm cycl}^{\rm p}/B = e/m_{\rm p}$	9.578 833 92(24)×10 ⁷ rad s ⁻¹ T ⁻¹	25
Avogadro constant	N_{A}	6.022 141 79(30)×10 ²³ mol ⁻¹	50
Boltzman constant	*	$1.380\ 650\ 4(24)\times10^{-23}\ J\ K^{-1} = 8.617\ 343(15)\times10^{-5}\ eV\ K^{-1}$	1700
molar volume, ideal gas at STP	NAk (273.15 K)/(101 325 Pa)	22.413 996(39)×10 ⁻³ m ³ mol ⁻¹	1700
π = 3.141 592 653 589 793 238	e = 2.71	$e = 2.718\ 281\ 828\ 459\ 045\ 235$ $\gamma = 0.577\ 215\ 664\ 901\ 532\ 861$	861
*The meter is the length of the pa	th traveled by light in vacuum during	*The meter is the length of the path traveled by light in vacuum during a time interval of 1/299 792 458 of a second.	
l in. = 2.54 cm l ne	l newton = 10 ⁵ dyne	$1 \text{ eV/}c^2 = 1.782 662 \times 10^{-33} \text{ g}$ 1 coulomb = 2.997 924 58×10 ⁹ esu	109 esu
$1 \text{ A} = 10^{-8} \text{ cm}$ 1 jo	1 joule = 10^7 erg	$hc/(1 \text{ eV}) = 1.239 842 \mu\text{m}$ 1 tesla = 10 ⁴ gauss	
$1 \text{ fm} = 10^{-13} \text{ cm}$	1 cal = 4.184 joule	$1 \text{ eV/h} = 2.417989 \times 10^{14} \text{ Hz}$ $1 \text{ atm} = 1.01325 \times 10^6 \text{ dyne/cm}^2$	dyne/cm ²
$1 \text{ barn} = 10^{-24} \text{ cm}^2$	1 eV = 1.602 176 5×10 ⁻¹² erg	$1 \text{ eV/k} = 11604.5 \text{ K}$ $0^{\circ}\text{C} = 273.15 \text{ K}$	

The NIST Reference on Constants, Units, and Uncertainty: http://physics.nist.gov/cuu/Constants/index.html

5.2 PHYSICAL PROPERTIES OF THE ELEMENTS

Table 5-2 lists several important properties of the elements. Data were taken mostly from D. R. Lide, Ed., CRC Handbook of Chemistry and Physics, 80th ed. (CRC Press, Boca Raton, Florida, 1999). Atomic weights apply to elements as they exist naturally on earth; values in parentheses are the mass numbers for the longest-lived isotopes. Some uncertainty exists in the last digit of each atomic weight. Specific heats are given for the elements at 25°C and a pressure of 100 kPa. Densities for solids and liquids are given as specific gravities at 20°C unless otherwise indicated by a superscript temperature (in °C); densities for the gaseous elements are given in g/cm³ for the liquids at their boiling points. The ionization energies were taken from

 $http://physics.nist.gov/PhysRefData/IonEnergy/ionEnergy. \\ html.$

A periodic table of the elements follows Table 5-2, on page 5-10. A more detailed periodic table can be found at http://www.cxro.lbl.gov/.

Table 5-2. Properties of the elements.

Z Element	Atomic weight	Density	Melting point (°C)	Boiling point (°C)	Ground-state configuration	Ground	Ionization energy (eV)	Specific heat (J/g·K)
1 Hydrogen	1.00794	0.0708	-259.34	-252.87	Is	$^{2}S_{1/2}$	13.598	14.304
2 Helium	4.002602	0.122	I	-268.93	$1s^2$	$^{1}S_{0}$	24.587	5.193
3 Lithium	6.941	0.534	180.50	1342	1s ² 2s	² S _{1/2}	5.392	3.582
4 Beryllium	9.012182	1.848	1287	2471	$1s^2 2s^2$	1S ₀	9.323	1.825
5 Boron	10.811	2.34	2075	4000	$1s^2 2s^2 2p$	² P° _{1/2}	8.298	1.026
6 Carbon	12.0107	1.9-2.3 (graph)	449210.3 MPa	3825b	$1s^2 2s^2 2p^2$	$^{3}P_{0}$	11.260	0.709
7 Nitrogen	14.00674	0.808	-210.00	-195.79	$1s^2 2s^2 2p^3$	4S°3/2	14.534	1.040
8 Oxygen	15.9994	1.14	-218.79	-182.95	$1s^2 2s^2 2p^4$	³ P ₂	13.618	0.918
9 Fluorine	18.9984032	1.50	-219.62	-188.12	$1s^2 2s^2 2p^5$	² P°3/2	17.423	0.824
10 Neon	20.1797	1.207	-248.59	-246.08	$1s^2 2s^2 2p^6$	1S ₀	21.565	1.030
11 Sodium	22.989770	0.971	97.80	883	[Ne] 3s	² S _{1/2}	5.139	1.228
12 Magnesium	24.3050	1.738	920	1090	[Ne] 3s ²	$^{1}S_{0}$	7.646	1.023
13 Aluminum	26.981538	2.6989	660.32	2519	[Ne] 3s ² 3p	$^{2}P^{\circ}_{1/2}$	5.986	0.897
14 Silicon	28.0855	2.3325	1414	3265	[Ne] $3s^2 3p^2$	$^{3}P_{0}$	8.152	0.705
15 Phosphorus	30.973761	1.82	44.15	280.5	[Ne] $3s^2 3p^3$	⁴ S°3/2	10.487	0.769
16 Sulfur	32.066	2.07	119.6	444.60	[Ne] $3s^2 3p^4$	³ P ₂	10.360	0.710
17 Chlorine	35.4527	1.56-33.6	-101.5	-34.04	[Ne] 3s ² 3p ⁵	$^{2}P^{\circ}_{3/2}$	12.968	0.479
18 Argon	39.948	1.40	-189.35	-185.85	[Ne] $3s^2 3p^6$	$^{1}S_{0}$	15.760	0.520
19 Potassium	39.0983	0.862	63.5	759	[Ar] 4s	² S _{1/2}	4.341	0.757
20 Calcium	40.078	1.55	842	1484	[Ar] 4s ²	$^{1}S_{0}$	6.113	0.647
21 Scandium	44.955910	2.98925	1541	2836	[Ar] 3d 4s ²	² D _{3/2}	6.562	0.568
22 Titanium	47.867	4.54	1668	3287	[Ar] 3d ² 4s ²	³ F ₂	6.828	0.523
23 Vanadium	50.9415	6.1118.7	1910	3407	[Ar] 3d ³ 4s ²	4F3/2	6.746	0.489
24 Chromium	51.9961	7.18-7.20	1907	2671	[Ar] 3d ⁵ 4s	7S3	992.9	0.449
25 Manganese	54.938049	7.21-7.44	1246	2061	[Ar] 3d ⁵ 4s ²	6S5/2	7.434	0.479
26 Iron	55,845	7.874	1538	2861	[Ar] 3a6 4s2	$^{5}D_{4}$	7.902	0.449

z	Z Element	Atomic weight	Density	Melting point (°C)	Boiling point (°C)	Ground-state configuration	Ground	Ionization energy (eV)	Specific heat (J/g·K)
27	27 Cobalt	58.933200	8.9	1495	2927	[Ar] 3d ⁷ 4s ²	⁴ F9/2	7.881	0.421
28	Nickel Nickel	58.6934	8.90225	1455	2913	[Ar] 3d ⁸ 4s ²	3F4	7.640	0.444
29	Copper	63.546	8.96	1084.62	2562	[Ar] 3d ¹⁰ 4s	² S _{1/2}	7.726	0.385
30	Zinc	65.39	7.13325	419.53	200	[Ar] 3d ¹⁰ 4s ²	1S ₀	9.394	0.388
31	Gallium	69.723	5.90429.6	29.76	2204	[Ar] 3d ¹⁰ 4s ² 4p	$^{2}P^{\circ}_{1/2}$	5.999	0.371
32	Germanium	72.61	5.32325	938.25	2833	[Ar] 3d ¹⁰ 4s ² 4p ²	$^{3}P_{0}$	7.899	0.320
33	3 Arsenic	74.92160	5.73	8173.7 MPa	e03p	[Ar] 3d ¹⁰ 4s ² 4p ³	⁴ S°3/2	682.6	0.329
34	34 Selenium	78.96	4.79	220.5	685	[Ar] 3d ¹⁰ 4s ² 4p ⁴	³ P ₂	9.752	0.321
35	5 Bromine	79.904	3.12	-7.2	58.8	[Ar] 3d ¹⁰ 4s ² 4p ⁵	² P°3/2	11.814	0.226
36	6 Krypton	83.80	2.16	157.38 ^{73.2} kPa	-153.22	[Ar] 3d ¹⁰ 4s ² 4p ⁶	1S ₀	14.000	0.248
37	Rubidium	85.4678	1.532	39.30	889	[Kr] 5s	$^{2}S_{1/2}$	4.177	0.363
38	38 Strontium	87.62	2.54	777	1382		1S ₀	5.695	0.301
39	99 Yttrium	88.90585	4.46925	1522	3345		² D _{3/2}	6.217	0.298
9	40 Zirconium	91.224	905'9	1855	4409	[Kr] 4d ² 5s ²	³ F ₂	6.634	0.278
4	41 Niobium	92.90638	8.57	2477	4744	[Kr] 4d ⁴ 5s	6D1/2	6.759	0.265
42	42 Molybdenum	95.94	10.22	2623	4639	4,	783	7.092	0.251
43	43 Technetium	(86)	11.50ª	2157	4265	[Kr] 4d ⁵ 5s ²	6S5/2	7.28	1
4	44 Ruthenium	101.07	12.41	2334	4150	[Kr] 4d ⁷ 5s	$^{5}\text{F}_{5}$	7.360	0.238
45	45 Rhodium	102.90550	12.41	1964	3695	[Kr] 4d ⁸ 5s	⁴ F9/2	7.459	0.243
46	46 Palladium	106.42	12.02	1554.9	2963	[Kr] 4d ¹⁰	180	8.337	0.246
47	47 Silver	107.8682	10.50	961.78	2162	[Kr] 4d ¹⁰ 5s	² S _{1/2}	7.576	0.235
48	48 Cadmium	112.411	8.65	321.07	191	[Kr] 4d ¹⁰ 5s ²	1 S ₀	8.994	0.232
49	49 Indium	114.818	7.31	156.60	2072	[Kr] 4d ¹⁰ 5s ² 5p	$^{2}P^{\circ}_{1/2}$	5.786	0.233
20	Tin 1	118.710	7.31	231.93	2602	[Kr] 4d ¹⁰ 5s ² 5p ²	$^{3}P_{0}$	7.344	0.228
51	51 Antimony	121.760	6.691	630.73	1587	$[Kr] 4d^{10} 5s^2 5p^3$	⁴ S°3/2	8.608	0.207
52	52 Tellurium	127.60	6.24	449.51	886	$[Kr] 4d^{10} 5s^2 5p^4$	$^{3}P_{2}$	9.010	0.202
53	53 Iodine	126.90447	4.93	113.7	184.4	$[Kr] 4d^{10} 5s^2 5p^5$	$^{2}P^{\circ}_{3/2}$	10.451	0.145
54	54 Xenon	131.29	3.52	-111.7981.6 kPa	-108.12	$[Kr]$ $4d^{10}$ $5s^2$ $5p^6$	$^{1}S_{0}$	12.130	0.158

Table 5-2. Properties of the elements (continued).

Z Element	Atomic	Density	Melting point (°C)	Boiling point (°C)	Ground-state	d-state rration	Ground level	Ionization energy (eV)	Specific heat (J/g·K)
55 Cesium	132.90545	1.873	28.5	671	[Xe]	es es	281/2	3.894	0.242
56 Barium	137.327	3.5	727	1897	[Xe]	6.52	1S ₀	5.212	0.204
57 Lanthanum	138.9055	6.14525	918	3464	[Xe] 5d	6.52	² D _{3/2}	5.577	0.195
58 Cerium	140.116	6.77025	798	3443	[Xe] 4f 5d	6.52	lG°4	5.539	0.192
59 Praseodymium	140.90765	6.773	931	3520	[Xe] 4y ³	6.52	⁴ I°9/2	5.473	0.193
60 Neodymium	144.24	7.00825	1021	3074	[Xe] 4/4	6.52	5 I ₄	5.525	0.190
61 Promethium	(145)	7.26425	1042	3000	[Xe] 4/6	6.82	6H°5/2	5.582	1
62 Samarium	150.36	7.520 ²⁵	1074	1794	[Xe] 4/6	6.52	$^{7}\text{F}_{0}$	5.644	0.197
63 Europium	151.964	5.24425	822	1529	[Xe] 4/7	6.82	8S°7/2	5.670	0.182
64 Gadolinium	157.25	7.901 ²⁵	1313	3273	[Xe] 4y ⁷ 5d	6.82	$^{9}D^{\circ}_{2}$	6.150	0.236
65 Terbium	158.92534	8.230	1356	3230	[Xe] 4/9	652	⁶ H° _{15/2}	5.864	0.182
66 Dysprosium	162.50	8.55125	1412	2567	[Xe] 4/ ¹⁰	6.82	5 ₁₈	5.939	0.170
67 Holmium	164.93032	8.79525	1474	2700	[Xe] 4/ ^{d1}	6.82	⁴ I° _{15/2}	6.022	0.165
68 Erbium	167.26	9.06625	1529	2868	[Xe] 4y ^{d2}	6.82	3H6	6.108	0.168
69 Thulium	168.93421	9.32125	1545	1950	[Xe] 4y ^{d3}	652	² F°7/2	6.184	091.0
70 Ytterbium	173.04	996.9	819	1196	[Xe] 4y ⁴⁴	6.82	1S ₀	6.254	0.155
71 Lutetium	174.967	9.84125	1663	3402	[Xe] 4y ¹⁴ 5d	6.82	$^{2}D_{3/2}$	5.426	0.154
72 Hafnium	178.49	13.31	2233	4603	[Xe] 4 ⁴⁴ 5d ²	2 es ²	3 F ₂	6.825	0.144
73 Tantalum	180.9479	16.654	3017	5458	[Xe] 4/14 5d3	3 652	4F3/2	7.550	0.140
74 Tungsten	183.84	19.3	3422	5555	[Xe] 4y4 5d4	4 6.52	δD ₀	7.864	0.132
75 Rhenium	186.207	21.02	3186	9655	[Xe] 47 ⁴⁴ 5a ⁵	5 652	6S5/2	7.834	0.137
76 Osmium	190.23	22.57	3033	5012	[Xe] 4/14 5d6	5 652	$^{5}D_{4}$	8.438	0.130
77 Iridium	192.217	22.4217	2446	4428	[Xe] 4/14 5d	7 652	4F9/2	8.967	0.131
78 Platinum	195.078	21.45	1768.4	3825	[Xe] 4/ ⁴⁴ 5d ⁹	9 68	$^{3}D_{3}$	8.959	0.133
79 Gold	196.96655	~19.3	1064.18	2856	[Xe] 4y ⁴⁴ 5d ¹⁰	10 68	$^{2}S_{1/2}$	9.226	0.129
80 Mercury	200.59	13.546	-38.83	356.73	[Xe] 4y14 5d10 6s2	10 es2	1S ₀	10.438	0.140
81 Thallium	204.3833	11.85	304	1473	[Xe] 47 ⁴⁴ 5d ¹⁰ 6s ² 6p	10 6s ² 6p	$^{2}P^{\circ}_{1/2}$	6.108	0.129
82 Lead	207.2	11.35	327.46	1749	[Xe] 4f ¹⁴ 5d ¹⁰ 6s ² 6p ²	$10 6s^2 6p^2$	$^{3}P_{0}$	7.417	0.129

Table 5-2. Properties of the elements (continued).

Z Element	Atomic weight	Density	point (°C)	(°C)	Ground-state configuration	Ground	energy (eV)	heat (J/g·K)
83 Bismuth	208.98038	9.747	271.40	1564	[Xe] 4/14 5d10 6s2 6p3	⁴ S°3/2	7.286	0.122
84 Polonium	(209)	9.32	254	962	[Xe] $4f^{14} 5d^{10} 6s^2 6p^4$	³ P ₂	8.417?	1
85 Astatine	(210)	I	302	1	[Xe] $4f^{14}$ $5d^{10}$ $6s^2$ $6p^5$	² P°3/2	I	I
86 Radon	(222)	ŀ	-71	-61.7	[Xe] 4y ¹⁴ 5d ¹⁰ 6s ² 6p ⁶	1S ₀	10.748	0.094
87 Francium	(223)	I	27	1	[Rn] 7s	2S1/2	4.073	l
88 Radium	(226)	1	700	1	[Rn] 7.5 ²	1S0	5.278	1
89 Actinium	(227)	1	1051	3198	[Rn] 6d 7s ²	² D _{3/2}	5.17	0.120
90 Thorium	232.0381	11.72	1750	4788	[Rn] 6d ² 7s ²	³ F ₂	6.307	0.113
91 Protactinium	231.03588	15.37a	1572	1	[Rn] 5/2(3H4) 6d 7s ²	(4,3/2)11/2	5.89	I
92 Uranium	238.0289	~18.95	1135	4131	$[Rn]5\beta^{(4}\Gamma^{9}_{9/2})6d7s^{2}$	(9/2,3/2)°6	6.194	0.116
93 Neptunium	(237)	20.25	644	1	$[Rn]5f^{4}(^{5}I_{4})6d7s^{2}$	(4,3/2)11/2	6.266	
94 Plutonium	(244)	19.8425	640	3228		$^{7}\mathrm{F}_{0}$	6.026	I
95 Americium	(243)	13.67	1176	2011	[Rn] 5f ² 7s ²	8S°7/2	5.974	I
96 Curium	(247)	13.51a	1345	3100	[Rn] 5f ⁷ 6d 7s ²	$^{9}D^{\circ}_{2}$	5.992	I
97 Berkelium	(247)	14 (est.)	1050	I	[Rn] 5/9 7.5 ²	⁶ H° _{15/2}	6.198	ĺ
98 Californium	(251)	I	006	1	$[Rn] 5/^{40} 7s^2$	5 ₁₈	6.282	I
99 Einsteinium	(252)	I	860	1	[Rn] 5y ⁴¹ 7s ²	⁴ I°15/2	6.42	I
100 Fermium	(257)	1	1527		[Rn] 5y ⁴² 7s ²	$^{3}\mathrm{H}_{6}$	6.50	I
101 Mendelevium	(258)	1	827	I	[Rn] 5/ ⁴³ 7.s ²	² F°7/2	6.58	1
102 Nobelium	(259)	1	827	1		1 S 0	6.65	I
103 Lawrencium	(262)	I	1627	1	$[Rn] 5f^{d4} 7s^2 7p?$	$^{2}P^{\circ}_{1/2}$?	4.9 ?	I
104 Rutherfordium	(261)		1	1	[Rn] 5j ¹⁴ 6d ² 7s ² ?	3F2?	6.0 %	I
105 Dubnium	(262)	1	I	ŀ	I	-	1	1
106 Seaborgium	(266)	1	I	I	ı	1		1
107 Bohrium	(264)	1	1	1	I	1	1	
108 Hassium	(269)	1	1	1	1	I	I	1
109 Meitnerium	(268)	1	1	1	1	1	1	1

					1	
- He	\$ 4 8 8 8 8	× 5 8 3;	131.28	8 (322)		
	_ ± 50 € €	έ φ ες.	126.90	85 (210)		174 97 103 103 (262)
	် စည်း လ	% % % %	0 le	26		70 173 04 102 NO (259)
	_ S	2 × 2	Sb	83 208.98		ir Tm 726 126 137 101 1
	္တည့္နယ္လ		2 [8]	82 Pb 207.2	(287)	2 T 3
ıts	°5 E E E	_ 2 2 g g.	11 82	81 T 704.38		66 67 10 HO HO 162 33 38 39 59 Cf ES (253)
me		2 85 38 85 38	3 2	80 H g 200.59	(272) (283)	⁸ 55 € 55 € 55 € 55 € 55 € 55 € 55 € 55
Ele		25 g -	Ag 107.87	Au 196.97		28 28 28 28 28 28 28 28 28 28 28 28 28 2
ţ		8 5 € S	Pd	³⁶ ₽	110	*35°5°5°5°5°5°5°5°5°5°5°5°5°5°5°5°5°5°5°
o elc		್ವಿ	Rh	" 92.22	109 (268)	Am Ser 38
c Tal		°5. ₹	Rn	0 0 190 23	108 HS (269)	E 80 2 8
Periodic Table of the Elements		2 2 W	ည 🫞	V Re 7	107 (264)	PE SE
Pe		ۣ ٷٷ؞ ٷٷ؞	S 8	× > 58	.Sg (266)	Ce Pr Nd 14012 14091 14421 30 91 97 Th Pa U
		2 2 2	S 58	73 180 95	105 D b (262)	8 - 5 - 5 E
		~ = = -	27 16	La + Hf	104 (261)	*35 € E E E
		28 48 S	− 15 88	28 1 138 91	Ac; Rf	Lanthanide series > Ce 14012 90 The Actinide series The Table The Table
	Be Zg	,	87.62 87.62	S 88 18	88 Ra (226)	anide :
= 5		² × 2 × 2 × 2	8547	န္တ လိုင္မ	87 (223)	Lanth Act

5.3 ELECTROMAGNETIC RELATIONS

	Gaussian CGS	SI
Units and conversions:		
Charge	$2.997 92 \times 10^9 \text{ esu}$	= 1 C = 1 A s
Potential	(1/299.792) statvolt = (1/299.792) erg/esu	= 1 V = 1 J C ⁻¹
Magnetic field	10^4 gauss = 10^4 dyne/esu	$= 1 T = 1 N A^{-1} m^{-1}$
Electron charge	$e = 4.803 \ 204 \times 10^{-10} \text{ esu}$	= $1.602\ 176 \times 10^{-19}\ C$
Lorentz force	$\mathbf{F} = q \left(\mathbf{E} + \frac{\mathbf{v}}{c} \times \mathbf{B} \right)$	$\mathbf{F} = q \left(\mathbf{E} + \mathbf{v} \times \mathbf{B} \right)$
Maxwell equations	$\nabla \cdot \mathbf{D} = 4\pi \rho$	$\nabla \cdot \mathbf{D} = \rho$
	$\nabla \times \mathbf{E} + \frac{1}{c} \frac{\partial \mathbf{B}}{\partial t} = 0$	$\nabla \times \mathbf{E} + \frac{\partial \mathbf{B}}{\partial t} = 0$
	$\nabla \cdot \mathbf{B} = 0$	$\nabla \cdot \mathbf{B} = 0$
	$\nabla \times \mathbf{H} - \frac{1}{c} \frac{\partial \mathbf{D}}{\partial t} = \frac{4\pi}{c} \mathbf{J}$	$\nabla \times \mathbf{H} - \frac{\partial \mathbf{D}}{\partial t} = \mathbf{J}$
Linear media	$\mathbf{D} = \varepsilon \mathbf{E}, \mathbf{B} = \mu \mathbf{H}$	$\mathbf{D} = \varepsilon \mathbf{E}, \mathbf{B} = \mu \mathbf{H}$
Permittivity of free space	$\varepsilon_{\rm vac} = 1$	$\varepsilon_{\rm vac} = \varepsilon_0$
Permeability of free space	$\mu_{\text{vac}} = 1$	$\mu_{\rm vac} = \mu_0$
Fields from potentials	$\mathbf{E} = -\nabla V - \frac{1}{c} \frac{\partial \mathbf{A}}{\partial t}$	$\mathbf{E} = -\nabla V - \frac{\partial \mathbf{A}}{\partial t}$
	$\mathbf{B} = \nabla \times \mathbf{A}$	$\mathbf{B} = \nabla \times \mathbf{A}$
Static potentials (coulomb gauge)	$V = \sum_{\text{charges}} \frac{q_i}{r_i}$	$V = \frac{1}{4\pi\varepsilon_0} \sum_{\text{charges}} \frac{q_i}{r_i}$
	$\mathbf{A} = \frac{1}{c} \oint \frac{I \mathbf{d} \ell}{ \mathbf{r} - \mathbf{r}' }$	$\mathbf{A} = \frac{\mu_0}{4\pi} \oint \frac{I \mathbf{d} \ell}{ \mathbf{r} - \mathbf{r}' }$
Relativistic transformations	$\mathbf{E}_{\parallel}' = \mathbf{E}_{\parallel}$	$\mathbf{E}_{ }' = \mathbf{E}_{ }$
(v is the velocity of primed system	$\mathbf{E}'_{\perp} = \gamma \left(\mathbf{E}_{\perp} + \frac{1}{c} \mathbf{v} \times \mathbf{B} \right)$	$\mathbf{E}'_{\perp} = \gamma (\mathbf{E}_{\perp} + \mathbf{v} \times \mathbf{B})$
as seen in un- primed system)	$\mathbf{B}'_{ } = \mathbf{B}_{ }$	$\mathbf{B}'_{ } = \mathbf{B}_{ }$
1 y y	$\mathbf{B}'_{\perp} = \gamma \left(\mathbf{B}_{\perp} \pm \frac{1}{c} \mathbf{v} \times \mathbf{E} \right)$	$\mathbf{B}'_{\perp} = \gamma \left(\mathbf{B}_{\perp} - \frac{1}{c^2} \mathbf{v} \times \mathbf{I} \right)$

$$4\pi\epsilon_0 = \frac{1}{c^2} 10^7 \text{A}^2 \text{ N}^{-1} = \frac{1}{8.987 \cdot 55...} \times 10^{-9} \text{F m}^{-1}$$

 $\frac{\mu_0}{4\pi} = 10^{-7} \text{N A}^{-1} ; c = 2.997 \cdot 924 \cdot 58 \times 10^8 \text{ m s}^{-1}$

Impedances (SI units)

 ρ = resistivity at room temperature in 10⁻⁸ Ω m:

For alternating currents, instantaneous current I, voltage V, angular frequency ω :

$$V = V_0 e^{j\omega t} = ZI$$
.

Impedance of self-inductance L: $Z = i\omega L$.

Impedance of capacitance C: $Z = 1/j\omega C$.

Impedance of free space: $Z = \sqrt{\mu_0 / \epsilon_0} = 376.7 \Omega$.

High-frequency surface impedance of a good conductor:

$$Z = \frac{(1+j)\rho}{\delta}$$
, where $\delta =$ effective skin depth;

$$\delta = \sqrt{\frac{\rho}{\pi \nu \mu}} \cong \frac{6.6~\text{cm}}{\sqrt{\nu [\text{Hz}]}}~\text{for Cu}~.$$

Capacitance \hat{C} and inductance \hat{L} per unit length (SI units) Flat rectangular plates of width w, separated by $d \ll w$ with linear medium (ε, μ) between:

$$\hat{C} = \varepsilon \frac{w}{d} \; ; \quad \hat{L} = \mu \frac{d}{w} \; ; \quad$$

 $\frac{\varepsilon}{\varepsilon_0}$ = 2 to 6 for plastics; 4 to 8 for porcelain, glasses;

$$\frac{\mu}{u_0} \cong 1$$
.

Coaxial cable of inner radius r_1 , outer radius r_2 :

$$\hat{C} = \frac{2\pi\varepsilon}{\ln(r_2/r_1)} \; ; \qquad \hat{L} = \frac{\mu}{2\pi} \ln(r_2/r_1) \; .$$

Transmission lines (no loss):

Impedance: $Z = \sqrt{\hat{L}/\hat{C}}$.

Velocity:
$$v = 1/\sqrt{\hat{L}\hat{C}} = 1/\sqrt{\mu\varepsilon}$$
.

Motion of charged particles in a uniform, static magnetic field

The path of motion of a charged particle of momentum p is a helix of constant radius R and constant pitch angle λ , with the axis of the helix along \mathbf{B} :

$$p[\text{GeV}/c]\cos \lambda = 0.29979 \ qB[\text{tesla}] \ R[\text{m}]$$
,

where the charge q is in units of the electronic charge. The angular velocity about the axis of the helix is

$$\omega[\mathrm{rad}\;\mathrm{s}^{-1}] = 8.98755 \times 10^7\,qB[\mathrm{tesla}]/\,E[\mathrm{GeV}]\ ,$$

where E is the energy of the particle.

This section was adapted, with permission, from the 1999 web edition of the *Review of Particle Physics* (http://pdg. lbl.gov). See J. D. Jackson, *Classical Electrodynamics*, 2d ed. (John Wiley & Sons, New York, 1975) for more formulas and details.

5.4 RADIOACTIVITY AND RADIATION PROTECTION

The International Commission on Radiation Units and Measurements (ICRU) recommends the use of SI units. Therefore, we list SI units first, followed by cgs (or other common) units in parentheses, where they differ.

A. DEFINITIONS

Unit of activity = becquerel (curie):

1 Bq = 1 disintegration s⁻¹ [= $1/(3.7 \times 10^{10})$ Ci]

Unit of absorbed dose = gray (rad):

1 Gy = 1 J kg⁻¹ (= 10^4 erg g⁻¹ = 100 rad)

= 6.24×10^{12} MeV kg⁻¹ deposited energy

Unit of exposure, the quantity of x- or γ-radiation at a point in space integrated over time, in terms of charge of either sign produced by showering electrons in a small volume of air about the point:

= 1 C kg⁻¹ of air (roentgen; 1 R = 2.58×10^{-4} C kg⁻¹)

= 1 esu cm⁻³ (= 87.8 erg released energy per g of air) Implicit in the definition is the assumption that the small test volume is embedded in a sufficiently large uniformly irradiated volume that the number of secondary electrons entering the volume equals the number leaving.

Unit of equivalent dose for biological damage = sievert. 1 Sv = 100 rem (roentgen equivalent for man). The equivalent dose in Sv = absorbed dose in grays \times w_R , where w_R is the radiation weighting factor (formerly the quality factor Q), which depends upon the type of radiation and other factors, as shown in Table 5-3. The equivalent dose expresses the long-term risk (primarily due to cancer and leukemia) from low-level chronic exposure.

B. RADIATION LEVELS

Natural annual background from all sources. In most of the world, the whole-body equivalent dose rate ≈ 0.4–4 mSv (40–400 mrem). It can range up to 50 mSv (5 rem) in certain areas. The U.S. average ≈ 3.6 mSv, including about 2 mSv (≈ 200 mrem) from inhaled natural radioactivity, mostly

Table 5-3. Radiation weighting factors.

1 total of Tradition Weighting Jacier	<i>-</i>
Type of radiation	$w_{\mathbf{R}}$
X- and γ-rays, all energies	1
Electrons and muons, all energies	1
Neutrons:	
< 10 keV	5
10-100 keV	10
0.1-2 MeV	20
2–20 MeV	10
> 20 MeV	5
Protons (other than recoils), > 2 MeV	5
Alphas, fission fragments, and heavy nuclei	20

radon and radon daughters. This radon exposure value is for a typical house; radon exposure varies by more than an order of magnitude.

Cosmic ray background in counters (Earth's surface): ~1 min⁻¹cm⁻² sr⁻¹.

Man-made radiation dose: The greatest contribution to manmade radiation dose has been from irradiation from x-ray diagnostics in medicine, which accounts for about 20% of the average natural radiation dose.

Fluxes (per cm²) to deposit one Gy, assuming uniform irradiation:

For photons:

≈ 6.24 × 10⁹ λ Ef, for photons of energy E [MeV], attenuation length λ (g cm⁻²), and fraction $f \le 1$ expressing the fraction of the photon's energy deposited in a small volume of thickness $< \lambda$ but large enough to contain the secondary electrons. ≈ 2 × 10¹¹ photons cm⁻² for 1-MeV photons on carbon (f = 0.5).

For charged particles:

 $\approx 6.24 \times 10^9 / (dE/dx)$; where dE/dx [MeV g⁻¹ cm²), the energy loss per unit length, may be obtained from range-energy figures.

 $\approx 3.5 \times 10^9$ cm⁻² for minimum-ionizing singly-charged particles in carbon.

Quoted fluxes are good to about a factor of two for all materials

Recommended exposure limits for radiation workers (wholebody dose):

ICRP: 20 mSv yr⁻¹ averaged over 5 years, with the dose in any one year \leq 50 mSv.

U.S.: 50 mSv yr⁻¹ (5 rem yr⁻¹). Many laboratories in the U.S. and and elsewhere set lower limits.

Lethal dose: Whole-body dose from penetrating ionizing radiation resulting in 50% mortality in 30 days (assuming no medical treatment), about 5 Gy (500 rads) as measured internally on body longitudinal center line. Surface dose varies owing to variable body attenuation and may be a strong function of energy.

This section was adapted, with permission, from the 1999 web edition of the Review of Particle Physics (http://pdg.lbl.gov). For further information, see ICRP Publication 60, 1990 Recommendation of the International Commission on Radiological Protection (Pergamon Press, New York, 1991) and E. Pochin, Nuclear Radiation: Risks and Benefits (Clarendon Press, Oxford, 1983).

5.5 USEFUL EQUATIONS

The following pages include a number of equations useful to x-ray scientists, either expanding on subjects covered in this booklet or addressing topics not covered here. The equations have been drawn from D. T. Attwood, Soft X-Rays and Extreme Ultraviolet Radiation: Principles and Applications (Cambridge Univ. Press, Cambridge, 1999) [www.coc) berkeley.edu/AST/sxreuv], and the equation numbers refer to that volume, which should be consulted for further explanation and discussion. That reference also expands on the discussions in this booklet on zone plate optics, synchrotron radiation, and other topics.

General X-Ray Formulas

Wavelength and photon energy relationship:

$$\hbar\omega \cdot \lambda = hc = 1239.842 \text{ eV} \cdot \text{nm}$$
 (1.1)

Number of photons required for 1 joule of energy:

1 joule
$$\Rightarrow 5.034 \times 10^{15} \lambda$$
 [nm] photons (1.2a)

X-Ray Scattering and Absorption

Thomson cross section for a free electron:

$$\sigma_e = \frac{8\pi}{2}r_e^2 \qquad (2.45)$$

$$r_e = \frac{e^2}{4\pi\epsilon_0 mc^2} = 2.82 \times 10^{-13} \text{cm}$$
 (2.44)

and r_e is the classical electron radius.

Scattering cross section for a bound electron:

$$\sigma = \frac{8\pi}{3} r_e^2 \frac{\omega^4}{(\omega^2 - \omega_s^2)^2 + (\gamma \omega)^4} \eqno(2.51)$$

Rayleigh cross section ($\omega^2 \ll \omega_*^2$):

$$\sigma_R = \frac{8\pi}{3} r_e^2 \left(\frac{\omega}{\omega_s}\right)^4 = \frac{8\pi}{3} r_e^2 \left(\frac{\lambda_s}{\lambda}\right)^4 \qquad (2.52)$$

Scattering by a multi-electron atom:

$$\frac{d\sigma(\omega)}{d\Omega} = r_e^2 |f|^2 \sin^2 \Theta \qquad (2.68)$$

$$\sigma(\omega) = \frac{8\pi}{3} |f|^2 r_e^2 \qquad (2.69)$$

where the complex atomic scattering factor represents the electric field scattered by an atom, normalized to that of a single electron:

$$f(\Delta \mathbf{k}, \omega) = \sum_{s=1}^{Z} \frac{\omega^2 e^{-i\Delta \mathbf{k} \cdot \Delta \mathbf{r}_s}}{(\omega^2 - \omega_s^2 + i\gamma\omega)}$$
 (2.66)

For forward scattering or long wavelength this reduces to

$$f^{0}(\omega) = \sum_{s=1}^{Z} \frac{\omega^{2}}{(\omega^{2} - \omega_{s}^{2} + i\gamma\omega)} = f_{1}^{0} - if_{2}^{0}$$
 (2.72 & 2.79)

Refractive index for x-ray radiation is commonly written * as

$$n(\omega) = 1 - \delta + i\beta = 1 - \frac{n_a r_e \lambda^2}{2} (f_1^0 - i f_2^0)$$
 (3.9 & 3.12)

where

$$\delta = \frac{n_a r_e \lambda^2}{2\pi} f_1^0(\omega) \qquad (3.13a)$$

$$\beta = \frac{n_a r_e \lambda^2}{2\pi} f_2^0(\omega) \qquad (3.13b)$$

Absorption length in a material:

$$\ell_{abs} = \frac{\lambda}{4\pi\beta} = \frac{1}{2n_a r_e \lambda f_2^0(\omega)}$$
 (3.22 & 3.23)

Mass-dependent absorption coefficient:

$$\mu = \frac{2r_e\lambda}{Am_u}f_2^0(\omega) \qquad (3.26)$$

Atomic absorption cross section:

$$\sigma_{abs} = 2r_e \lambda f_2^0(\omega) = Am_u \mu(\omega)$$
 (3.28a&b)

Relative phase shift through a medium compared to a vacuum:

$$\Delta \phi = \left(\frac{2\pi \delta}{\lambda}\right) \Delta r \qquad (3.29)$$

where Δr is the thickness or propagation distance.

^{*} The choice of $+i\beta$ is consistent with a wave description $E=E_0\exp[-i(\omega t-kr)]$. A choice of $-i\beta$ is consistent with $E=E_0\exp[i(\omega t-kr)]$.

Snell's law:

$$\sin \phi' = \frac{\sin \phi}{n}$$
(3.38)

Critical angle for total external reflection of x-rays:

$$\theta_c = \sqrt{2\delta}$$
 (3.41)

$$\theta_c = \sqrt{2\delta} = \sqrt{\frac{n_a r_e \lambda^2 f_1^0(\lambda)}{\pi}}$$
(3.42a)

Brewster's angle (or polarizing angle):

$$\phi_B \simeq \frac{\pi}{4} - \frac{\delta}{2} \qquad (3.60)$$

Multilayer Mirrors

Bragg's law:

$$m\lambda = 2d \sin \theta$$
 (4.6b)

Correction for refraction:

$$m\lambda = 2d\sin\theta\sqrt{1-\frac{2\bar{\delta}}{\sin^2\theta}} = 2d\sin\theta\left(1-\frac{4\bar{\delta}d^2}{m^2\lambda^2}\right)$$

where $\bar{\delta}$ is the period-averaged real part of the refractive index.

$$\Gamma = \frac{\Delta t_{\rm H}}{\Delta t_{\rm H} + \Delta t_{\rm L}} = \frac{\Delta t_{\rm H}}{d}$$
(4.7)

Plasma Equations

Electron plasma frequency:

$$\omega_p^2 = \frac{e^2 n_e}{\epsilon_0 m}$$
(6.5)

Debye screening distance:

$$\lambda_D = \left(\frac{\epsilon_0 \kappa T_e}{e^2 n_e^2}\right)^{1/2} \tag{6.6}$$

No. of electrons in Debye sphere:

$$N_D = \frac{4\pi}{2} \lambda_D^3 n_e \qquad (6.7)$$

Electron cyclotron frequency:

$$\omega_c = \frac{eB}{m}$$
(6.8)

Maxwellian velocity distribution for electrons characterized by a single-electron temperature κT_e :

$$f(\mathbf{v}) = \frac{1}{(2\pi)^{3/2}\mathbf{v}_s^3} e^{-\mathbf{v}^2/2\mathbf{v}_e^2}$$
(6.1)

where

$$v_e = \left(\frac{\kappa T_e}{m}\right)^{1/2} \qquad (6.2)$$

Electron sound speed:

$$a_e = \left(\frac{\gamma \kappa T_e}{m}\right)^{1/2} \tag{6.79}$$

Critical electron density:

$$n_{\rm c} \equiv \frac{\epsilon_0 m \omega^2}{e^2} = 1.11 \times 10^{21} \; \frac{\rm e/cm^3}{\lambda^2 (\mu \rm m)} \eqno(6.112 \rm a~\&~b)$$

Refractive index of plasma is

$$n = \sqrt{1 - \frac{n_e}{n_c}}$$
(6.114b)

Ratio of electron energy in coherent oscillations to that in random motion:

$$\left|\frac{\mathbf{v}_{os}}{\mathbf{v}_{e}}\right|^{2} = \frac{e^{2}E^{2}}{m\omega^{2}\kappa T_{e}} = \frac{I/c}{n_{c}\kappa T_{e}}$$
(6.131a)

$$\left|\frac{{\rm v_{os}}}{{\rm v_e}}\right|^2 = \frac{0.021 I(10^{14}~{\rm W/cm^2}) \lambda^2~(\mu{\rm m})}{\kappa T_{\rm e} ({\rm keV})} \eqno(6.131b)$$

Spectral brightness of blackbody radiation within $\Delta\omega/\omega = 0.1\%BW$:

$$B_{\Delta\omega/\omega} =$$

$$3.146 \times 10^{11} \left(\frac{\kappa T}{eV}\right)^3 \frac{(\hbar \omega/\kappa T)^3}{(e^{\hbar \omega/\kappa T} - 1)} \frac{\text{photons/sec}}{(\text{mm})^2 (\text{mr})^2 (0.1\% \text{BW})}$$
(6.136)

Photon energy at peak spectral brightness:

$$\hbar \omega |_{pk} = 2.822 \kappa T$$
 (6.137)

where κ is the Boltzmann constant.

Stefan-Boltzmann radiation law (blackbody intensity at any interface):

$$I = \sigma T^4$$
 (6.141b)

where the Stefan-Boltzmann constant is

$$\sigma = \frac{\pi^2 \kappa^4}{60c^2\hbar^3}$$
(6.142)

With κT in eV:

$$I = \hat{\sigma}(\kappa T)^4 \qquad (6.143a)$$

where $\hat{\sigma}$ is the modified Stefan-Boltzmann constant

$$\widehat{\sigma} = \frac{\pi^2}{60\hbar^3 c^2} = 1.027 \times 10^5 \frac{\text{watts}}{\text{cm}^2 (\text{eV})^4} \tag{6.143b}$$

Coherence

Longitudinal coherence length:*

$$\ell_{\text{coh}} = \lambda^2/2\Delta\lambda$$
 (8.3)

Spatial or transverse coherence (rms quantities):

$$d \cdot \theta = \lambda/2\pi$$
 (8.5)

or in terms of FWHM values

$$d \cdot 2\theta|_{PWHM} = 0.44\lambda$$

Spatially coherent power within a relative spectral bandwidth $\lambda/\Delta\lambda=N$ for an undulator with N periods:

$$\bar{P}_{\text{coh},N} = \frac{e\lambda_u I}{8\pi\epsilon_0 d_x d_y \theta_x \theta_y \gamma^2} \cdot \left(\frac{\hbar\omega_0}{\hbar\omega} - 1\right) f(\hbar\omega/\hbar\omega_0) \quad (8.7c)$$

where $\hbar\omega_0$ corresponds to K=0, and where

$$f(\hbar\omega/\hbar\omega_0) = \frac{7}{16} + \frac{5}{8} \frac{\hbar\omega}{\hbar\omega_0} - \frac{1}{16} \left(\frac{\hbar\omega}{\hbar\omega_0}\right)^2 + \dots$$
 (8.8)

When the undulator condition $(\sigma' \ll \theta_{\text{cen}})$ is satisfied, the coherent power within a relative spectral bandwidth $\Delta \lambda / \lambda < 1/N$, is

$$\begin{split} \bar{P}_{\mathrm{coh},\lambda/\Delta\lambda} &= \frac{e\lambda_{\mathrm{u}} I\eta(\lambda/\Delta\lambda)N^{2}}{8\pi\epsilon_{0}d_{x}d_{y}} \cdot \left(1 - \frac{\hbar\omega}{\hbar\omega_{0}}\right) f(\hbar\omega/\hbar\omega_{0}) \\ & (\sigma'^{2} \ll \theta_{\mathrm{cen}}^{2}) \end{split} \tag{8.10c}$$

where η is the combined beamline and monochrometer efficiency.

^{*} The factor of two here is somewhat arbitrary and depends, in part, on the definition of $\Delta\lambda$. Equation (26) on page 2-14 omits this factor. See Attwood, op.cit., for further discussion.

Spatially coherent power available from a laser is

$$P_{\text{coh}} = \frac{(\lambda/2\pi)^2}{(d_x\theta_x)(d_y\theta_y)} P_{\text{laser}}$$
(8.11)

where P_{laser} is the total laser power.

Normalized degree of spatial coherence, or complex coherence factor:

$$\mu_{12} = \frac{\langle E_1(t)E_2^*(t)\rangle}{\sqrt{\langle |E_1|^2\rangle}\sqrt{\langle |E_2|^2\rangle}}$$
(8.12)

The van Cittert-Zernike theorem for the complex coherence factor is

$$\mu_{\rm OP} = \frac{e^{-i\psi} \int \int I(\xi, \eta) e^{ik(\xi\theta_x + \eta\theta_y)} d\xi d\eta}{\int \int I(\xi, \eta) d\xi d\eta}$$
(8.19)

For a uniformly but incoherently illuminated pinhole

$$\mu_{OP}(\theta) = e^{-i\psi} \frac{2J_1(ka\theta)}{(ka\theta)}$$
(8.27)

which has its first null ($\mu_{\rm OP}=0$) at $ka\theta=3.832$, which for d=2a corresponds to $d\cdot\theta=1.22\lambda$.

EUV/Soft X-Ray Lasers

Growth of stimulated emission:

$$\frac{I}{I_0} = e^{GL}$$
(7.2)

where L is the laser length and G is the gain per unit length. For an upper-state ion density n_u and a density inversion factor $F(\leq 1)$

$$G = n_u \sigma_{\text{stim}} F$$
 (7.4)

where the cross section for stimulated emission is

$$\sigma_{\text{stim}} = \frac{\lambda^3 A_{u\ell}}{8\pi c(\Delta \lambda/\lambda)}$$
(7.16)

$$\sigma_{\text{stim}} = \frac{\pi \lambda r_e}{(\Delta \lambda / \lambda)} \left(\frac{g_\ell}{q_u} \right) f_{\ell u} \qquad (7.18)$$

where $A_{u\ell}$ is the spontaneous decay rate, $f_{\ell u}$ is the oscillator strength and g_{ℓ}/g_u is the ratio of degeneracy factors.

Laser wavelength scaling goes as $1/\lambda^4$:

$$\frac{P}{A} = \frac{16\pi^2 c^2 \hbar (\Delta \lambda / \lambda) GL}{\lambda^4}$$
(7.22)

Doppler-broadened linewidth:

$$\frac{(\Delta \lambda)}{\lambda}\Big|_{\text{EWUM}} = \frac{v_i}{c} = \frac{2\sqrt{2 \ln 2}}{c} \sqrt{\frac{\kappa T_i}{M}}$$
 (7.19a)

where v_i is the ion thermal velocity, κT_i is the ion temperature, and M is the ion mass. With κT_i expressed in eV and an ion mass of $2m_p Z$

$$\frac{(\Delta \lambda)}{\lambda}\bigg|_{\text{FWHM}} = 7.68 \times 10^{-5} \left(\frac{\kappa T_i}{2Z}\right)^{1/2} \tag{7.19b}$$

Lithography

Minimum printable line width:

$$L_w = k_1 \frac{\lambda}{N \Delta}$$
(10.1)

where k_1 is a constant dominated by the optical system, but affected by pattern transfer processes.

Depth of focus:

$$DOF = \pm k_2 \frac{\lambda}{(NA)^2}$$
(10.2)

Degree of partial coherence:

$$\sigma = \frac{\text{NA}_{\text{cond}}}{\text{NA}_{\text{obj}}} \tag{10.3}$$

where the subscript cond refers to the condenser or illumination optics, and obj refers to the objective lens of the reduction optics.

International Technology Road Map for Semiconductors

		Years		
1:1 lines (nm) Isolated lines (nm)	2005 100 65	2008 70 45	2011 50 30	2014 35 20

http://www.sematech.org

lightsources.org

Additional information about light sources around the world can be found at http://lightsources.org